Revista Română de Inginerie Civilă

Indexată în bazele de date internationale (BDI)

ProQuest, INSPEC, EBSCO, GOOGLE SCHOLAR, CROSSREF, TDNET, DIMENSIONS, DRJI, JGATE, INDEX COPERNICUS, ULRICH'S și JOURNALSEEK

Volumul 14 (2023), Numărul 4

MATRIX ROM
3 Politehnicii Street, Bucharest, Romania
Tel. +4021.4113617, +40733882137
e-mail: office@matrixrom.ro
www.matrixrom.ro

EDITORIAL BOARD

Romanian Journal of Civil Engineering is founded, published and funded by publishing house MATRIX ROM
Executive Director: mat. Iancu ILIE

Online edition ISSN 2559-7485
Print edition ISSN 2068-3987; ISSN-L 2068-3987

Occupant-Centred Lighting (OCL) to well-being: a review

Iluminatul centrat pe ocupant (OCL) pentru bunăstare: o revizuire

M Simtinica, M Husch, S Caluianu

Technical University of Civil Engineering of Bucharest, Bucharest, Romania

Email: marian-catalin.simtinica@phd.utcb.ro

DOI: 10.37789/rjce.2023.14.4.1

Abstract. *People in the past spent most of their time outdoors and received the benefits of exposure to natural light. Nowadays we spend a large part of our day indoors where we predominantly use artificial lighting. Against the backdrop of the accelerating climate change we are experiencing, the need to reduce energy consumption in the lighting component of buildings can be achieved by maximising the use of natural daylight during the day in conjunction with identifying the human presence in indoor spaces for efficiency. Occupant Lighting Control technologies offer a real tool to achieve these goals. Adaptive lighting automation controllers, sensor networks and wireless actuators for occupancy-based lighting control, user-centric lighting control based on video cameras, platforms for intelligent lighting control based on life logs are just some of the techniques and methods used to apply Occupant Lighting Control principles. Although lowering energy consumption in buildings is the primary goal of lighting management systems, taking into account the inhabitants' feeling of comfort and their general level of wellbeing is just as vital, if not more so. The adoption of integrative lighting, by complementing natural light with artificial lighting in an articulated manner and in conjunction with the human presence in interior spaces, is the efficient and human-accepted path to sustainable energy efficiency. A collective effort by society is needed to make human-centred lighting an everyday reality.*

Key words. Lightning**,** services, natural light

1. Introduction

Earth's natural day-night cycle has had a defining influence on human biological and social evolution. Light has been a fundamental factor in human activities, and its changes over a 24-hour period in light intensity and color temperature at different times of the day starting from low values in the morning, peaking in the middle of the

day and then falling to a very low level at night has defined the circadian rhythm for humans.

In the past, 90% of our time was spent outdoors. Humans were immersed in natural light radiation streams, receiving through their sense organs all these changes, and reacting accordingly to these external stimuli. In modern times we spend 10% of our active time in the outside environment, exposed to natural environmental factors. Most of the time we use artificial lighting, present in residential, office, commercial and factory buildings as well as on the streets. The quantitative (illuminance level and luminous flux distribution) and quantitative (luminaire distribution, light color, color rendering, etc.) aspects of lighting can influence the condition of lighting system users, both for better and for worse. In a positive sense, the effects can be increased attention and concentration, increased productivity, physiological and psychological comfort, relaxation, and efficient recovery, etc. In a negative sense, it can lead to disruption of the circadian rhythm and the appearance of health problems, affecting the general state of well-being.

Humankind is facing an accelerating phenomenon of climate change [1]. Against this backdrop of instability, the energy consumption of buildings is increasing. Buildings consume about 30% of the electricity produced worldwide. A review of design thinking for building installations using advanced technologies and renewable energy is needed. The Near Zero Energy Building (NZEB) concept is important to consider, and to apply on a large scale [9].

Building technologies have evolved and buildings with good thermal envelope insulation are now being built. We can even say that they are energy efficient in this respect.

But lighting technologies, although they have moved to LED lighting sources in most buildings, have not evolved that much. There is a phenomenon of increasing electricity consumption generated by lighting systems, due to the level of demand for comfort in indoor spaces, the extended time people spend in buildings, especially late at night, and the lack of an articulated automation system that reduces the level of artificial lighting in proportion to the natural light input, correlates the shading system with the artificial lighting and switches off the lights when people leave the spaces, all done in an efficient but user interactive way.

The concepts of well-being and human centered lighting coordinate aspects of human perception and perception of an interior space and beyond. But the concept that coordinates energy efficiency, and how to achieve comfort while keeping energy consumption at the right level, is Occupant Centric Control (OCC). For lighting, the subject of this article, the concept is Occupant-Centered Lighting (OCL). By implementing in buildings automation systems that employ occupant centered lighting techniques for the actuation and control of lighting systems, optimal energy consumption is ensured while preserving for the occupants the characteristics of human lighting but very importantly also the state of well-being.

A person's well-being is not a concept defined in scientific terms. Even so, there are some parameters that can be considered with serious arguments in influencing the general state of a person in a building (lighting, room temperature, humidity, solar

radiation, brightness (glare), air currents speed, thermal radiation of objects in the room, etc.).

It is universally true that the weighting of one at the expense of another can produce imbalances, and a saving made in one-part leads to cost increases in another. A classic example is that of increasing the glazed area of a facade, which favors access to natural light and leads to lower energy consumption with artificial lighting, but which leads to higher heat input and therefore higher heating and cooling costs for the interior space in question.

A balance is needed, and this involves a fine balancing of energy parameters to achieve a situation that, in the best assessments, can induce a state of comfort and therefore a state of "well-being".

2. Lighting in buildings - economy versus well-being

Building-related activities considerably increase the world's energy usage. 25% of the energy used in commercial buildings in the US is ascribed to lighting, while 12% is allocated to the residential sector. In the EU, lighting accounts for 14% of all energy usage in commercial buildings and 11% in residential ones. To achieve energy-efficient energy consumption, automated lighting control systems are therefore required [10]. Numerous innovations in technology over the years have been successful in lowering the amount of energy used by lighting systems. For instance, traditional passive infrared occupancy sensors have been utilized in structures for more than 20 years. According to numerous studies, these sensors, used to turn on lights when a room is occupied and turn them off after a predetermined amount of time, defined duration of non-occupancy, or time delay, can save up to 38% more energy than human operation [2].

However, there are some drawbacks to control via conventional passive sensor monitoring of occupant presence:

On the one hand, false positive detection may result in the use of illumination that is not necessary. On the other hand, false-negative detection might result in unintended light switching off, such as when a person sits motionless for a lengthy time using a computer. This frequently makes the residents angry.

A system that exclusively employs occupancy sensors does not take the environment into account. Regardless of whether there is any natural light present in the space, the lights will be turned on to their highest setting if a human is identified.

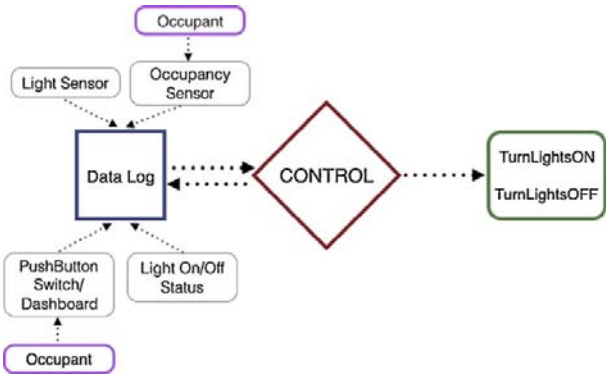

Figure 1. Lighting control system with a focus on the user. [2]

Improved automation system design has been a focus of research and development as of late. Because of this, cutting-edge automatic control methods have been offered, which may not only save more energy but also modify their operations in response to the preferences of the building's occupants.

Research shows that people don't generally prioritize energy efficiency when making home adjustments; rather, they prioritize the comfort of themselves and their guests.

It is necessary to integrate intelligent lighting automation systems in buildings that take into account inhabitants' impression of comfort and well-being, even if the primary goal of lighting control systems is to reduce energy consumption. There is a pressing demand for implementations that can adapt to their surroundings and improve over time.

How well these systems function in terms of energy efficiency and how well they are received by their intended occupants depends on this.

3. User-centred lighting control (OCL): approaches

A comfortable working atmosphere while consuming the least amount of energy are the goals of the current generation of intelligent lighting control systems. Better human-room interaction requires an occupant-centered design approach (a person in a space in a room) [5]. Given the following goals of an intelligent building automation system, occupant context-based lighting control design is required:

- locate a person and, while turning off the lights in empty spaces, change the lighting control to suit the space they are using.
- comprehend the activity of individuals around them to give suitable illumination conditions for various situations and activities.
- integrating lighting and shade technologies to maximize natural light while preserving the indoor climate.

The automation system can be configured to reflect the user's preferences for lighting. For instance, varying light levels and color temperatures can be used to generate various moods based on the time of day or during particular activities (watching films, eating, studying, etc.).

There are algorithms for smart buildings that manage lighting based on the needs of the occupants. A lighting control algorithm based on observations of a network of

sensors situated in one or more rooms is taken into consideration to give suitable lighting settings for various conditions. The system may modify lighting settings to provide an environment that is comfortable for the user while also saving energy by dimming or reducing the light output for particular luminaires after learning a person's position and activities.

3.1. LightLearn: An adaptive occupant-centred controller

Because they concentrate only on energy consumption rather than occupant comfort, lighting controllers that incorporate occupancy and brightness sensors to increase energy efficiency are frequently useless. The perfect controller will adjust to the preferences of the users and the surrounding environment.

In their research, Nagy et al. [3] used LightLearn, an occupant-centered controller (OCC) for learning-based lighting.

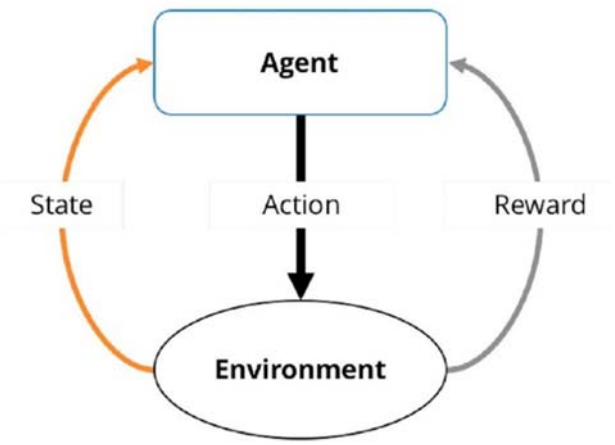

Figure 2. To choose the best course of action, the control agent engages with the environment [3].

It keeps an eye on the amount of both natural and artificial light present in the space as well as how the tenant and the lighting system interact. The best actions for the controller are then decided upon using this data.

LightLearn successfully strikes a balance between consumer energy use and occupant comfort. LightLearn's adaptive features imply that occupant-centered control-based learning is a workable strategy to reduce the disparity between occupant comfort and energy usage.

The Light Utilization Ratio (LUR), which was developed to normalize energy consumption depending on human presence, was one of the initial two metrics employed in the study.

$$\text{LUR} = \frac{\text{time with lights on}}{\text{occupied time}}$$

- The UNC Ratio for Evaluating Human Comfort. This parameter was employed by Nagy et al. [2] to assess the efficacy of their OCC lighting controller by determining how long occupants were subjected to an unsuitable lighting environment before reporting discomfort.

Comfort-to-light levels Sunlight utilization (as measured by LUR) and human comfort (as measured by UNC) are both indicators. The two metrics are not sufficient for evaluating OCC performance, however, for two main reasons: - neither indicator takes into account the connection between occupants, occupant behavior, and energy use. There is also the energy used implicitly by the controller to maintain a pleasant environment and turn off lights when not needed or when the room is deserted if there is ample natural light. However, LUR and UNC have limitations in these types of scenarios.

- Given that LUR and UNC were originally conceived as design criteria, it is possible that they are not well suited for assessing controller performance in the field.

To evaluate the effectiveness of occupant-focused lighting management systems, we propose the Light Comfort-Ratio (LCR) to combat this problem.

Table 1.

LCR performance scores [3].

Controller performance scores in LCR.

Goal	Score
Occupant is comfortable with lights off	1.0
Occupant is comfortable with necessary energy consumption	1.0
Occupant is comfortable with unnecessary energy consumption	0.5
Occupant is uncomfortable	0.0
Space is vacant with lights off	1.0
Space is vacant with lights on	0.0

To put it simply, the goal is to assign a value between 0 (worst) and 1 (best) to each time step t when the controller is in effect (best). As can be seen in Table 1, LightLearn assigns a value of 0 to occupant discomfort and energy waste and a value of 1 to occupant comfort and mandatory energy usage. Both goals are equally reinforced by the confusing scenario of a happy occupant who uses too much energy. With this grading system, we can see how well a controller strikes a balance between occupant satisfaction and energy efficiency.

An eight-week experiment in five offices demonstrates that LightLearn can learn the habits of its occupants and the state of the building's surroundings, then adjust its control parameters to achieve the desired effects. Overall, participants felt the illumination had improved slightly from before.

3.2. Network of wireless sensors and actuators for lighting control occupancy

Approximately 35 percent of current buildings in the EU are older than 50 years. These historic buildings, the majority of which have deteriorating infrastructure and insufficient operational resources, consume a substantial amount of energy. The retrofitting of these older buildings, however, gives an excellent chance to accomplish significant increases in energy efficiency while still preserving the built environment [4].

In modern buildings, automation relies on a combination of communication mediums, including both wired and wireless communication systems. Despite the fact that wired solutions are typically favored, wireless devices have grown more widespread as a result of advancements in communication technology, such as the speed and security of connections and the battery life. Batteries for sensors today have a lifespan of several years on average. Consequently, wireless sensors are already replacing or, in some cases, augmenting old wired systems, resulting in versatile and cost-effective building automation solutions.

In building automation, numerous wireless devices employing diverse protocols, such as Wi-Fi, ZigBee, Z-wave, and Bluetooth, are available. In addition to its versatility and adaptability, wireless gadgets of the present day are cost-effective and allow unobtrusive installation in existing structures without cables or cable ducts.

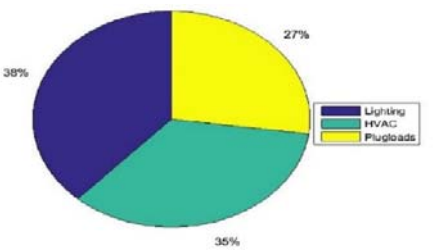

Figure 3. Distribution of annual power consumption among the three most common end uses: lighting, HVAC, and outlets [4].

The Wireless Sensors and Actuators Network (WSAN), which was once seen as expensive and immature for practical large-scale commercial applications, is now utilized in a variety of contexts.

Since lighting systems in open areas of the majority of commercial office buildings are frequently centrally controlled, WSAN promotes the deployment of optimal lighting systems. This dynamic system can alter the lighting in open-plan spaces according to the tastes and demands of the occupants in the most energy-efficient manner possible. By using the individual addressability of luminaires, they can be coordinated to give occupants with customized lighting for specific job functions, while ensuring that unoccupied rooms stay dark or at a background level of illumination.

The condition of structures with excellent insulation is contradictory. Heating and cooling systems do not consume the majority of the building's energy. Even when high-efficiency lighting solutions (LED) are utilized, illumination becomes a significant factor. Up to 30-35% of the annual energy used in buildings with strong thermal insulation is for lighting [4]. It is therefore crucial to seek out new techniques to lower the energy consumption of lighting in buildings, especially those that have already been completed.

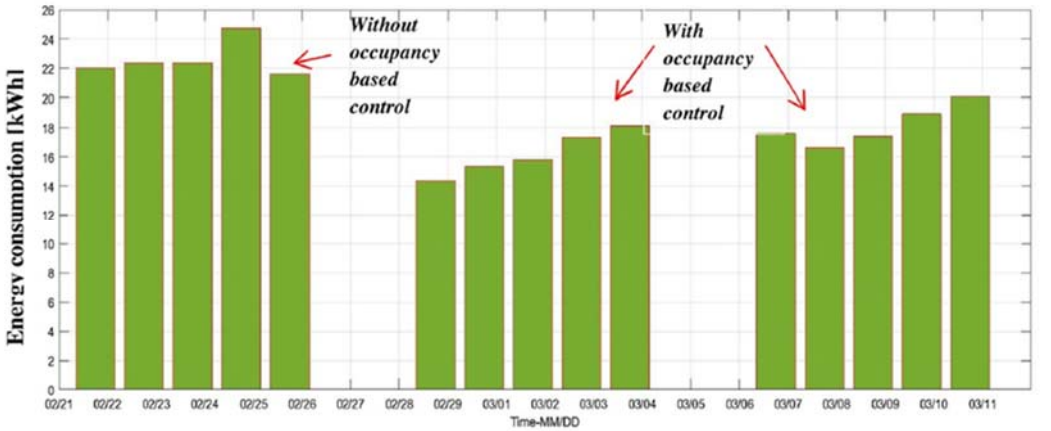

Figure 4. Daily illumination energy use [kWh] during the course of three weeks of studies [4].

Motion sensors in the space and pressure sensors in the seat (detection of the weight of the individual seated on the seat) were utilized and were programmed to only communicate data to an interface (gateway) when a change in state was detected. This meant that occupancy information was only provided to the gateway when the presence or absence of a human was recognized. Consequently, battery life is extended.

Existing building retrofitting is not a low-cost solution, but it offers significant energy savings. Thus, higher up-front expenses and a lack of understanding of the technologies and their potential might be considered as significant contributors to the relatively slow rate of building restoration.

In a medium-sized commercial office building, the feasibility of wireless sensors and actuators was assessed. In an open area of the office building, wireless sensors and actuators were installed for occupancy detection and presence-based lighting management. During the first week of the experiment with occupancy-based control, lighting energy usage was reduced by 28%. To preserve a pleasant relationship between the system and the user, the time delay between turning off the lighting and the occupant leaving the workstation was increased from 2 minutes to 5 minutes the next week, resulting in a 20% decrease in lighting electricity use.

3.3. User-centred lighting control based on video cameras

To gain a finer resolution of user position and activity, we examine a lighting control system based on data collected from a network of visible-spectrum video cameras. In the video camera, useful features are derived from the video image data. These characteristics from each camera are then collated by the central unit. The central unit can determine the location and activities of the user based on data collected from all cameras. The system then determines the best illumination level and sends commands to the lighting automation system.

The vast majority of studies employ sensors to monitor illumination levels and offer feedback for lighting management. This study is mainly concerned with the occupant. As a result, instead of using illumination sensors, it employs video cameras as room

sensors to acquire user position and activity as well as contextual data pertaining to the inhabitant.

A few tasks have been chosen to illustrate the provided topics. The selected activities represent a set of simple but frequent actions observed in ordinary users while seated in a room: - walking around the room, - sitting at a desk to study, - sitting on the sofa to watch television, - lying on the couch.

A module for image processing and a module for optimization construct the method. The image processing module uses a human silhouette-based 3D form reconstruction approach for logical reasoning on room occupancy. It has been demonstrated that silhouette-based 3D form has significant promise in a variety of applications [5], such as to construct the 3D silhouette-contour of a user and then generate a graphical model to determine the user's posture.

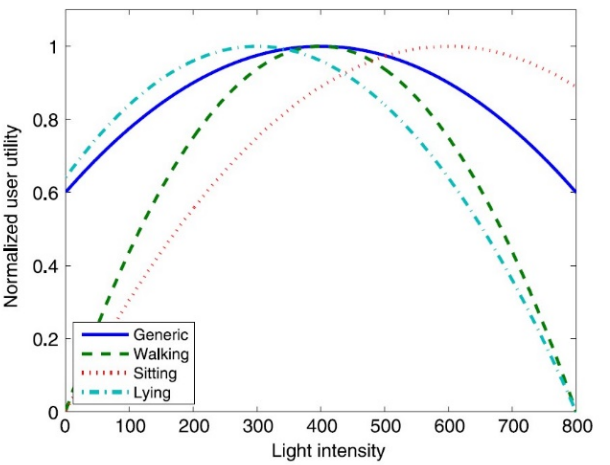

Figure 5. Multipurpose utility functions [5].

The analysis of human activity has been the subject of extensive research, but it remains a difficult endeavor due to variables such as the difficulty of dealing with an articulated human body model, changeable imaging settings, and the complexity of human activities.

There have been two lighting control algorithms proposed. The first consists of variable light intensity settings, while the second consists of on/off controls. For the light intensity control, it was expected that the light intensity can be adjusted constantly within a specific range, however for the on-off controls, it was considered that the lights can only be switched on or off.

The purpose of this study is to reduce lighting energy usage while preserving user satisfaction with lighting settings. To quantify a user's pleasure with the lighting condition, utility functions are utilized. A utility function establishes a relationship between light intensity and user happiness, represented by a value within a specific range. For various positions and occupations, distinct utility functions can be defined. For instance, the utility function in the area surrounding the desk may differ from the

utility function in the region surrounding the entrance, or we may have separate utility functions for sleeping and reading.

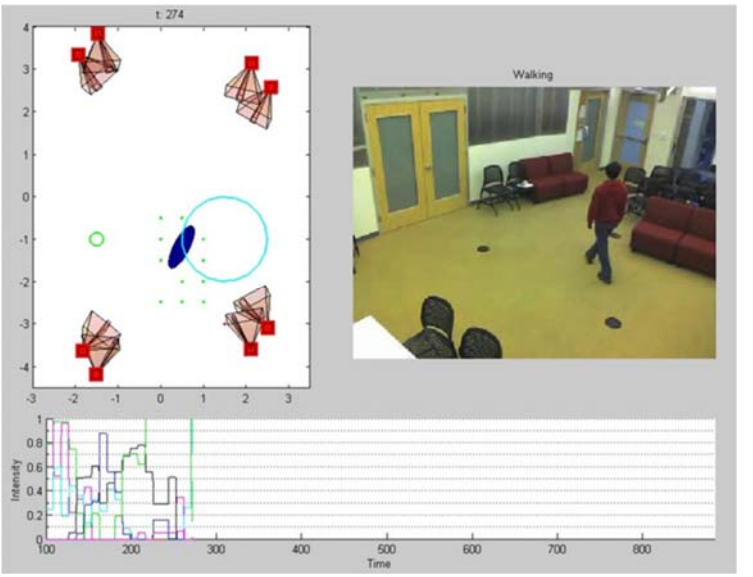

Figure 6. User-controlled light intensity snapshots [5].

The technology continuously monitors the area but only adjusts the lighting when the user's position or activity changes. Figure 5 depicts the flowchart of the light control system. When the system detects a change in the user's position or activity, it verifies the new utility values for every occupied point. The system reoptimizes the light control if one of the points has a lower utility value than the predefined value.
It is meant to expand the number of activities included in the human activity analysis algorithm. In this work, it was assumed that the light intensity delivered to the user can be computed; however, in the future, it is planned to include lighting sensors and real-time measurement of light intensity as a form of system feedback. Future development will also focus on enabling the user to customize the utility features for different tasks using a simple and intuitive interface. This can be accomplished, for instance, by a user-device interface by which the user offers incremental level changes in the system's lighting intensity for a certain position.

3.4. Intelligent lighting management system based on LifeLog

LifeLog is a record of a person's daily activities, including environmental behavior, activity, emotional and biological information. The usage of life logs enables the customization of the lighting environment to the user's characteristics. Nonetheless, such a tailored lighting environment has not yet been presented because the necessary data collecting and classification methods and a platform to synthesis these data are not yet physically feasible [6].
Sensors, lighting controllers, and control interfaces required for intelligent lighting control based on life logging were installed in a test space, a machine learning method was configured on a machine learning server, and a cloud-based platform for

implementing an optimal lighting environment was created by connecting these devices. This study's platform provides a tailored lighting environment by utilizing life logs, which are comprised of emotional information acquired by instant message (IM), text, activity information obtained using a location and activity tracker, and meteorological data.

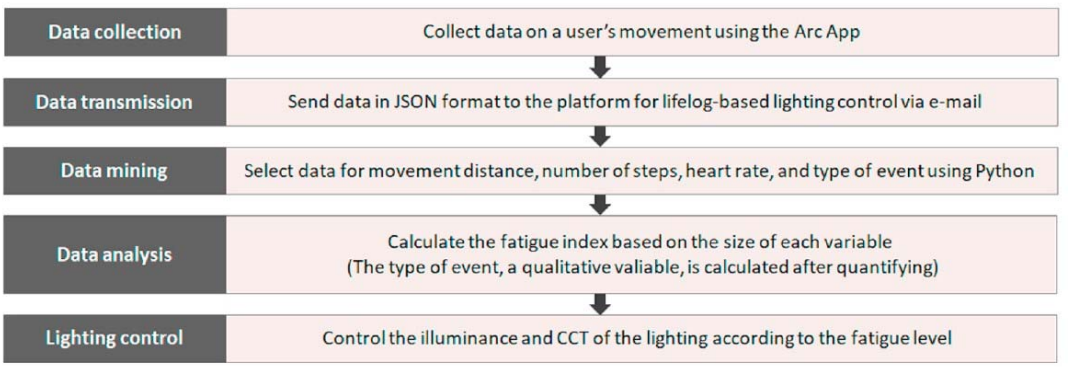

Figure 7. Method for intelligently regulating lights based on activity data [6].

LifeLog-based intelligent lighting control is proposed as a concept. It implements methods for gathering environmental data, emotional and activity information of users, as well as a system for recommending a suitable lighting mode for a particular individual based on an analysis of the information acquired about that individual.

A platform for intelligent lighting control based on lifelog aims to deliver an appropriate lighting environment based on the user's mood and situation, even without human input, by continuously collecting and storing lifelog data and by analyzing and learning from the stored data.

Smart lighting should be integrated with IoT, big data, artificial intelligence, and machine learning in order to provide a platform for lifelog-based smart lighting control.

The study proposes a lifelog-based smart lighting control technology that collects lifelog information via MI, activity, and weather data. Life log data are separated into: - emotional data, - activity data, - environmental information.

In Korea, the KakaoTalk social networking platform was utilized to adjust lights based on emotional data. The user sends the discussion text to an email account associated with the platform, and the email is examined for emotion analysis every 10 minutes. Therefore, there is a constraint in that user participation is necessary to collect text data, and emotion analysis cannot be conducted in real time.

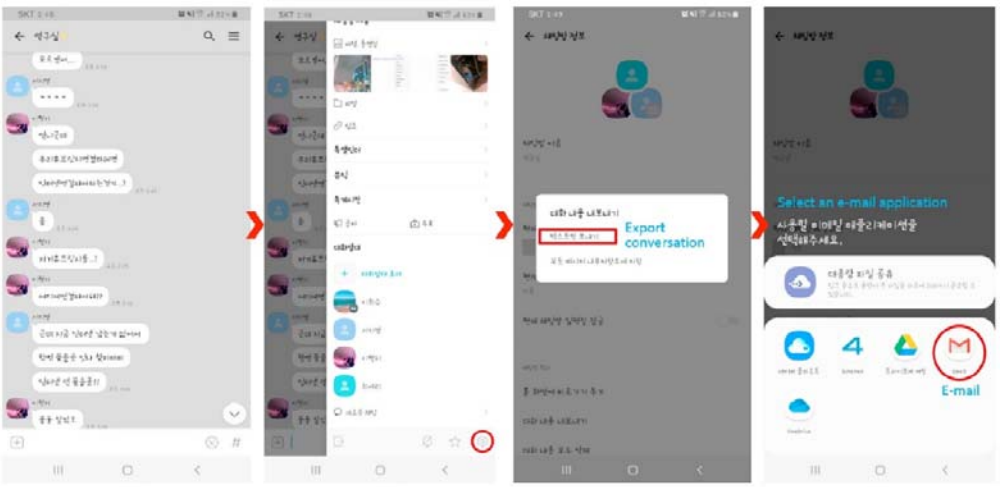

Figure 8. Procedure for Exporting Conversation Text from KakaoTalk for Emotion Analysis: To email a copy of your KakaoTalk chat history, you must first (a) open a chat window, (b) select the "Chat Window Setup" option, and (d) use the "Export Conversation" option [6].

For more precise emotion analysis in the future, physiological data acquired via wearable devices (e.g., heart rate, ECG, and PPG) should be added to the IM text and platform for intelligent, real-time control.

Importantly, the platform in the study goes beyond simple information like location, occupancy, and users' light usage patterns to recommend a lighting environment that is best suited to the user based on the result of a comprehensive analysis of users' emotional activity, activity, and environmental information.

Custom lighting is determined by three distinct types of data analysis:

In the first step, the user's mood is gauged by analyzing their IM chat logs for textual cues indicative of their emotional state. Once the relevant text has been extracted, it is translated from Korean into English using Node-RED and Google's Watson language translator. Then, IBM Watson's NLU is used to do an analysis of the user's emotions, categorizing them as either happy, sad, angry, scared, or disgusted.

The findings of this analysis of the five different emotions are then used to determine the optimal lighting mode for reducing the user's negative feelings via adjustments to the Correlated Color Temperature (CCT) and brightness.

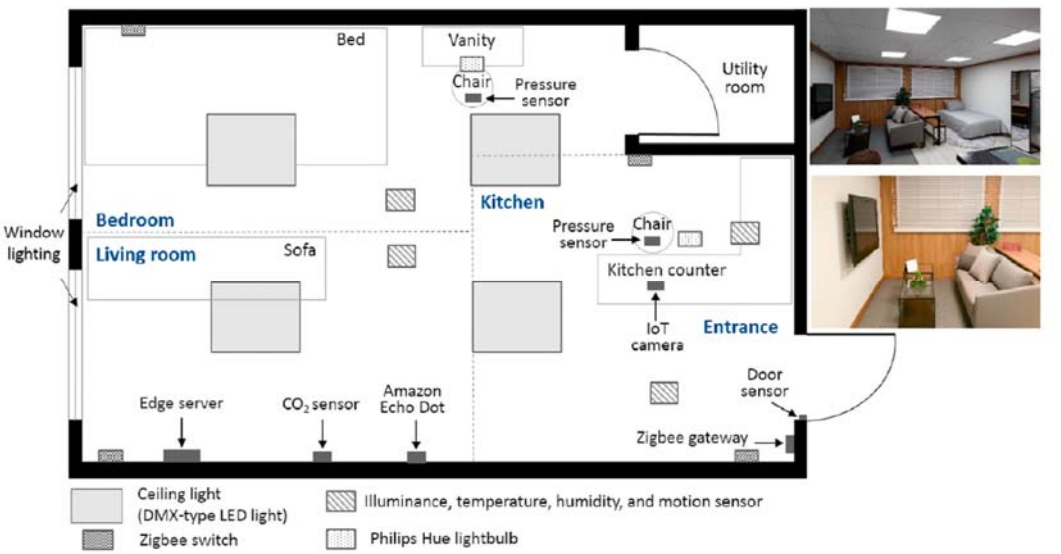

Figure 9. Plan and photos of the layout space [6]

Second, information on user behavior is gathered with the aid of a GPS and activity tracker and an Apple Watch. The data is sent to the platform through email in JSON format. Python is used to pick data on user attributes including walking distance, number of steps, heart rate, and the sort of event that occurred at the area visited by the user. The fatigue index is then computed after these factors have been quantified, and the user's tiredness is taken into account while selecting an appropriate lighting mode.
Third, data from the Korea Meteorological Administration KMAweather's stations is used to compile statistics about the local ecosystem. The sky conditions used in this analysis fall into three categories: clear, cloudy, and entirely cloudy.
Once data and forecasts for the desired region have been extracted from the KMA website using RSS (RSS provides this information as an XML file called RSS feed), Node-RED can use this data to adjust the DMX (standard for special lighting scenes effects) lighting in the sample space based on the weather outside.
Using information about the user's emotions, activities, and the surrounding environment, this platform intelligently modifies the lighting to create the desired mood.

4. Conclusions

In recent decades, electric lighting has been a significant contributor to the rise in worldwide energy expenditures. Increasing the proportion of glazed building facades is a relative solution, since it raises additional difficulties of thermal and visual comfort, but the impacts on lighting consumption have lowered the energy savings of LED technology. [7].

The building sector faces enormous issues relating to energy efficiency, greenhouse gas emissions, and visual features, with health and well-being-related goals becoming increasingly ambitious.

Office spaces can easily achieve an annual energy consumption of less than 5 kWh/m^2 by integrating natural illumination effectively; lighting energy consumption can be cut

considerably. Advanced automation technologies have demonstrated the potential to deliver dependable solutions (e.g., self-learning or self-adaptive lighting systems).

To attain the planned goals for new buildings, rigorous architectural design for daylight and solar control will be required.

Current technological developments are characterized by integrative lighting, which will become widely used in projects, but only when technical expertise among specialized designers becomes more popular [8]. Artificial lighting will be activated in a "integrative" mode when natural light is insufficient, as a result of improvements in the efficiency of LED technology used in the manufacture of lighting sources, as well as the increased processing capabilities of automation system controllers. As a result of insufficient scientific and mathematical understanding and models, the use of daylight in integrative lighting is still fairly limited in practice. To make human-centered lighting an everyday activity, architects, designers, engineers, luminaire and automation manufacturers, and policymakers must make a concerted effort.

References

[1] Lin B, Chen Z. Net zero energy building evaluation, validation and reflection – A successful project application. Energy and Buildings. 2022;261:111946.

[2] Nagy Z, Yong F, Schlueter A. Occupant centered lighting control: A user study on balancing comfort, acceptance, and energy consumption. Energy and Buildings. 2016;126:310-322.

[3] Park J, Dougherty T, Fritz H, Nagy Z. LightLearn: An adaptive and occupant centered controller for lighting based on reinforcement learning. Building and Environment. 2019;147:397-414.

[4] Labeodan T, De Bakker C, Rosemann A, Zeiler W. On the application of wireless sensors and actuators network in existing buildings for occupancy detection and occupancy-driven lighting control. Energy and Buildings. 2016;127:75-83.

[5] Lee H, Wu C, Aghajan H. Vision-based user-centric light control for smart environments. 2022.

[6] Cho Y, Seo J, Lee H, Choi S, Choi A, Sung M et al. Platform design for lifelog-based smart lighting control. Building and Environment. 2020;185:107267.

[7] Papinutto M, Boghetti R, Colombo M, Basurto C, Reutter K, Lalanne D et al. Saving energy by maximising daylight and minimising the impact on occupants: An automatic lighting system approach. Energy and Buildings. 2022;268:112176.

[8] Gentile N, Lee E, Osterhaus W, Altomonte S, Naves David Amorim C, Ciampi G et al. Evaluation of integrated daylighting and electric lighting design projects: Lessons learned from international case studies. Energy and Buildings. 2022;268:112191.

[9] European Commission. 2050 long-term strategy [Internet]. Climate Action. 2022 [cited 11 August 2022]. Available from: https://ec.europa.eu/clima/eu-action/climate-strategies-targets/2050-long-term-strategy_en

[10] The International Energy Agency I. Annual Reports || IEA EBC [Internet]. Iea-ebc.org. 2022 [cited 11 August 2022]. Available from: https://www.iea-ebc.org/publications/annual-reports

Virtual instrumentation control for evaluation and compensation of the three-phased grid's unbalanced operations

Controlul instrumentației virtuale pentru evaluarea și compensarea operațiunilor dezechilibrate ale rețelei trifazate

Robert Pecsi[1], Magdalena Culcea[1], Eleonora Darie[1] and Elena Sanda[1]

[1] Electric Engineering in Constructions and Building Services Department, Technical University of Civil Engineering in Bucharest, Romania

E-mail: robert.pecsi@utcb.ro; magdalena.culcea@utcb.ro; elena.sanda@utcb.ro

DOI: 10.37789/rjce.2023.14.4.2

Abstract. *The unbalanced operation of the three-phase grid has a large number of negative consequences. The solution to this problem of unbalance, problem that appears whenever an unbalanced or single-phase load is connected to the network can be based either on conversion, or on compensation. Compensation based methods are capable of compensating not only the unbalanced operations, but also the non-sinusoidal and reactive operations. Former papers of the authors study the compensations methods. In this paper there is developed a LabView virtual instrument capable to calculate the unbalance factor of the grid and to control the active power filter used for compensation. The developed virtual instrument enables the activation of the compensation depending on the values of the measured and calculated unbalance factor. The method compensates the non-sinusoidal, reactive and unbalanced operations of the three-phase grid. Measurements prove the instrument's efficient operation and the method's viability.*

Key words. *Virtual instrumentation, three phased grid*

1. Introduction

The three-phase grid was designed for an operation that should be sinusoidal, direct-sequenced, nonreactive and balanced. If these objectives were easy to be obtained and maintained at the beginnings of the three-phase grid, nowadays, due to the great diversity of the single-phase loads connected to the grid, the operation is mostly non-sinusoidal, reactive and / or unbalanced. For sinusoidal operation the loads should be linear, for non-reactive operation they should be resistive (or the power factor must be compensated), and for the balanced operation the loads on the grid's three phases have to be equal.

Any unbalanced three-phase load connected to the grid, leads to an unbalanced operation, that can be considered a superposition of an inverse and a homopolar symmetrical operation on the direct symmetrical operation. The non-sinusoidal, reactive and unbalanced operations have a lot of disadvantages, like the supplementary power losses in the grid's lines, differences from the voltage rating, the too fast aging of the grid's components and of the loads connected to it. The current knowledge about the studied matter through the analysis of similar or related published work is described by the author in the former papers on this topic [1-6].

The grid's unbalance is evaluated by some unbalance factors that can be calculated as proportions between the symmetrical components of the three-phase system. There are different types of unbalance factors:

- The dissymmetry factor, defined as:

$$\xi_d = \frac{V_i}{V_d} \tag{1}$$

- The inverse sequence factor:

$$\xi_i = \frac{V_i}{V_n} \tag{2}$$

- The total unbalance factor:

$$\xi_d = \frac{V_i}{V_d}, \tag{3}$$

where the homopolar and inverse components of the three phase voltage system can be determined by the symmetrical components' method, by the following equations:

$$\begin{cases} \underline{V}_d = \frac{1}{3} \cdot \left(\underline{V}_{10} + a \cdot \underline{V}_{20} + a^2 \cdot \underline{V}_{30} \right) \\ V_i = \frac{1}{3} \cdot \left(\underline{V}_{10} + a^2 \cdot \underline{V}_{20} + a \cdot \underline{V}_{30} \right), \\ \underline{V}_h = \frac{1}{3} \cdot \left(\underline{V}_{10} + \underline{V}_{20} + \underline{V}_{30} \right) \end{cases} \tag{4}$$

where $\underline{V}_{10}$, $\underline{V}_{20}$, $\underline{V}_{30}$ are the complex images of the phase voltages, and:

$$\begin{cases} a = \cos\left(2\pi/3\right) + j \cdot \sin\left(2\pi/3\right) = -1/2 + j \cdot \sqrt{3}/2 \\ a^2 = = \cos\left(2\pi/3\right) - j \cdot \sin\left(2\pi/3\right) = -1/2 - j \cdot \sqrt{3}/2 \end{cases} \tag{5}$$

are the complex roots of the equation $\underline{z}^3 = 1$.

2. The principle and the physical unit used to compensate the unbalanced, reactive and/or non-sinusoidal operation

The authors have studied for some years and have a significant number of scientific paper and books written [1-6].

As detailed in [1], whenever connected to the grid there is an unbalanced three-phase load or a single-phase load, the balancing solution can be either the *conversion*, or the *compensation*, in such a way that the grid „feels" a balanced consumption, although the consumer is unbalanced. Conversion has the disadvantage that the entire unbalanced load-power must be handled by the conversion unit. Compensation units handle only the consumed power's difference between the phase-loads, the part of the unbalance from the entire power. These compensation unit are known as electronic active power filters. The active power filter can also be used to compensate the harmonics and the power factor of the three-phase grid.

The compensation of the unbalanced utility currents is performed by the active power filter at a really high frequency – the authors used in their measurements a frequency of 10800 Hz. The passive filter in figure 1 has the role of canceling the harmonics given by this high frequency command operation. The control unit of the active filter has to perform some operations of evaluating the unbalance, of calculating the necessary compensation currents and of building the command signal for the IGBT transistors of the voltage inverter. These necessary operations are the following:

- Measuring the actual currents of the utility (i_a, i_b, i_c), the utility voltages (u_a,u_b,u_c) and the load currents (i_{a_load},i_{b_load},i_{c_load});
- Calculating the rms values for the load currents ($\bar{I}_a$,$\bar{I}_b$,$\bar{I}_c$) and for the utility voltages ($\bar{U}_a$,$\bar{U}_b$,$\bar{U}_c$);
- Calculating the mean rms value of the utility current:

$$\bar{I}_{mean}=\frac{\bar{I}_a+\bar{I}_b+\bar{I}_c}{3} \tag{6}$$

- Calculating the phases of the utility voltages:

$$\phi_a=\frac{u_a}{\bar{U}_a},\phi_b=\frac{u_b}{\bar{U}_b},\phi_c=\frac{u_c}{\bar{U}_c} \tag{7}$$

- Calculating the reference currents of the utility, balanced currents in phase with the utility voltages that are to be obtained after the compensation:

$$i_{ax}=\bar{I}_{mean}\cdot\phi_a,i_{bx}=\bar{I}_{mean}\cdot\phi_b,i_{cx}=\bar{I}_{mean}\cdot\phi_c \tag{8}$$

- Calculating and building the command signals for the inverter transistors.

These compensation operations have already been performed and experimentally tested by the authors, what is new in this paper is the control of the compensation unit by a virtual instrument developed in LabView. The developed and tested virtual instrument allows the evaluation of the measured grid's unbalance factors, the activation of the compensation when the unbalance factor's value exceeds a certain threshold (usually the threshold values indicated by the valid and applicable regulations) and the effective control of the active power filter. The measurements performed through the

virtual instrument connected to the grid were also verified by measurements with physical measurement devices.

The following figure illustrates the active power filter used for the compensation of the unbalanced, reactive and non-sinusoidal operations. The figure does not contain the components that form the power source and the physical connection to the grid. The meaning of the symbols from this figure is explained in the following equations, with the amendment that in the figure, for the voltage there is used „U" instead of „V".

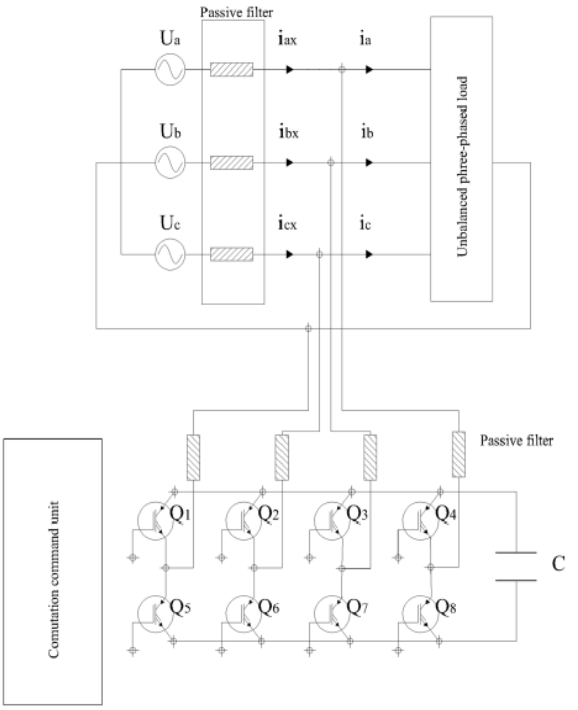

Figure 1: The active power filter used for the compensation of the unbalanced, reactive and non-sinusoidal operations.

3. The virtual instrument developed for the calculation and display of the grid's unbalance factors

The developed virtual instrument includes a part of signal acquisition, for the acquisition - with a proper frequency - of the instantaneous values of the voltages and currents from the grid lines and performs the following steps:

- The acquisition of the three voltage signals from the three-phase grid (V_{10}, V_{20}, V_{30});
- The calculation of the true rms values for each phase voltage;
- The calculation of the complex images of the phase voltages, $\left(\underline{V}_{10}, \underline{V}_{20}, \underline{V}_{30}\right)$, by using the following definition:

$$\underline{V}_x = V_x \cdot (\cos\varphi + j \cdot \sin\varphi), \tag{9}$$

For the calculation of the initial phases of the acquired voltages, we used the fact that we have the freedom to define the value of one of them the significant part being their difference:

$$\begin{cases} \varphi_{10} \equiv 0 \\ \varphi_{20} = \varphi_2 - \varphi_1 = (\omega \cdot t + \varphi_{20}) - (\omega \cdot t + \varphi_{10}) \\ \varphi_{30} = \varphi_3 - \varphi_1 = (\omega \cdot t + \varphi_{30}) - (\omega \cdot t + \varphi_{10}) \end{cases} \quad (10)$$

- The calculation of the complex images of the symmetrical components, defined by equations (4);
- The calculation of the modulus for each symmetrical component, by using the equations:

$$V = \sqrt{[\mathrm{Real}(\underline{V})]^2 + [\mathrm{Im}(\underline{V})]^2} \quad (11)$$

- The calculation of the unbalance factors with equations (1)-(3).

That part of the virtual instrument, which performs the calculation of the rms values, the initial phases and the complex images for the three voltages is illustrated (as Block diagram) in figure 2.

The following figure, 3, illustrates the synthesis of the two complex numbers (the roots of the complex equation $\underline{z}^3 - 1$.

Figure 4 shows the calculation of the symmetrical components, and the following figure 5 shows the last part of the unbalance evaluation virtual instrument, that one of calculating the unbalance factors.

The figures 2-5 illustrate the evaluation of the voltage unbalance factors. In the same way the virtual instrument evaluates the current unbalance factors, too.

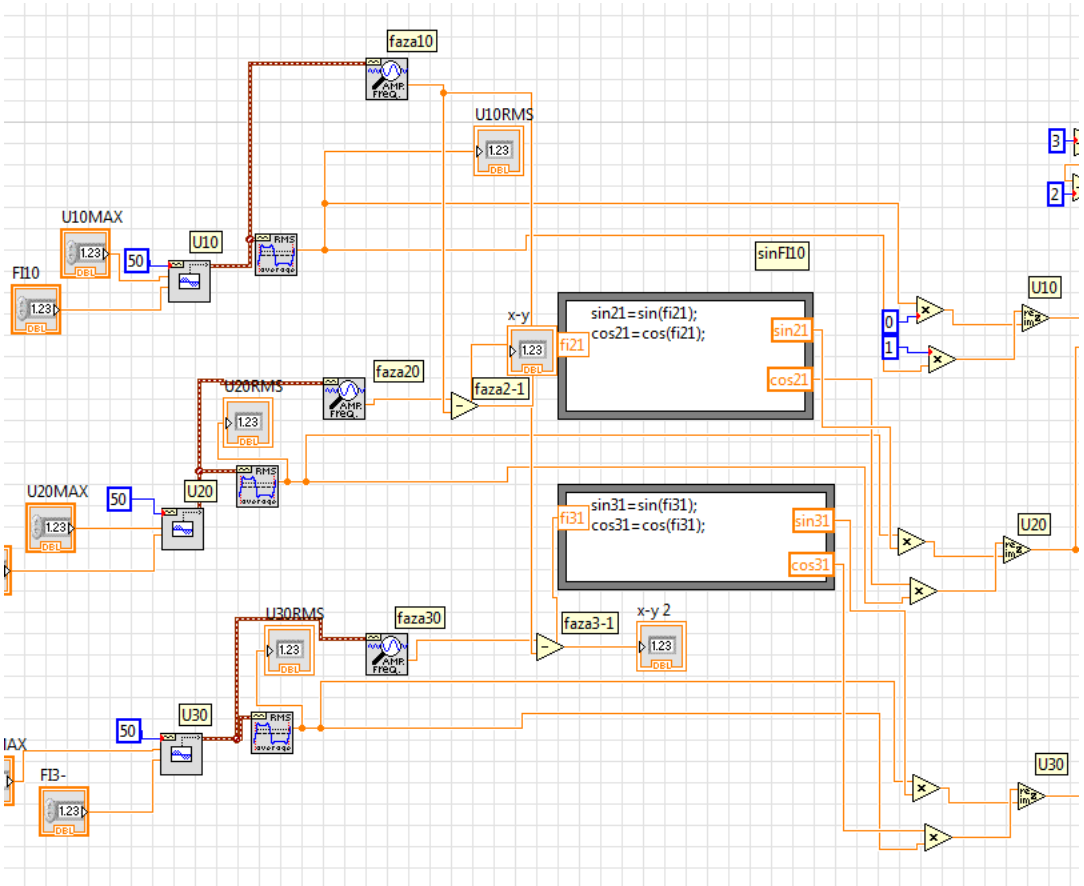

Figure 2: A first part of the unbalance evaluation virtual instrument.

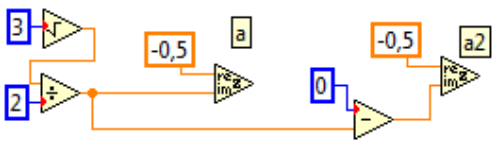

Figure 3: The synthesis of the two complex numbers a and a^2.

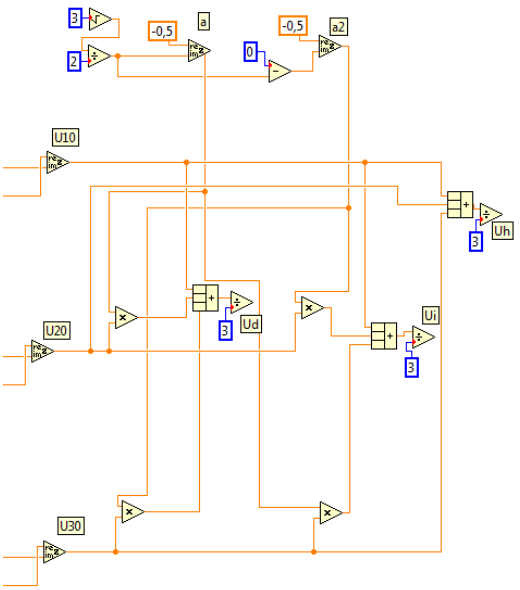

Figure 4: The calculation of the symmetrical components.

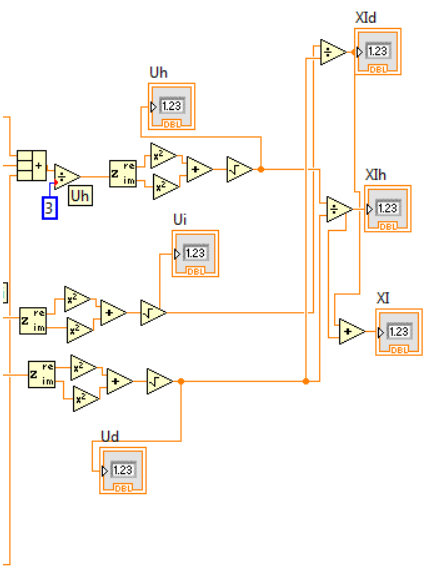

Figure 5: The last part of the unbalance evaluation virtual instrument.

4. The virtual instrument for the control of the compensation unit

This part of the virtual instrument has been developed in order to implement the steps described under point 2. After the signal acquisition of the phase lines' voltages and currents, their rms values are determined, then, the currents' mean rms value, the voltages phases and the equivalent balanced, non-reactive, sinusoidal currents are

calculated. The difference between these perfect currents and the load currents form the signal that will control the active power filter.

Although the first part – the evaluation part – of the virtual instrument performs a lot of the required operations, for the sake of modularity and of the better understanding, this control part of the virtual instrument is developed by the authors as an independent virtual instrument. Consequently, it will contain the following parts. Figure 6 illustrates the control virtual instrument – its block diagram.

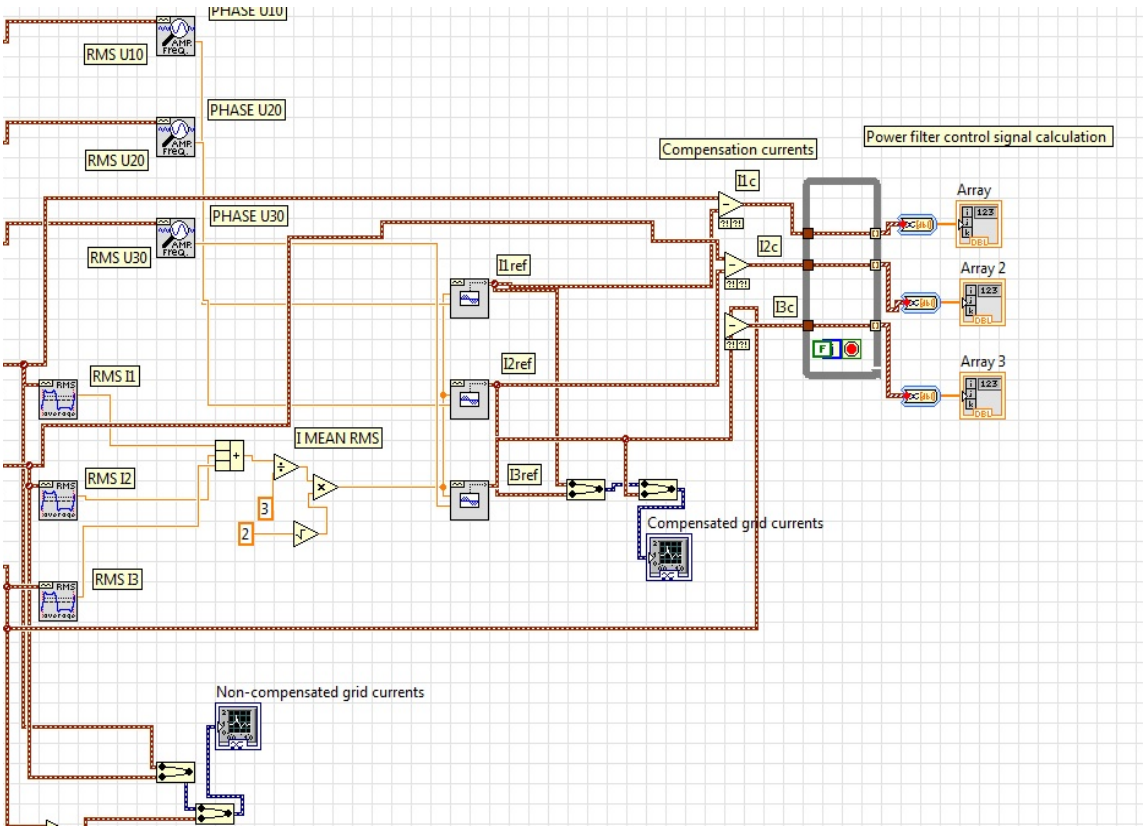

Figure 6: The compensation-control virtual instrument.

The sub-VI (virtual instrumentation subroutine) from figure 6 is integrated in the unbalance evaluation and compensation control virtual instrument inside a case structure activated by the positive result of the comparison between the unbalance factor calculated by the sub-VI presented in figure 5 and the threshold value, which can be introduced and modified by the virtual instrument's operator. For further development of this evaluation and compensation virtual instrument, it can be extended to:

- to evaluate also the power factor and to activate the compensation sub-Vi also for the exceeding of certain threshold values by this power factor (the evaluation of the non-reactive operations and the consequent activation of the compensation unit) and
- to evaluate the sinusoidal waveform of the grid's currents, by the comparison between the true rms, calculated by the evaluation sub-Vi through integration

method and the rms of the sinusoidal waveform ($I=I_{max}/\sqrt{2}$). For any significant difference between these two rms values of the same current, we can consider that there is a corresponding significant deviation from the sinusoidal waveform and that there is necessary to activate the compensation sub-VI

The active power filter controlled by this virtual instrument was tested in various load conditions and in all the measurements the results were excellent. The authors used unbalanced, reactive, non-linear loads and all the combinations between them. In every case the obtained phase currents were sinusoidal, non-reactive and balanced. Figure 7 illustrates some of the compensation results obtained with this evaluation and compensation virtual instrument.

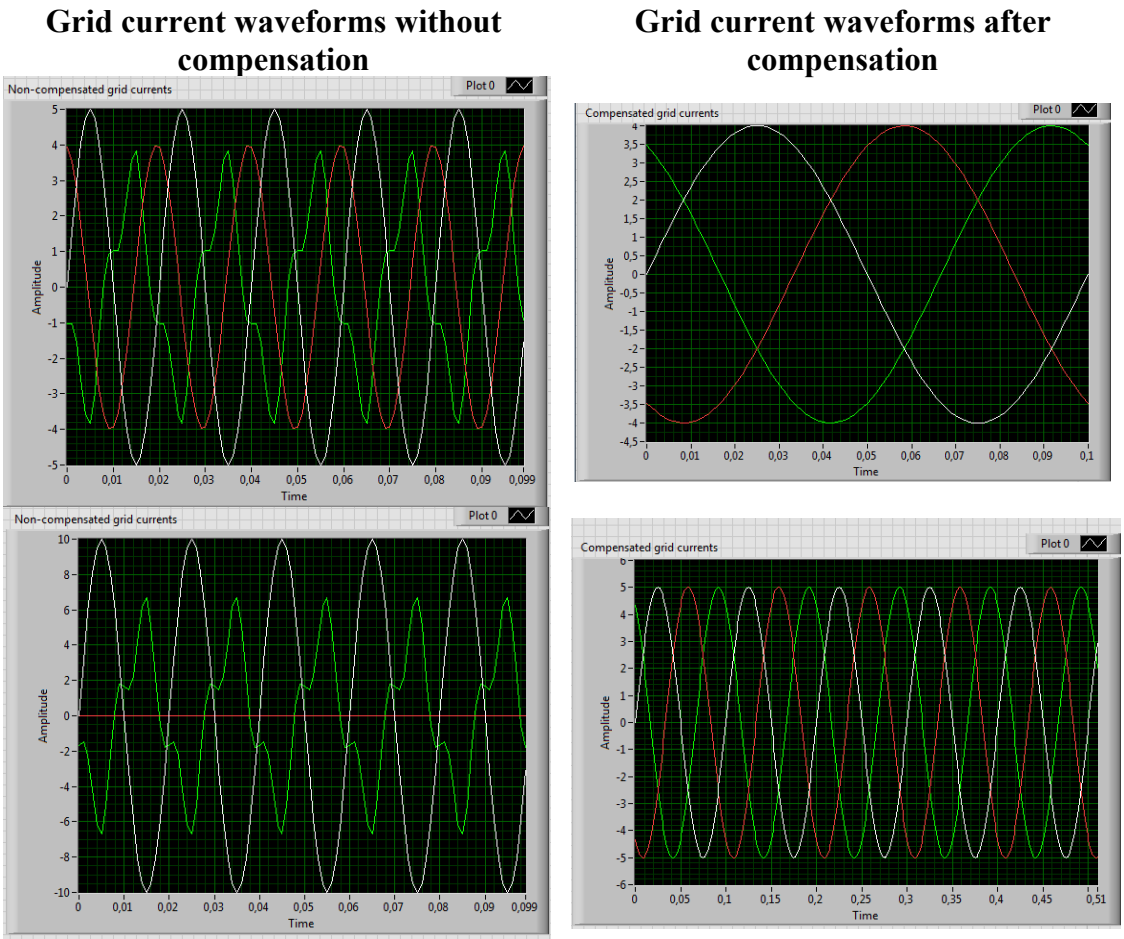

Figure 7: Some experimental results with the evaluation and compensation virtual instrument.

5. Conclusions

In conclusion we can state that the developed virtual instrument is a precise and elegant, flexible tool for the evaluation and the compensation of the unwanted operations of the three phase grid: unbalanced, nonlinear, reactive operations. Together with the active

power filter used by the authors in many measurements and balancing experiments, with the electronic control circuits and with the signal acquisition boards, the developed virtual instrument is a valuable tool [1] – [6].

The results of the measurements performed with the active power filter controlled by this virtual instrument proved very good compensation parameters. The virtual instrument enables the control al an active filter with results that are similar, identical with any other control device, physical of virtual. In fact, the results themselves prove that compensation is performed well enough, so the control of the active power filter can be done by using such a virtual instrument.

References

[1] Pecsi R 2015 Improving Energy Efficiency through Electric Utility Unbalance and Reactive Power Compensation, *Sustainable Solutions for Energy and Environment Conference*

[2] Pecsi R november 2002 Consideraţii privind efectele energetice în regimurile armonice asimetrice ale sistemelor trifazate, *Proceedings of the CIB 30.10 International Conference Transilvania University, Braşov*

[3] Pecsi R 16-17 december 2010Algoritmi de compensare a dezechilibrelor sarcinilor trifazate, *XVI National Conference for Building Machines - SINUC*,

[4] Pecsi R May 2004O metodă de compensare a dezechilibrelor din reţeaua de distribuţie a energiei electrice –*Ştiinţa Modernă şi Energia Cluj Napoca*,

[5] Pecsi R 2006 A Method And Device For Balancing A Three-Phase Power System, *Herculane International Conference*

[6] Pécsi R and Bostan V 2006 Transferul de putere între fazele reţelei realizat prin utilizarea unui filtru activ, the *Scientific Conference held by the Ploieşti University* .

[7] Măgureanu R Creangă D Ambrosi S and Bostan V May 2004 Particular Aspects of Shunt Power Active Filters Control, *Proceedings of the 9th International Conference on Optimization of Electrical and Electronic Equipment "Optim'04", Braşov*,

Geopolymer foam based on coal fly ash and metakaolin as an economic and environment friendly porous construction material

Spumă de geopolimer pe bază de cenușă zburătoare de cărbune și metacaolin ca un material de construcție poros, economic și ecologic

Lucian Paunescu[1], Bogdan-Valentin Paunescu[2], Enikő Volceanov[3,4]

[1] Cosfel Actual SRL
95-97 Calea Grivitei street, M4 room, sector 1, Bucharest 010705, Romania
E-mail: lucianpaunescu16@gmail.com

[2] Consitrans SA
56 Polona street, sector 1, Bucharest 010504, Romania
E-mail: pnscbogdan@yahoo.com

[3] University „Politehnica" of Bucharest
313 Independence Splai, sector 6, Bucharest 060042, Romania
E-mail: evolceanov@yahoo.com

[4] Metallurgical Research Institute SA
39 Mehadia street, sector 6, Bucharest 060543, Romania
E-mail: evolceanov@yahoo.com

DOI: 10.37789/rjce.2023.14.4.3

Abstract. *Geopolymer foam based on fly ash and metakaolin was designed and tested. The usual technique of activating alumino-silicate materials in a highly alkaline medium was applied, the generation of the geopolymer being favoured by developing the geopolymerization reaction. The traditional foaming agent (hydrogen peroxide) has been replaced by sodium perborate, which is more stable and easier to handle. The work originality was the use of a nanomaterial (bentonite clay), having the ability to increase the mechanical strength. Density and thermal conductivity of the new product had low values (470 kg·m^{-3} and 0.104 W·m^{-1}·K^{-1}) and compressive strength reached 7.5 MPa.*

Key words: geopolymer foam, geopolymerization, sodium perborate, nanomaterial, thermal insulating properties.

Rezumat. *O spumă de geopolimer pe bază de cenușă zburătoare și metacaolin a fost proiectată și testată. A fost aplicată tehnica uzuală de activare a materialelor aluminosilicatice în mediu înalt alcalin, generarea geopolimerului fiind favorizată prin desfășurarea reacției de geopolimerizare. Agentul tradițional de spumare (peroxid de hidrogen) a fost înlocuit cu perborat de sodiu, mai stabil și mai ușor de manipulat. Originalitatea lucrării a fost utilizarea unui nanomaterial (argilă de bentonită), având*

capacitatea creșterii rezistenței mecanice. Densitatea și conductivitatea termică ale noului produs au avut valori reduse (470 kg·m^{-3} și 0,104 W·m^{-1}·K^{-1}), iar rezistența la compresiune a atins 7,5 MPa.

Cuvinte cheie: spumă de geopolimer, geopolimerizare, perborat de sodiu, nanomaterial, proprietăți termoizolante.

1. Introduction

Under the current global conditions, in which the construction materials industry (especially cement) is strongly affected by the excessively high emissions of greenhouse gases responsible for the partial destruction of the planet's ozone layer as well as by the excessive consumption of fossil fuels [1], the use of silico-aluminous materials (natural or resulting as industrial by-products) has become a necessity. The remarkable invention of the French scientist Davidovits from the last decade of the last century created the possibility of turning this type of materials into geopolymers following the geopolymerization reaction favoured by a highly alkaline aqueous medium. Having excellent pozzolanic properties, geopolymers are suitable as construction materials with outstanding physical, thermal, mechanical, and structural characteristics [2]. According to their inventor, geopolymers are inorganic, ceramic materials based on aluminum and silicon covalently bonded, forming a three-dimensional polymer chain that includes Si-O-Al-O bonds [3]. In addition, their manufacture requires only a very low energy consumption and carbon dioxide emissions in the atmosphere are almost negligible.

Using different techniques and materials, a varied range of geopolymers was experimentally made, between very dense products with very high mechanical properties and porous products made by foaming the mixture with excellent thermal insulating properties and much lower strength. All of these are suitable for using in construction, their manufacture being economic and environmental friendly. In the current study, only the porous geopolymers forming the category of geopolymer foams were analyzed.

According to the literature [4], hydrogen peroxide (H_2O_2) is widely used in industry, having the tendency to decompose due to the instability of the hydrogen-oxygen bond. It is the most used expanding agent in the manufacturing process of fly ash-geopolymer foam, favourably influencing the thermal insulation properties (density, thermal conductivity, and porosity) of geopolymer [5]. The experiment presented in this paper included metakaolin (as a natural alumino-silicate material) and fly ash (as an industrial by-product) in a 2:1 weight ratio. The raw materials were activated with hydrated sodium silicate (Na_2SiO_3) and sodium hydroxide (NaOH) in the form of pellets dissolved in deionized water as alkaline activators [6]. Low values of thermal conductivity (below 0.107 W·m^{-1}·K^{-1}) were experimentally obtained. Also, the density of geopolymer foam had relatively low values below 560 kg·m^{-3}.

Parameters of making process of geopolymer foam based on metakaolin were experimentally optimized by Jaya et al. [7]. Thus, the optimal NaOH concentration

was established at 10M, the weight ratio of alkaline activator was limited at 1 %, and the metakaolin/alkaline activator ratio was determined at 0.8. The indicated foaming agent was H_2O_2, which together with the Tween 80 surfactant (polyethylene glycosorbitan monooleate) led to obtaining the following performances of the geopolymer foam characteristics: density within the limits of 471-1212 $kg \cdot m^{-3}$, porosity between 36-80 %, thermal conductivity in the range of 0.11-0.30 $W \cdot m^{-1} \cdot K^{-1}$, and compressive strength within the acceptable limits of 0.4-6 MPa.

Metakaolin and calcium phosphate $Ca_3(PO_4)_2$ biomass ash mixture in 1:1 weight ratio was activated with NaOH and Na_2SiO_3 solution and subjected to foaming with H_2O_2 (5 wt. %) for experimental manufacturing geopolymer foam [8]. Low values of density (310 $kg \cdot m^{-3}$) and thermal conductivity (0.073 $W \cdot m^{-1} \cdot K^{-1}$), but also a low level of compressive strength (0.6 MPa) characterized the optimal sample of geopolymer foam. Thermal-structural sandwich panel is the recommended application domain for this geopolymer.

The use of H_2O_2 as an expanding agent can create some difficulties related to the inhomogeneity of pores, which negatively influence the physical, thermal, and mechanical characteristics of geopolymer foam, according to [9]. It was found that the higher ratio of Na_2SiO_3 in the alkaline activator mixture can influence the stability of the H_2O_2 decomposition process. The open porosity observed in the geopolymer foam microstructure could be decreased from 58 to 22 vol. % by increasing the stability of the foaming process with H_2O_2. Also, the uniformity of the pore distribution is favoured, increasing from 82 to 98 % by stabilizing the same foaming process. The thermal insulation properties of metakaolin-based geopolymer foam can be improved by 16 % due to the foam homogenization. The compressive strength can be favourably influenced in the case of a more homogeneous microstructure.

According to Bai et al. [10], vegetable oil (sunflower oil, canola oil, olive oil). can successfully play the role of foam stabilizing agent. Its introduction in very low proportions (0.1-0.5 wt. %) in the manufacturing mixture of geopolymer foam together with H_2O_2 as an expanding agent allowed to obtain excellent features: density within the limits of 370-740 $kg \cdot m^{-3}$, porosity between 66-83 %, thermal conductivity in the range of 0.11-0.17 $W \cdot m^{-1} \cdot K^{-1}$, and compressive strength between 0.3-11.6 MPa. The work conclusion was that the highest ratio of vegetable oil as a stabilizer agent contributed to improving the thermal insulating properties (density, thermal conductivity, and porosity), even if the compressive strength was reduced within acceptable limits.

In the paper [11], lightweight geopolymer concrete based on class C-fly ash (with over 20 % CaO) was produced by activation of the alumina-silicate material in 12M NaOH solution by adding NaOH pellets to distilled water and Na_2SiO_3 solution (30.1 % SiO_2, 9.4 % Na_2O and 60.5 % water) with SiO_2/Na_2O molar ratio of 3.2. Polycarboxylate-based superplasticizer used as a foaming agent was added into the material mixture. Geopolymer paste obtained by mixing solid and liquid components was poured into molds and subjected to curing process in two variants: at 60 ºC and at room temperature. The measurement of the geopolymer characteristics after 1, 7, and

28 days led to the conclusion that the hot curing favoured the highest compressive strength values of a maximum of 18.2 MPa. Water absorption (1.22 vol. %) and porosity (6.78 %) were significantly decreased. Instead, the geopolymer density reached 1667 $kg \cdot m^{-3}$.

Authors of current paper previously tested the manufacture of geopolymer foam based on residual alumino-silicate materials (fly ash and old clay brick recovery from building demolition). The raw material activation was done in the highly alkaline aqueous environment consisting of NaOH and Na_2SiO_3. The foaming agent used in this experiment was H_2O_2 (1.99-3.32 wt. %). The experiment peculiarity was the addition of olive oil (0.06-0.19 wt. %) as a surfactant into the geopolymer paste. Other components of the starting mixture were expanded perlite (about 10.3 wt. %) as a siliceous additive, and fine sand (0.06-0.19 wt. %). The main geopolymer foam characteristics were: density between 420-560 $kg \cdot m^{-3}$, thermal conductivity within the limits of 0.08-0.122 $W \cdot m^{-1} \cdot K^{-1}$, porosity between 71.5-76.9 %, compressive strength in the range of 4.1-5.6 MPa, and water absorption between 3.1-3.8 vol. % [12].

Perlite, an amorphous alumino-silicate volcanic glass, is valorized as a by-product resulting from the industrial exploitation of the volcanic rock. The material containing over 70 % SiO_2 and over 13 % Al_2O_3 is in dusty state with extremely low mean particle size (below 7 μm). According to Vaou and Panias [13], perlite is suitable for its use as an alumino-silicate raw material in the manufacturing process of geopolymer. The geopolymer foam prepared from non-expanded perlite had the thermal conductivity of 0.03 $W \cdot m^{-1} \cdot K^{-1}$, compressive strength of 0.78 MPa, and maximum application temperature of 700 ºC.

Other expanding agent type used in manufacturing process of geopolymer foam based on metakaolin, according to Wattanarach et al. [14], was sodium perborate (NaH_2BO_4) between 0.5-2 wt. %. This was mixed with metakaolin and then with already known alkaline activator solution (NaOH and Na_2SiO_3) for forming a paste. The paste was poured into silicon mold for performing the curing process at 60 ºC for 24 hours, followed by keeping at room temperature for 28 days. The use of increasing weight proportion of NaH_2BO_4 had the effect of increasing the porosity from 54.7 to 67.6 % as well as decreasing the density from 1077 to 750 $kg \cdot m^{-3}$, the thermal conductivity from 0.325 to 0.218 $W \cdot m^{-1} \cdot K^{-1}$, and the compressive strength from 6.7 to 5.2 MPa. Decreasing the compressive strength is not disturbing due to the relatively high level of the strength.

Korat and Ducman [15] carried out studies on the manufacture of fly ash-based geopolymer foam by the already known method of alkaline activation using sodium perborate monohydrate (NaH_2BO_4) as a foaming agent and sodium dodecyl sulfate ($NaC_{12}H_{25}SO_4$) as a stabilizing agent, both in weight proportions between 0.9-2.8 %. The curing process was carried out at 70 ºC for 24 hours, continued with keeping the sample removed from the mold for 3 days. The results showed values of density within the limits of 330-670 $kg \cdot m^{-3}$, thermal conductivity between 0.143-0.205 $W \cdot m^{1} \cdot K^{-1}$, and compressive strength in the range of 1.02-6.33 MPa, corresponding to a fly ash with relatively low CaO content of 6.1 %.

Various types of additive ((polypropylene fiber, nano-silica, carbon nano-tubes, sodium dodecyl sulfate, rosin, sodium lauryl ether sulfate, proteins, etc.) and expanding agent (H_2O_2, NaH_2BO_4, sodium hypochlorite, etc.) can be used in manufacturing process of geopolymer foam. Organic materials (cellulose fiber, expanded perlite, etc.) are also adequate for manufacturing new environment friendly products [16, 17]. A 90/10 mixture of metakaolin and sand as alumina-silicate binder activated with aqueous solution of 8M NaOH and Na_2SiO_3 (1:2.5 weight ratio), H_2O_2 (3 wt. %) and aluminium powder (very low proportion) as foaming agents were used by Kurek et al. [16]. Expanded perlite as an additive contributed to decrease the thermal conductivity and density of the geopolymer foam. The compressive strength did not been significantly affected.

Other manufacturing technique of fly ash-geopolymer foam was tested by Phavongkham et al. [18], using Na_2SiO_3 as a foaming agent and detergent (0.1-0.5 wt. %) as a surfactant helping to increase the fineness of the geopolymer macrostructure. Thermal conductivity decreased from 0.32 to 0.27 $W \cdot m^{-1} \cdot K^{-1}$ and compressive strength reached 4.82 MPa starting from 4.21 MPa. The increase in mechanical strength is due to the 28 day-curing process. Also, the fire resistance increased due to the surfactant proportion increasing.

The paper [19] studied the effect of polypropylene fibers on thermal conductivity and mechanical properties of fly ash-geopolymer foam. Class C fly ash (with high CaO content of 14.6 %) was used as alumino-silicate raw material and NaOH and Na_2 SiO_3 solution mixture was used as an alkaline activator. The foam was prepared by mechanically mixing the surfactant Sika Poro 40 ID (produced in Indonesia) and distilled water into the foam generator. The homogenized foam was added in weight proportions of 40 and 60 % to the mixture of fly ash, fibers, and alkaline activator and mixed further for 5 min aiming at the formation of slurry. This was poured into a mold and the curing process of the fresh material was carried out at ambient temperature. The geopolymer characteristics determining was performed after 7 and 28 days. The polypropylene fibers had the effect of increasing the tensile strength (up to 1.35 MPa). Also, fibers led to increasing the thermal conductivity (0.6-0.8 $W \cdot m^{-1} \cdot K^{-1}$).

The objective of the current work is the manufacture of high-performance geopolymer foam based on a rich SiO_2 and Al_2O_3-industrial by-product of the energy industry (coal fly ash) and a widely available natural alumino-silicate material (metakaolin). The already well-known system invented by Davidovits of the activation of alumino-silicate materials in a highly alkaline liquid environment created by the combination of NaOH and Na_2SiO_3 solutions favourable for developing the geopolymerization reaction was generally kept. The technical solution originality is the addition of sunflower oil as a stabilizing agent for homogenizing the pore structure, the use of bentonite clay, a nanomaterial that has the ability to increase the mechanical strength of geopolymer as well as the replacement of the commonly used foaming agent (H_2O_2) with a more stable agent (NaH_2BO_4).

2. Methods and materials

As mentioned above, the foaming agent chosen for this experiment is sodium perborate. Through the hydrolysis of sodium perborate in contact with water, hydrogen peroxide (H_2O_2) and the tetrahydroxyborate anion $[B(OH)_4]^-$ are released [20]. More explicitly, in aqueous solution, the cyclic anion $\{[B(OH)_2OO]^2\}^{2-}$ hydrolyzes into two anions $[B(OH)_3(OOH)]^-$, which further enter into equilibrium with boric acid $B(OH)_3$, hydrogen peroxide H_2O_2, the hydroperoxyl anion OOH^-, and the tetrahydroxyborate anion $[B(OH)_4]^-$. Through the decomposition process, H_2O_2 releases molecular hydrogen and molecular oxygen in form of bubbles that contribute to expanding the mixture.

On the other hand, the conversion of alumino-silicate materials into geopolymer takes place by activating these materials in an aqueous high alkaline environment containing NaOH and Na_2SiO_3 solutions, which create appropriate conditions for the initiation and development of the geopolymerization reaction. The reaction leads to the formation of a „three-dimensional polymer chain and ring structure" including Si-O-Al-O bonds [21]. According to Provis and Rees [22], the geopolymerization is a particularly complex process, which develop in three stages, that can intersect and influence each other. Deep knowledge of the process mechanism is still difficult and its understanding requires additional research.

As in most manufacturing techniques involving solid and liquid materials, the preparation of each group of components was separately carried out in different containers. In the case of geopolymers making, it is known the recommendation on preparing the liquid mixture of the alkaline activator about 24 hours before mixing it with the solid components represented by the alumino-silicate materials (with the role of binder) and the foaming agent. The alkaline activator adopted for this experiment was composed of NaOH in the form of pellets dissolved in distilled water at a concentration of 10M and the 38 % Na_2SiO_3 aqueous solution commercially available in this state. The preparation of the alkaline activator involved the combination of the two solutions and their mechanical stirring at a rate of 1000 rpm for at least 3 min. Pouring the alkaline activator over the solid mixture and mixing them together with the supplementary addition of stabilizing agent (sunflower oil) and nanomaterial (bentonite clay) led to the formation of the geopolymer paste. The curing process of the geopolymer paste poured into metal molds of different forms and dimensions (depending on the conditions required by the device for determining the characteristics of geopolymer) took place at 80 ºC for 24 hours, followed by keeping the material removed from the molds at room temperature in a dry medium for 3 days. The testing of the geopolymer characteristics was carried out after a storage time at room temperature of 28 days.

Alumino-silicate materials adopted for experimental manufacturing process of the geopolymer foam were fly ash and metakaolin [23]. Given the considerations of the French researcher Davidovits regarding the adequate fly ash type for the geopolymerization process [3], class F fly ash (according to the ASTM C 618-12 standard), characterized by low CaO content (below 5 %) was chosen. 6-7 years ago,

Paroseni-thermal power station (Romania) supplied the companies Cosfel Actual SRL and Daily Sourcing & Research SRL with a batch of class F fly ash that was stored for future research works. The batch of fly ash came from the period of the station operation with anthracite. The chemical composition of the two mentioned alumino-silicate materials as well as of the bentonite clay nanomaterial is shown in Table 1.

Table 1

Chemical composition of alumino-silicate materials

Material	SiO_2	Al_2O_3	TiO_2	Fe_2O_3	CaO	MgO	Na_2O	K_2O	SO_3
Metakaolin	53.0	43.0	0.8	1.2	0.5	0.4	0.4	-	-
Fly ash	54.4	26.5	1.5	4.8	3.5	2.5	0.4	0.6	1.7
Bentonite clay	66.5	16.8	0.1	3.3	1.4	3.1	1.2	0.5	-

Fly ash available at a grain size below 200 μm required additional processing in a ball mill to reduce the maximum grain size limit below 40 μm. Metakaolin is commercially available as a very fine powder with a particle size of 1-2 μm. The dosing of fly ash and metakaolin was done in a 70/30 weight ratio. The foaming agent (NaH_2BO_4) as a crystalline material (more stable and easier to handle than H_2O_2) [14] was added together with the two mentioned materials in variable proportions between 0.5-2 wt. %. The mixing was done by stirring with an electric stirrer at a rate of 750 rpm for 2 min. After pouring the previously prepared alkaline activator over the solid mixture, stirring continued for 5 min, during which sunflower oil as a stabilizing agent and bentonite clay as a nanomaterial additive to increase mechanical strength were added, until the formation of the geopolymer paste.

Investigation methods for determining geopolymer foam characteristics were those presented below. The density was measured by weighing the mass with an electronic balance relating this value to that of the specimen volume [24]. The apparent porosity was determined using a vacuum saturation method [25]. Compressive strength was tested with TA.XTplus Texture Analyzer and the flexural strength was determined according to SR EN ISO 1412:2000 [26]. Immersing method under water of specimen for 24 hours (ASTM D570) was adopted to determine the water volume absorbed into the geopolymer mass. The thermal conductivity was investigated by the guarded-comparative-longitudinal heat flow method (ASTM E1225-04) and the microstructural appearance of geopolymer foam specimens was examined with ASONA 100X Zoom Smartphone Digital Microscope.

3. Results and discussion

Four experimental variants were adopted for manufacturing the geopolymer foam based on fly ash and metakaolin. The weight ratio of the two types of alumino-silicate material varied between 70.7/29.3-72.9/27.1. The alkaline activator composed of Na_2SiO_3 and NaOH solutions was designed under the conditions of 2.48 weight ratio, kept constant. The weight ratio between the total amount of alumino-silicate materials (fly ash and metakaolin) and the alkaline activator was 2.80, constant for all

variants. The additive in the form of nanomaterial (bentonite clay) had increasing values between 0.85-1.35 wt. % and the stabilizing agent (sunflower oil) had also increasing values between 0.36-1.43 wt. % (from variant 1 to variant 4). The composition of the experimental variants is shown in Table 2.

Table 2

Composition of experimental variants

Material ($kg \cdot m^{-3}$)	Variant 1	Variant 2	Variant 3	Variant 4
Fly ash	297	300	303	306
Metakaolin	123	120	117	114
Bentonite clay	5	6	7	8
10M NaOH solution	46	46	46	46
Na_2SiO_3 solution	114	114	114	114
Sodium perborate	5	7	9	11
Sunflower oil	2	4	6	8
Water addition	10	10	10	10

Determining the physical, thermal, mechanical, and morphological characteristics of geopolymer foam specimens was performed after 28 days, while the mechanical characteristics (compressive strength and flexural strength) were also measured after 7 days. The results of the measurements are presented in Table 3.

Table 3

Characteristics of geopolymer foam specimens

Characteristic	Variant 1	Variant 2	Variant 3	Variant 4
Density ($kg \cdot m^{-3}$)	516	502	487	470
Apparent porosity (%)	70.8	73.9	75.2	76.4
Thermal conductivity ($W \cdot m^{-1} \cdot K^{-1}$)	0.122	0.119	0.111	0.104
Compressive strength (MPa)				
- after 7 days	3.9	4.4	5.0	5.2
- after 28 days	6.8	7.2	7.5	7.5
Flexural strength (MPa)				
- after 7 days	2.9	2.9	3.0	3.3
- after 28 days	3.1	3.3	3.5	3.4
Water absorption (vol. %)	3.7	3.0	2.4	1.8
Pore size (mm)	0.2-0.5	0.4-0.7	0.6-0.9	0.7-1.0

According to the data in Table 3, the thermal insulating properties of geopolymer foam samples (density, thermal conductivity, and porosity) exhibit qualities suitable for this role as construction materials. Thus, the density of the porous material had values in the range of 470-516 $kg \cdot m^{-3}$, the thermal conductivity fell within excellent limits (0.104-0.122 $W \cdot m^{-1} \cdot K^{-1}$), and apparent porosity had relatively high values between 70.8-76.4 %. The density and thermal conductivity had decreasing values with the increase of the foaming agent (NaH_2BO_4) ratio from 5 to 11 $kg \cdot m^{-3}$ as well as the increase of the proportion of sunflower oil from 2 to 8 $kg \cdot m^{-3}$, although in percentage terms these values are very low (below 2 wt. %). According to the literature [10], the use of vegetable oil as a stabilizing agent contributes to

improving the thermal insulation properties and the foaming agent obviously favoured the increase of the material porosity as well as the reduction of density and thermal conductivity. Usually, having a porous structure, the geopolymer foam has quite low mechanical strength. To compensate for this disadvantage, the manufacturing recipe included a nanomaterial that contributes to increasing the concrete strength. Bentonite clay in very small amounts (5-8 $kg.m^{-3}$) was chosen in this experiment. Thus, the compressive strength had increasing values reaching 7.5 MPa after 28 days of curing and 5.2 MPa after 7 days. The flexural strength, which usually has much lower values compared to compressive strength, increased to 3.5 MPa after 28 days (3.3 MPa after 7 days), but the role of the nanomaterial was not very conclusive in this case.

Appearance images of geopolymer foam specimens are presented in Fig. 1 and microstructural pictures of these specimens are shown in Fig. 2.

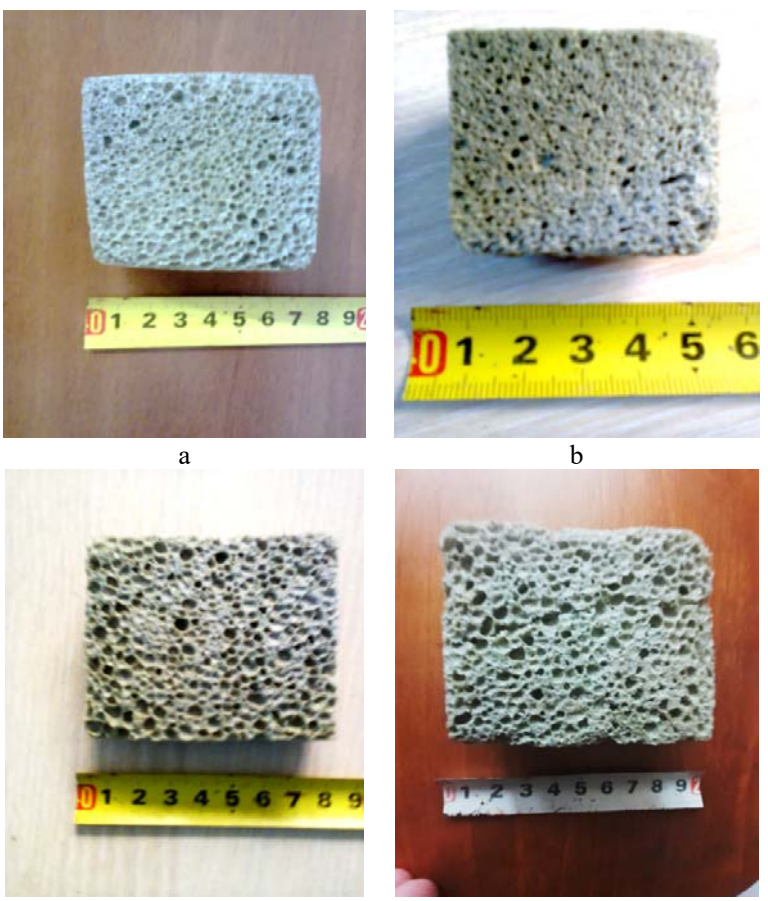

a b c d

Fig. 1. Appearance images of geopolymer foam specimens
a – variant 1; b – variant 2; c – variant 3; d – variant 4.

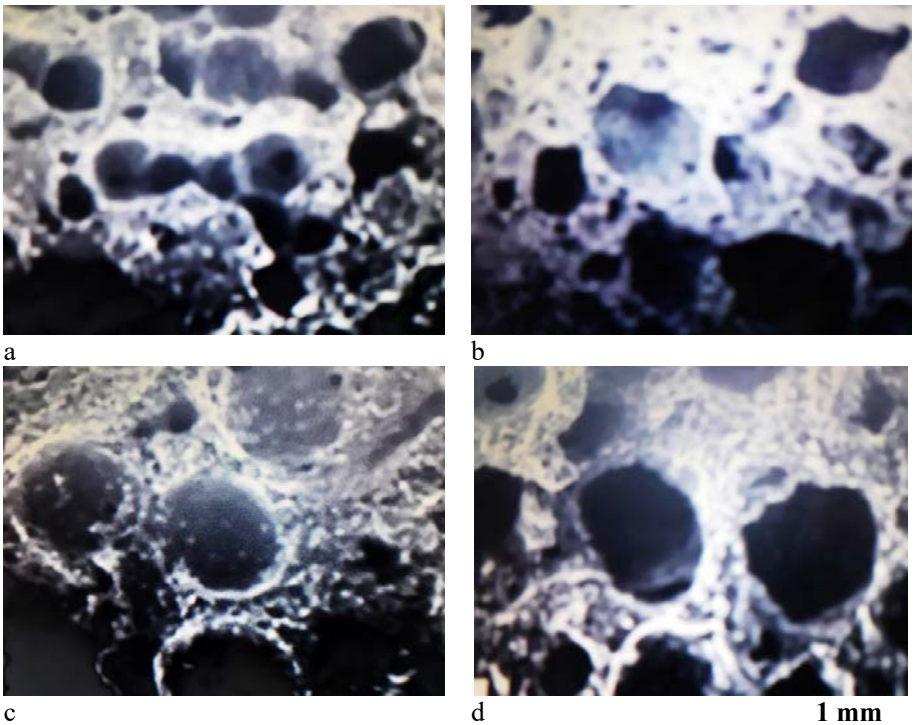

Fig. 2. Microstructural pictures of geopolymer foam specimens
a – variant 1; b – variant 2; c – variant 3; d – variant 4.

From a macro- and microstructural point of view, the porous aspect of specimens is accentuated from variant 1 to variant 4. In this experiment, a higher Na_2SiO_3/NaOH weight ratio of the alkaline activator (2.48) was adopted, which has the ability to homogenize the material pores according to the literature [9]. Fig. 2 is eloquent in terms of obtaining a microstructure with uniformly distributed pores, significantly improved compared to microstructures obtained in the case of using H_2O_2 as a foaming agent. On the other hand, according to the images in Fig. 2, the open porosity was greatly diminished. Microstructural homogenization plays an important role in improving all types of geopolymer characteristics (physical, thermal, and mechanical). The pore size had low values (below 1mm) according to the data indicated in Table 3.

4. Conclusions

Producing an economic and environment friendly geopolymer foam based on fly ash and metakaolin in 2.3-2.5 weight ratio was the research objective in this work. The basic principle of the alkaline activation of the two alumino-silicate materials in a highly alkaline aqueous medium containing NaOH and Na_2SiO_3, which created the conditions for the initiation and developing the geopolymerization reaction as well as the basic technique of the curing process of the geopolymer paste before the investigation of physical, thermal and mechanical properties of the final product were the relatively constant elements of manufacturing the foamed material. In the last two

decades, numerous methods have been tested in the world regarding the nature and amount of the used materials (additives and foaming agents) aiming to improve the properties of the geopolymer. The current work used an unusual type of foaming agent (NaH_2BO_4) as a substitute for H_2O_2, a nanomaterial (bentonite clay) not used in the manufacture of geopolymer foam, but applied in the case of concrete manufacture to increase mechanical strength, and a vegetable oil (sunflower oil) for the stabilization and homogenization of the foam. Optimum results were obtained in the case of variant 4, characterized by the highest proportions of the foaming agent and the additives mentioned above. The density of geopolymer foam had the value of 470 $kg \cdot m^{-3}$, apparent density reached 76.4 %, thermal conductivity was 0.104 $W \cdot m^{-1} \cdot K^{-1}$, compressive strength reached the maximum value after 28 days of 7.5 MPa and after 7 days of 5.2 MPa. Flexural strength had much lower values of 3.4 MPa after 28 days and 3.3 MPa after 7 days. The water absorption recorded the minimum value of 1.8 vol. % and the pore size was the highest (between 0.7-1.0 mm) compared to the other variants, but at a satisfactory level. Comparing the obtained results with those reported in the literature, the values of physical, mechanical, thermal, and microstructural characteristics are approximately at the level of those obtained in the world. The work originality is the use of nanomaterial in this process as well as replacing the usual H_2O_2 with NaH_2BO_4.

References

[1] R. A. Simmons, E. D. Coyle, „Understanding the Global Energy Crisis", Purdue University Press West Lafayette, Indiana, the United States, 2021.

[2] J. Davidovits, „Geopolymers, Inorganic Polymeric New Materials", Journal of Thermal Analysis and Calorimetry, vol. **37**, no. 8, 2008, pp. 1633-1656.

[3] J. Davidovits, „High-Alkali Cements for 21st Century Concretes", in Concrete Technology, Past, Present and Future, Proceedings of V. Mohan Malhotra Symposium, P. Kumar Metha (ed.), ACI Publisher, Detroit, Michigan, the United States, SP-144, 1994, pp. 383-397.

[4] P. Pedziwiatr, F. Mikotajczyk, D. Zawadski, K. Mikotajczyk, A. Bedka, „Decomposition of Hydrogen Peroxide-Kinetics and Review of Chosen Catalyst", Acta Innovations, no. 26, 2018, pp. 45-62.

[5] R. M. Movais, L. H. Burubberi, G. Ascensão, M. P. Scabra, J. A. Labrincha, „Porous Biomass Fly Ash-Based Geopolymers with Tailored Thermal Conductivity", Journal of Cleaner Production, vol. **119**, Elsevier Publishing, Amsterdam, The Netherlands, 2016, pp. 99-107.

[6] A. Chithambar Ganesh, M. Muthukannan, „A Review of Recent Developments of Geopolymer Concrete", International Journal of Engineering and Technology, vol. **774**, Sept. 2018. https://doi.org/10.14419/ijet.v774.5.25061

[7] N. A. Jaya, Y-M. Liew, C-Y. Heah, A. Mohd Mustafa Al Bakri, H. Kamarudin, „Correlation between Pore Structure, Compressive Strength and Thermal Conductivity of Porous Metakaolin Geopolymer", Construction and Building Materials, vol. **247**, Elsevier Publishing, Amsterdam, The Netherlands, 2020. https://doi.org/10.1016/j.combuildmat.2020.118641

[8] A. N. Muri, V. Medri, E. Papa, L. Laghi, C. Mingazzini, E. Landi, „Porous Geopolymer Insulating Core from a Metakaolin/Biomass Ash Composite", Environments, vol. **4**, 2017, pp. 86-99. https://doi.org/10.3390/environments4040086

[9] A. Hajimohammadi, T. Ngo, P. Mendis, T. Nguyen, A. Kashani, J. S. J. van Deventer, „Pore Characteristics in One-Part Mix Geopolymer Foamed by H_2O_2: The Impact of Mix Design",

Materials & Design, vol. **130**, Elsevier Publishing, Amsterdam, The Netherlands, 2017, pp. 381-391.

[10] C. Bai, T. Ni, Q. Wang, H. Li, P. Colombo, „Porosity, Mechanical and Insulating Properties of Geopolymer Foams Using Vegetable Oil as the Stabilizing Agent", Journal of the European Ceramic Society, vol. **38**, no. 2, 2018, pp. 799-805. https://doi.org/10.1016/j.jeurceramsoc.2017.09.021

[11] A. Mohd Mustafa Al Bakri, H. Kamarudin, B. Mohamed, N. I. Khairul, Y. Zarina, A. R. Rafiza, „Fly Ash-Based Geopolymer Lightweight Concrete Using Foaming Agent", International Journal of Molecular Sciences, Material Sciences Section, vol. **13**, no. 6, 2012, pp. 7186-7198. https://doi.org/10.3390/ijms13067186

[12] B. V. Paunescu, A. Ioana, L. Paunescu, „Environmental Friendly Manufacturing the Geopolymer Foam from Aluminosilicate Wastes Completely Excluding the Cement", The Bulletin of the Polytechnic Institute from Iasi, Chemistry and Chemical Engineering Section, vol. **69 (73)**, Fasc. 1 (March), 2023. (in process of publishing).

[13] V. Vaou, D. Panias, „Thermal Insulating Foamy Geopolymers from Perlite", Minerals Engineering, vol. **23**, Elsevier Publishing, Amsterdam, The Netherlands, 2010, pp.1146-1151.

[14] S. Wattanarach, S. Supothina, P. Thavorniti, „Preparation and Properties of Metakaolin-Based Porous Geopolymer Formed with Sodium Perborate", Journal of Asian Ceramic Society, vol. **10**, no. 3, 2022, pp. 567-574. https://doi.org/10.1080/21870764.2022.2088755

[15] L. Korat, V. Ducman, „ Characterization of Fly Ash Alkali Activated Foams Obtained Using Sodium Perborate Monohydrate as a Foaming Agent at Room and Elevated Temperatures", Frontiers in Materials, Structural Materials Section, vol. **7**, 2020. https://doi.org/10.3389/fmats.2020.572347

[16] I. Kurek, E. Florek, W. Gozdur, C. Ziejewska, J. Marczyk, M. Łach, K. Korniejenko, P. Duzy, „Foamed Eco-Geopolymer Modified by Perlite and Cellulose as a Construction Material for Energy-Efficient Buildings", Energies, vol. **15**, no. 12, 2022. https://doi.org/10.3390/en1512497

[17] X. Zhang, C. Bai, Y. Qiao, „Porous Geopolymer Composites: A Review", Composites Part A: Applied Science and Manufacturing, vol. **150**, 2021. https://doi.org/10.1016/j.compositesa.2021.106629

[18] V. Phavongkham, S. Wattanasiriwech, T-W. Cheng, D. Wattanasiriwech, „Effects of Surfactant on Thermo-Mechanical Behavior of Geopolymer Foam Paste Made with Sodium Perborate Foaming Agent", Construction and Building Materials, vol **243**, Elsevier Publishing, Amsterdam, The Netherlands, 2020. https://doi.org/j.conbuildmat.2020.118282

[19] N. K. A. Agostini, A. Triwiyono, D. Sulistyo, S. Suyitno, „Mechanical Properties and Thermal Conductivity of Fly Ash-Based Geopolymer Foams with Polypropylene Fibers", Applied Sciences, vol. **11**, 2021, pp. 4886-4898. https://doi.org/10.3390/app11114886

[20] B. J. Brotherton, „Boron: Inorganic Chemistry", in: Encyclopedia of Inorganic Chemistry, 2nd edition, Bruce King R. (ed.), John Wiley & Sons, New Jersey, the United States, 1994.

[21] V. C. Nguyen, D. T. Bui, V. T. Dang, „Recent research geopolymer concrete", The 3rd ACF International Conference-ACF/VCA, vol. **A.8**, pp. 235-241, Ho Chi Minh, Vietnam, Novemver 11-13, 2008.

[22] J. L. Provis, C. A. Rees, „Geopolymer Synthesis Kinetics", in: Geopolymers-Structures, Processing, Properties and Industrial Applications, Woodhead Publishing Series in: Civil and Structural Engineering, J. L. Provis and J. S. J. van Deventer (eds.), Sawston, Cambridge, UK, 2009, pp. 118-136.

[23] K. Mermerdas, M. Gesoğlu, E. Güneyisi, T. Ozturan, „Strength development of concretes incorporated with metakaolin and different types of calcined kaolins", Construction and Building Materials, vol. **37**, 2012, pp. 766-774. https://doi.org/10.1016/j.conbuildmat.2012.07.077

[24] *** „Metrology in Laboratory-Measurement of Mass and Derived Values", in: Radwag Balances and Scales, 2nd edition, Randon, Poland, 2015, pp. 72-73.

[25] E. P. Kearsley, P. J. Wainwright, „The Effect of Porosity on the Strength of Foamed Concrete", Cement and Concrete Research, vol. **32**, no. 2, pp. 233-239, Elsevier Publishing, Amsterdan, The Netherlands, 2002. https://doi.org/10.1016/S0008-8846(01)00665-2
[26] I. Curtu, A. E. Stanciu, „Determinarea Caracteristicilor Mecanice ale Epruvetelor din Material Compozit de Tip Mat&Roving", Buletinul AGIR, no. 1, 2011, pp. 78-81.

Correlations between geotechnical in situ investigations and geotechnical parameters of the Bucharest Loam layer

Corelații între încercările geotehnice de teren și parametrii geotehnici ai stratului Lutul de București

Alexandru Poenaru[1]

[1] Technical University of Civil Engineering Bucharest
Bd. Lacul Tei nr. 122 - 124, cod 020396, Sector 2, Bucureşti, România
E-mail: alexandru.poenaru13@gmail.com

Abstract. *The in situ geotechnical investigation methods are experiencing an upward trend in their use at national and international level. In the international literature there are numerous correlations between in situ tests and geotechnical parameters which have been developed mainly in Western European countries, the United States and Japan. This paper contributes to a better understanding of how to select, interpret and apply correlations between geotechnical soil parameters and in situ test results for the Bucharest Loam layer. New correlations between CPT and DMT tests and routine laboratory tests for the Bucharest Loam layer were developed.*

Key words: *Correlations, CPT, DMT, Bucharest Loam*

DOI: 10.37789/rjce.2023.14.4.4

1. Introduction

The recent national and European technical norms and standards – revision of Eurocode 7 and the Romanian technical norm on geotechnical documents, NP 074-2022 – are requiring, when using correlations for determining the geotechnical parameters based on in situ test results, to document them and provide information about the soils for which they have been developed and the correlation degree. In the national literature, there are certain correlations for specific Romanian soils, but their number is limited. Also, a good part of them were determined a few decades ago [1]. The limited existence of "national" correlations leads to the under- or improper use of field tests and to an excess or lack of caution in establishing characteristic and calculation values of geotechnical parameters. In order to increase the use of in situ tests in the Romanian practice and to have a proper interpretation of them, there is a need for new developed correlations for specific type of soils.

The main original contribution of the present paper is the determination of new correlations between in situ CPT and DMT tests and the usual laboratory tests for Bucharest Loam layer. On the basis of the literature review, an extensive investigation of the soil was carried out, including in situ investigations and geotechnical boreholes. Laboratory tests to determine geotechnical parameters were carried out on disturbed and undisturbed soil samples obtained from geotechnical boreholes. Parallel analysis of the geotechnical parameters obtained using the newly determined correlations and separately using laboratory tests helped to validate the proposed correlations. A total of 22 sites located in the North, South, Center, West and East of Bucharest were investigated. The table below summarizes the investigated sites and the investigations carried out for each of them.

Table 1

Investigated sites

Site nr.	Area	Address	Boreholes	CPT	DMT
1.	C-S	Splaiul Unirii 165	7	10	5
2.	N	Calea Floreasca 246	3	2	1
3.	N	Nicolae G. Caranfil 74	2	3	2
4.	S	Strada Povestei 10	3	12	3
5.	NV	Bulevardul Bucureștii Noi 25	6	7	2
6.	E	Șos. Vergului 4	2	2	2
7.	C-V	Șoseaua Orhideelor 46	4	3	-
8.	N	Str. Barbu Văcărescu 164	4	9	2
9.	N	Calea Floreasca 242-244	6	18	3
10.	C	Tudor Arghezi 1-3	5	3	1
11.	C-V	Strada Sg Constantin Ghercu 1b	4	5	5
12.	N	Bulevardul Pipera 1/8, Voluntari	13	-	4
13.	N-NV	Strada Menuetului Nr. 8	2	-	-
14.	E	Șos. Vergului 20	2	-	1
15.	C	Strada Logofăt Luca Stroici 45	2	-	-
16.	N-NE	Bulevardul Dimitrie Pompeiu 2D	1	-	-
17.	N-NV	Strada Jiului nr. 10	2	7	1
18.	C-E	Șoseaua Mihai Bravu nr. 321	2	-	-
19.	C-N	Bulevardul Mircea Eliade nr. 18	7	-	-

Site nr.	Area	Address	Boreholes	CPT	DMT
20.	C	Strada Mântuleasa nr. 10-18	2	3	-
21.	NV	Bd. Expoziției nr. 2	-	3	1
22.	V	Bd. Preciziei nr. 6	-	3	1

Reviewing the information in Table 1 a total of 79 boreholes, 88 CPT (Cone Penetration Tests) and no less than 34 DMT (Dilatometer Marchetti Tests) were analyzed to determine the new correlations.

2. Selection process of relevant high-quality samples

To achieve the objectives of this research a laborious selection process in order to select high-quality samples was necessary.

The following in-situ and laboratory tests were used to determine new correlations:

- Cone Penetration Tests (CPT)
- Dilatometer Marchetti Tests (DMT)
- Geotechnical Boreholes
- Laboratory tests for identification and classification of soils
- Mechanical laboratory tests

The sample selection steps are detailed below.

Step 0 consisted of the pre-selection of sites. Before starting the actual process of selecting the different laboratory samples or in situ tests, sites with a typical stratification for the Municipality of Bucharest were selected. For example, sites that have been subject to extensive changes in the recent past were excluded. The following were considered as significant changes: the site has been subject to pollution with hydrocarbons or other liquids \ materials that may affect the geotechnical characteristics or the bearing capacity, land on which excavations and fills have been carried out.

Step 1 of the actual screening process consisted in the selection of investigation points (geotechnical borehole, CPT and DMT tests) that could fit into a circle with a radius of no more than 3 m. The 3 m criterion was chosen because, for technological reasons, it is sometimes not possible to set points closer than 1.5 m without influencing each other. The distance of 1.5 m was chosen assuming that the test/survey deviates less than 1°/m from the vertical position. This is also the rejection criterion for DMT equipment and can also be assimilated with the rejection criterion for CPT equipment, if an average survey depth of 25 m and a maximum allowable inclination of 25° are considered.

In Step 2 geotechnical profiles were created and analyzed. The geotechnical profiles included, as a minimum, the geotechnical borehole log with stratification description and field test plots, as well as tests not covered by this report. This allowed for the removal of tests that showed anomalies compared to the other 2 corresponding

tests. As an example, if the laboratory tests corresponding to a geotechnical borehole in the vicinity of the CPT/DMT tests showed significantly lower or significantly higher modulus values than the other boreholes on site, while the CPT/DMT tests showed similar values, the borehole or sample was eliminated from the analysis.

Step 3 consisted of eliminating laboratory and field tests with implausible values. For example, if a laboratory compressibility test showed a modulus $E_{oed\ 0\text{-}50}$ higher than $E_{oed200\text{-}300}$, the test was eliminated. Another example of eliminated samples due to implausible values are those in which the oedometric modulus corresponding to 200-300 kPa was higher than 30-40 MPa or q_c values higher than 5 MPa for Bucharest Loam. These values are outside the range of variation of the respective parameters. On top of that, the Bucharest Loam layer is a cohesive soil with a consistency ranging from stiff to hard. Values of $E_{oed200\text{-}300}$ higher than 30-40 MPa for q_c above 5 MPa are not typical.

3. Determination of new correlations for the Bucharest Loam layer

The following linear correlations were determined:

- Between cone resistance q_c and oedometric modulus $E_{oed200\text{-}300}$
- Between cone resistance q_c and dilatometer modulus M_{DMT}
- Between dilatometer modulus M_{DMT} and oedometric modulus $E_{oed200\text{-}300}$
- Between q_c and undrained shear resistance determined from DMT $c_{u,\ DMT}$

The "Bucharest Loam" layer has, probably, the most important contribution in the design of geotechnical structures in the Bucharest area. It develops immediately below the topsoil layer and down to depths of about 6 - 10 m usually, and in some areas, it can reach depths of approx. 20 m.

In terms of particle size distribution, the Bucharest Loam consists of silty clays to clayey silts and sandy clays with a slight loess character. According to SR EN ISO 14688-1 and 2, the soil can be predominantly classified as siCL (silty clay) and Cl (clay), less frequently as clSi (clayey silt). Rarely it may contain up to 5% gravel-sized particles, which can be observed especially in the central-southern part of the municipality.

The correlations that have been developed specifically for the Bucharest Loam layer are presented below. These were developed using the geotechnical parameters obtained from laboratory tests and those obtained directly from field or in situ tests and surveys.

To determine the correlations in situ investigations were performed. They consisted of Cone Penetration Tests (CPT) and Dilatometer Marchetti Tests (DMT). Common laboratory tests were also performed. Those were classification and identification tests as sieve analysis and Atterberg limits. Mechanical laboratory tests were also performed. They consisted of Direct Shear Test and Oedometer Tests.

Figure 1 shows the correlations between the cone resistance q_c and the oedometric modulus $E_{oed200\text{-}300}$. The correlations were determined on all available

samples (blue dots and line). During pre-screening a good correlation was observed for samples with a fine particle content (<0.063 mm) greater than 90%. For these samples another correlation was determined separately (red dots and line). The correlation factor r^2 was 0,75 and 0,99.

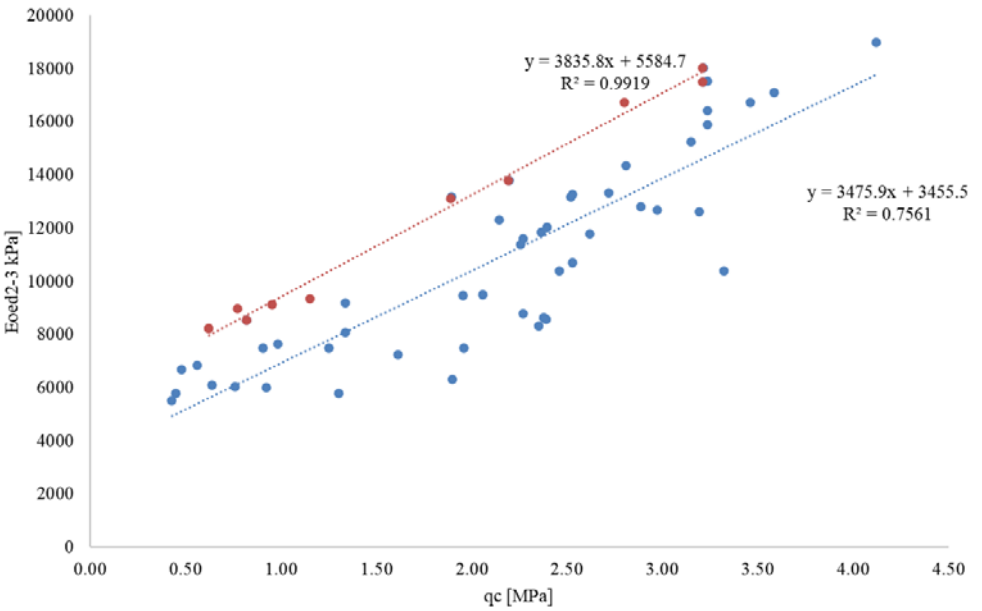

Fig. 1. Correlations between cone resistance qc and oedometric modulus $E_{oed200-300}$

In Figure 2 is presented the newly determined correlation between cone pressure q_c and M_{DMT} dilatometric modulus. The correlation was determined for 40 high quality samples. In this case a correlation coefficient of approx.. 0,85 was obtained.

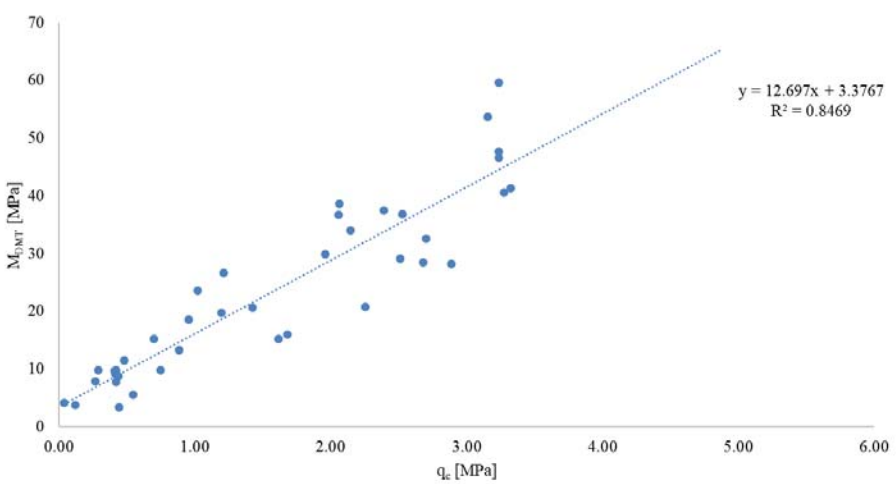

Fig. 2. Correlations between cone resistance q_c and dilatometer modulus M_{DMT}

Cone pressure q_c and undrained shear strength determined using DMT were correlated using a approximately 40 samples. As shown in Figure 3 a correlation coefficient of approx.. 0,70 was obtained.

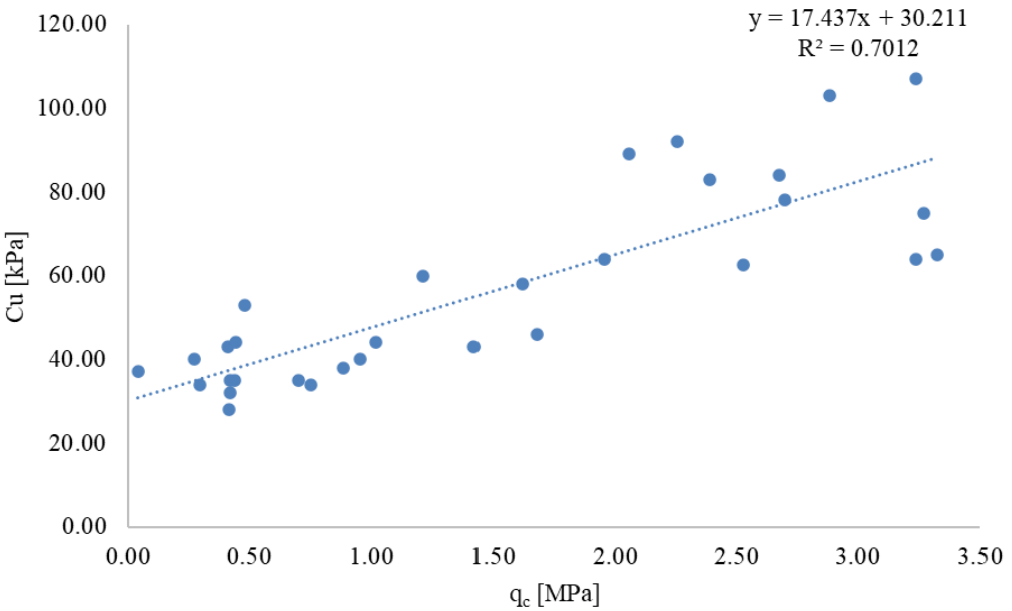

Fig. 3. Correlations between cone resistance q_c and undrained shear strength $c_{u\ DMT}$

The dilatometric modulus and the $E_{oed200\text{-}300}$ oedometric modulus were correlated using 38 common points. As shown in Figure 4, a correlation coefficient of $r^2 = 0{,}58$ was obtained, which corresponds to a correlation coefficient r of approximately 0,70.

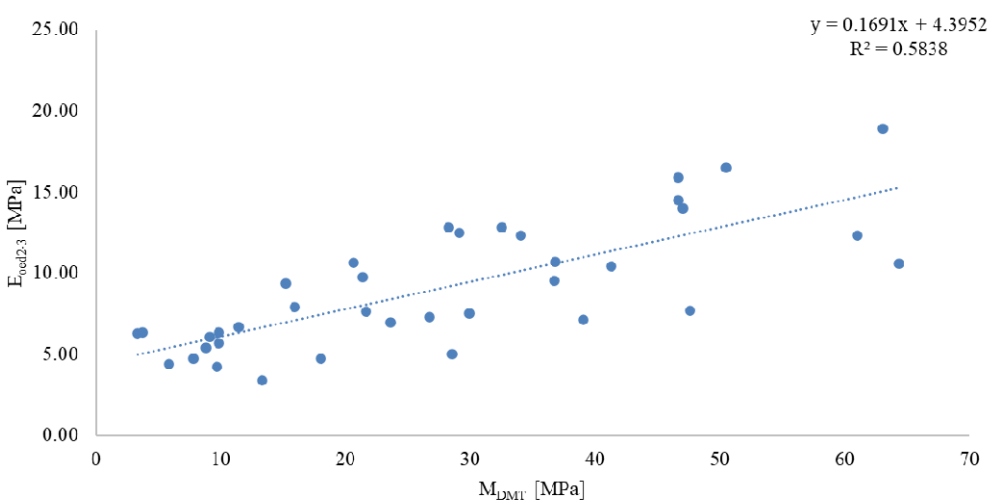

Fig. 4. Correlations between the dilatometer modulus M_{DMT} and the oedometric modulus $E_{oed200\text{-}300}$

Figure 5 shows the correlation between the cone pressure q_c and the tangent of the internal friction angle φ, determined using 20 points . The correlation coefficient r^2 is of about 0.70.

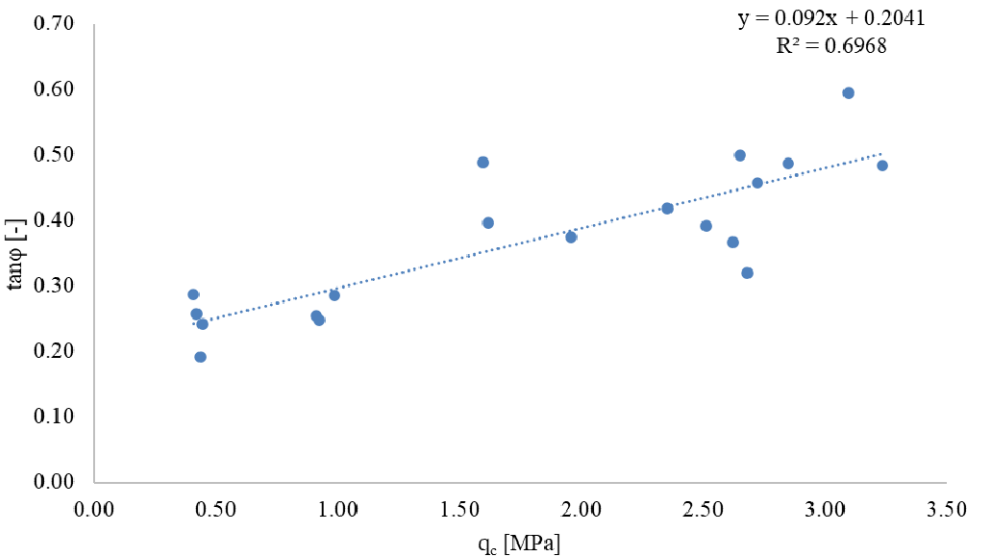

Fig. 5. Correlations between cone resistance q_c and the internal friction angle φ

Figure 6 shows the correlation of the cone pressure q_c and the cohesion c obtained from the shear box tests under natural moisture content and undrained conditions (CUn). 20 points were used in determining the correlation. The correlation coefficient is about $r^2 = 0,67$, respectively $r = 0,85$.

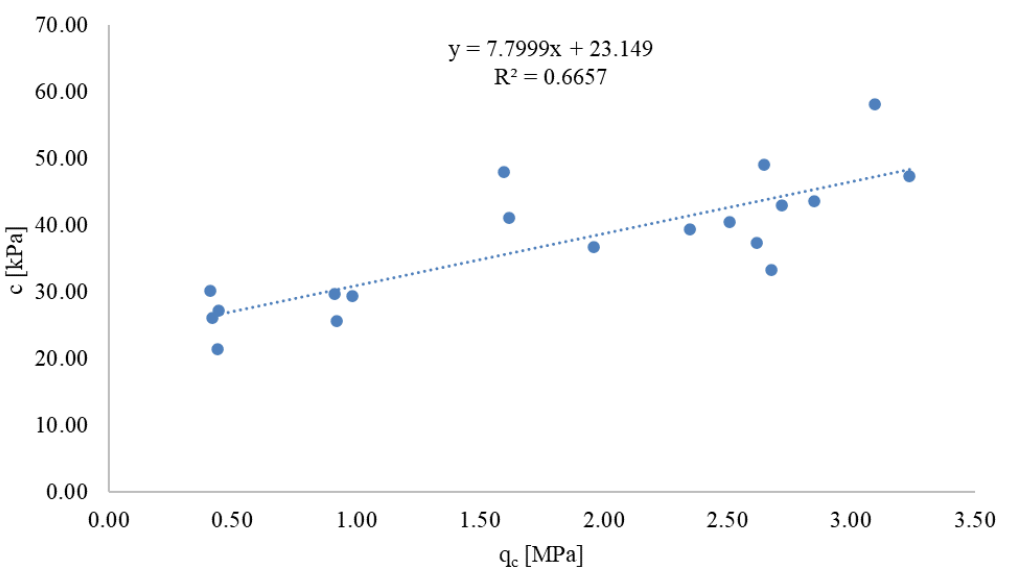

Fig. 6. Correlations between cone resistance q_c and the cohesion c

The correlations between the different parameters presented in Fig. 1 to Fig. 6 are summarized in the following table. The safe correlation gives an assured value and involves translating the correlation slope by the value of the standard deviation.

Table 2

New correlations between different soil parameters specific to Bucharest Loam

Parameters	New correlations	Correlation coef.	Nr. of Samples	Standard deviations	Safe correlation
q_c vs. $E_{oed}2$-3	3476 q_c + 3456 kPa	0,870	50	300 kPa	3476 q_c + 3156 kPa
q_c vs. $E_{oed}2$-3*	3836 q_c + 5584 kPa	0.996	10	122 kPa	3836 q_c + 5462 kPa
q_c vs. tanφ	0,092 qc + 0,204	0,834	20	0,015	0,092 qc + 0,189
q_c vs. c	7,8 qc + 23 kPa	0,816	20	1,35 kPa	7,8 qc + 21 kPa
q_c vs. M_{DMT}	12,7 q_c + 3,4 MPa	0,920	40	0,88 MPa	12,7 q_c + 2,5 MPa
q_c vs. $c_{u,DMT}$	14,4 q_c + 30 kPa	0,837	32	2,11 kPa	14,4 q_c + 28 kPa
M_{DMT} vs $E_{oed200-300}$	0,17 M_{DMT} + 4,4 MPa	0,764	38	1,7 MPa	0,17 M_{DMT} + 2,7 MPa

*Samples with over 90% fine particles (<0,063 mm)

4. Validation of the new correlations

This chapter aims to validate the new correlations proposed in chapter 3. To this end, in order to be able to analyze the validity of the new correlations, they were compared with some well-established correlations available in the literature. The main aim of the present paper is to obtain new correlations specific to the Bucharest area. Since the field and laboratory tests carried out, as well as the processing methods, are similar to those from which the existing correlations were obtained, the new correlations are practically a calibration of the existing correlations for the specific soils of the Bucharest area.

Table 3

New and literature correlations for the deformation modulus for the Bucharest Loam layer

Parameter	Deformation modulus E		
	Correlation	Soil type	Observations
New correlation	$E_{oed200-300}$ = 3,48 q_c + 3,45	Cohesive soil	Oedometric modulus between 200 and 300 kPa vertical stress
New safe correlation	$E_{oed200-300}$ = 3,48 q_c + 3,15	Cohesive soil	Oedometric modulus between 200 and 300 kPa vertical stress
Marcu, 1983 [1]	E = 4,8 q_c	Cohesive soil	In this case E can be approx. with $E_{oed200-300}$

Figure 7 shows the theoretical values (linear variation) of the deformation modulus E for the Bucharest loam layer that can be assigned to a value of q_c ranging from 0.5 to 4 MPa using the new proposed correlations and the literature ones [1]. The area shaded in green represents the range of values corresponding to a 95% confidence level of the deformation modulus determined for the Bucharest Loam soil [2]. By analyzing the graph, a good fit between the new proposed correlation and the one known from the literature can be observed [1]. Considering the information presented in [1], the correlation available in the literature is affected by a safety coefficient, which leads to more conservative values. It should be noted, however, that literature correlations [1] better covers the range of values of the deformation moduli [2]. This may be due to the determination of the correlation in [1] between q_c and the deformation modulus determined with the static loading plate and not the one determined in the laboratory, as is the case for the current correlation.

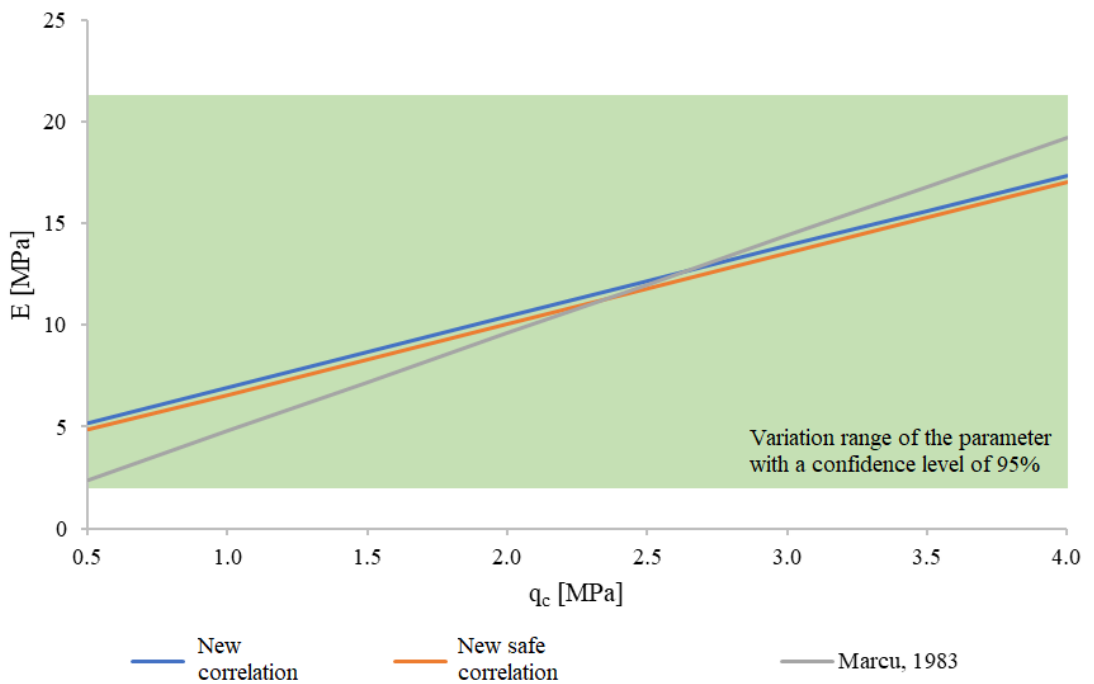

Fig. 7. Bucharest Loam layer, comparison of results for the proposed correlation and those in the literature for deformation modulus E

Table 4 presents the new correlations determined as described above. The shear parameters from Table 4 and Table 5 correspond to those determined by shear box tests on samples with natural moisture content and sheared in undrained conditions.

Table 4

New and literature correlations for the friction angle φ for the Bucharest Loam layer

Parameter	Friction angle		
	Correlation	Soil type	Observations
New correlation	$\tan\varphi = 0{,}092\ q_c + 0{,}204$	Cohesive soils	tanφ determined using direct shear test CUn
New safe correlation	$\tan\varphi = 0{,}092\ q_c + 0{,}189$	Cohesive soils	tanφ determined using direct shear CUn
Trofimenkov & Vorobkov, 1974 [3]	$\tan\varphi = 0{,}045\ q_c + 0{,}260$	Cohesive soils	-

Figure 8 shows the theoretical values (linear variation) of the tangent of the internal friction angle for the Bucharest Loam layer that can be assigned to a cone pressure q_c ranging from 0.5 to 4 MPa, using the new proposed correlations and those available in the literature [3]. The analyzed q_c values represent typical values for the Bucharest Loam layer. The area hatched in green represents the range corresponding to a 95% confidence level of the tangent of the angle of internal friction determined in [2]. By analyzing the graph, a similarity can be observed between the new correlation and the one known from the literature [3].

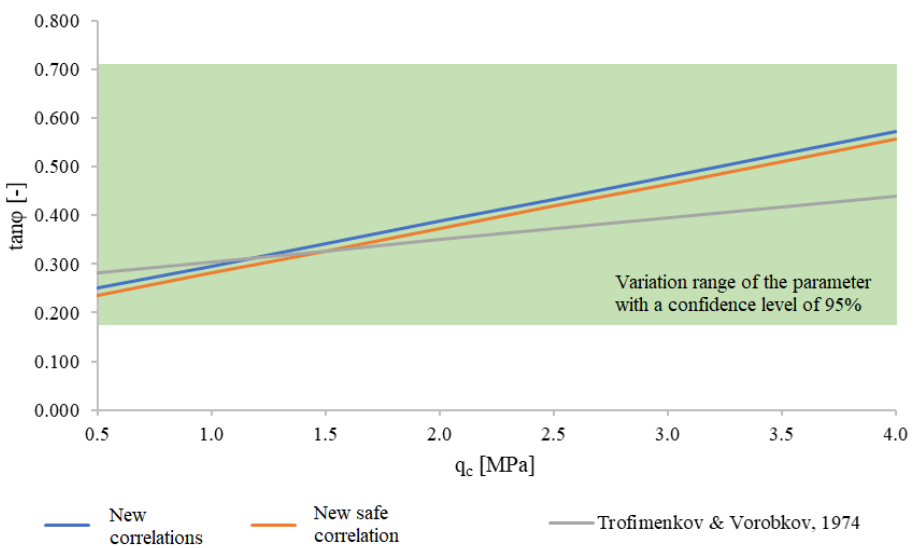

Fig. 8. Bucharest Loam, comparison of results for new correlations and literature correlations for internal friction angle φ

The new proposed correlation tends to underestimate the values of the tangent of the internal friction angle for q_c values below 1.25 MPa and to overestimate the same value for q_c higher than 1.25 MPa, in comparison with the correlation proposed by [3]. Given the information presented in [1], the correlation in the literature [3] is affected by a certain safety coefficient, which is however not known, leading to more

conservative values. Even in comparison with the new safe correlation, when using correlation [3] more conservative parameters are obtained. However, the proposed correlation better covers the range of usual values of the Bucharest Loam layer. The differences between the new and existing correlations can be explained by the fact that the new correlations are optimized for the Bucharest Loam layer.

Table 5 shows the new proposed correlations and the correlations from the literature [3] for the indirect determination of cohesion. In the case of the present paper the new proposed correlation corresponds to the cohesion obtained from the shear box test on sample at natural water content in CU conditions (CUn).

Table 5

New and literature correlations for the cohesion for the Bucharest Loam layer

Parameter	Cohesion c (kPa)		
	Correlation	Soil type	Observations
New correlation	$c = 0{,}078\ q_c + 0{,}023$	Cohesive soils	c determined using direct shear CUn
New safe correlation	$c = 0{,}078\ q_c + 0{,}021$	Cohesive soils	c determined using direct shear CUn
Trofimenkov & Vorobkov, 1974 [3]	$c = 0{,}0116\ q_c + 0{,}0125$	Cohesive soils	-

Fig. 9 shows the typical cohesion range values for the Bucharest Loam layer that can be assigned to cone pressure values q_c ranging from 0.5 to 4 MPa using the new proposed and the literature correlations. It should be noted that all correlations underestimate the cohesion value which leads to conservative results.

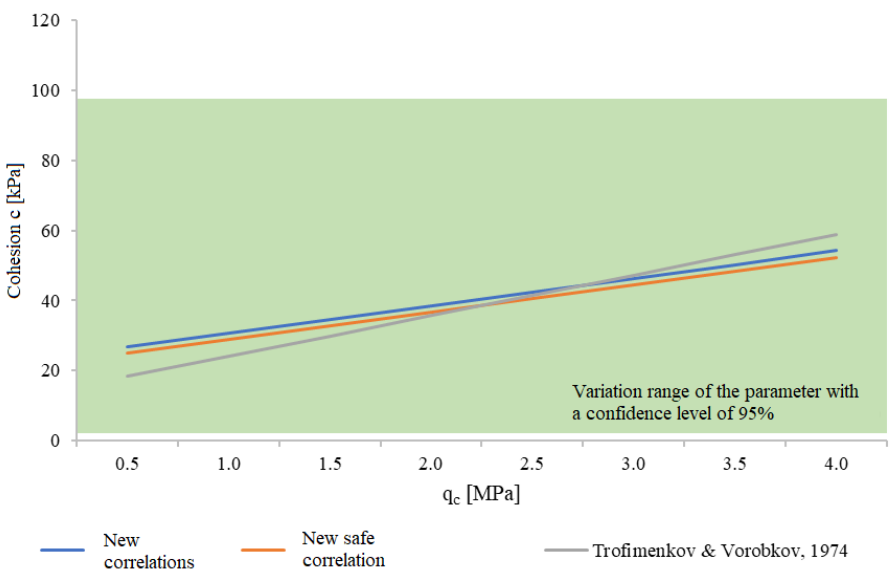

Fig. 9. Bucharest Loam, comparison of results for new correlations and literature correlations for cohesion c

For q_c values lower than 1 MPa the correlations tend to overestimate the cohesion value.

6. Conclusions

In the present paper new correlations between the geotechnical parameters of the Bucharest Loam layer and the in situ geotechnical investigations have been proposed. Correlations were obtained by comparing the results of the in-situ investigations with the geotechnical laboratory results. The newly proposed correlations were validated by comparing their results with those obtained using correlations available in the literature and currently used [1],[3]. Thus, it can be concluded that the newly proposed correlations better cover the range of variation of the studied parameters compared to the parameters obtained using correlations from the literature [1],[3]. Using the newly proposed correlations in the current geotechnical design can lead to an optimized design of the foundations and deep excavation support systems in Bucharest area.

References

[1] *A. Marcu*, Fundații speciale. Cercetarea terenului de fundare și determinarea caracteristicilor geotehnice de calcul. Institutul de Construcții București, 1983
[2] *A. Poenaru*, Variația parametrilor geotehnici în zona municipiului București, a XIV-a Conferință Națională de Geotehnică și fundații – București 2-3 iunie 2021, pp. 193 – 200, Printech, București, 2021
[3] *I. Trofimenkov, L. Vorobkov*, Polevie metodi issledovania stritelnih svoistv gruntov. Gosetroiizdat, Moskva, 1974

Thermal analysis of storage tank PCM

Analiza termică a unui rezervor de stocare

Emilian-Florin Țurcanu[1], Vasilică Ciocan[1], Nelu-Cristian Chereches[1], Sebastian-Valeriu Hudișteanu[1], Ana Diana Ancas[1], Verdeș Marina[1], Cătălin-George Popovici[1]

[1] Technical University "Ghe. Asachi" of Iasi, Faculty of Civil Engineering and Building Services, Department Building Services, D. Mangeron 67 str., 700050, Romania,
E-mail: florin-emilian.turcanu@academic.tuiasi.ro

DOI: 10.37789/rjce.2023.14.4.5

Abstract. *In this research, we investigate the thermal behavior of storage tanks subjected to varying environmental conditions. Through numerical simulations and experimental analysis, we assess heat transfer mechanisms, temperature distribution, and energy consumption patterns of both insulated and non-insulated tanks. Our study aims to optimize tank design and insulation materials to minimize heat losses, improve energy efficiency, and enhance the safety and longevity of storage tanks. Findings reveal that incorporating optimal insulation materials and techniques can significantly reduce energy consumption and maintain the desired temperature range within the tank, thus providing valuable insights for future storage tank design and management.*

Keywords: Phase Change Materials (PCMs), Thermal energy storage, Computational Fluid Dynamics (CFD), Temperature distribution, Design optimization

1. Introduction

The increasing global demand for energy and the need to reduce greenhouse gas emissions have increased interest in efficient energy storage and management systems. Phase change materials (PCMs) have emerged as a promising solution for thermal energy storage due to their ability to store and release large amounts of latent heat during phase transitions, such as melting and solidification. In storage tanks, incorporating PCMs can significantly improve thermal performance, reduce energy consumption, and maintain temperature stability.[1, 2]

This research article focuses on the thermal analysis of storage tanks integrated with PCMs, aiming to optimize their design and enhance energy efficiency. The application of PCMs in storage tanks can have a wide range of benefits in various sectors, including solar thermal systems, building energy management, and industrial processes. To fully exploit the potential of PCMs in these applications, it is essential to understand the

complex heat transfer mechanisms, temperature distribution, and phase change dynamics within the storage tank. [3, 4]

Phase change materials (PCMs) have gained significant attention in recent years due to their high latent heat storage capacity and the ability to maintain a nearly constant temperature during phase transitions. Several types of PCMs, including organic, inorganic, and eutectic mixtures, have been investigated for thermal energy storage applications. Organic PCMs, such as paraffin waxes and fatty acids, are favored for their high energy density, low supercooling, and chemical stability. Inorganic PCMs, such as salt hydrates and metal alloys, offer high thermal conductivity and heat storage capacity but may experience phase segregation and subcooling issues. [5 ,6]

To improve the performance of PCM-based storage tanks, researchers have explored various techniques, such as using encapsulated PCMs, finned structures, and nanoparticle-enhanced PCMs (NEPCMs). Encapsulation enhances heat transfer and reduces the risk of leakage, while finned structures increase the surface area for heat exchange, improving the charging and discharging processes. NEPCMs, formed by dispersing nanoparticles into the base PCM, exhibit enhanced thermal conductivity and can reduce the charging/discharging time of the storage tank. [7, 8]

Computational Fluid Dynamics (CFD) analysis is a valuable tool for studying the complex heat transfer and phase change dynamics in PCM-based storage tanks. By solving the governing equations for mass, momentum, and energy conservation, CFD can predict temperature distribution, fluid flow patterns, and phase change rates within the tank. Researchers have employed CFD to optimize the design of storage tanks, investigate the influence of PCM properties, and develop effective control strategies for various applications. [9]

2. Material and method

In this study, we will conduct a comprehensive analysis of the thermal behavior of storage tanks containing PCMs by employing numerical simulations, experimental investigations, and analytical modeling. We will explore various factors that influence the performance of PCM-based storage tanks, such as PCM selection, tank geometry, and insulation materials. Moreover, we will evaluate the effect of different operating conditions on the thermal performance and energy efficiency of these systems.

The findings of this research will provide valuable insights into the design and optimization of PCM-based storage tanks and contribute to the development of more sustainable and efficient energy storage solutions. This work will address the current challenges in the field of thermal energy storage but also pave the way for the widespread adoption of PCM technology in various applications.

In this study, we will utilize CFD analysis to model the thermal behavior of PCM-based storage tanks under various operating conditions. We will employ the enthalpy-porosity method, which accounts for the latent heat associated with phase change and the varying porosity of the PCM during melting and solidification. The CFD simulations will be validated against experimental data to ensure the accuracy and reliability of the model.

The CFD analysis will provide insights into the temperature distribution, melting/solidification front progression, and the effect of PCM properties on the overall performance of the storage tank. Moreover, we will investigate the impact of different tank geometries, encapsulation techniques, and heat exchanger configurations on the thermal performance and energy efficiency of the system.
Through the CFD analysis, we aim to identify the optimal design parameters and operating conditions that maximize the energy storage capacity and minimize the energy losses in PCM-based storage tanks. The outcomes of this study will contribute to the advancement of PCM technology and its integration into various energy storage applications, promoting sustainable and efficient energy management solutions.
The 3-D domain of this simulation has been designed in ANSYS Design Modeler. Domain has an inlet and outlet and a wall for PCMs. (Figure 1)
The meshing of this present model has been generated by ANSYS Meshing software. The mesh grid is unstructured, and the total cell number is 339466 elements.
To simulate the present model, several assumptions are considered which are:

- The solver is pressure-based.
- The effect of gravity on the flow has yet to be considered.
- The present model is unsteady.

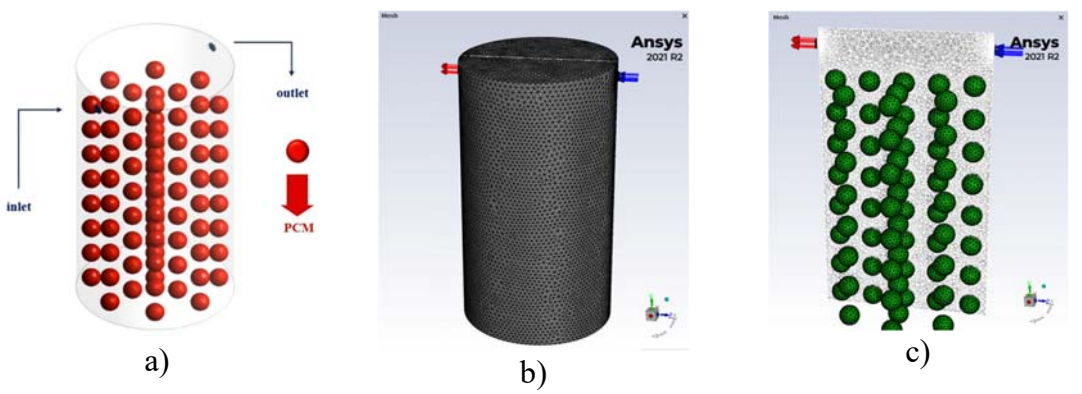

Fig. 1. a) Storage geometry; b), c) boundary conditions and geometry meshing

3. Results

Computational Fluid Dynamics (CFD) analysis of a storage tank with Phase Change Materials (PCMs) (Figure 2) provides valuable insights into the thermal behavior and performance of the system. PCMs are used in thermal energy storage systems for their ability to absorb, store, and release large amounts of thermal energy during phase transitions. In the case of a storage tank, the PCM is typically encapsulated in containers or integrated with the tank structure.
Results from a CFD analysis of a storage tank with PCM may include:

- Temperature distribution: The analysis reveals the spatial distribution of temperature inside the tank and PCM containers, which is critical for understanding the heat transfer and energy storage processes.

- Phase change visualization: CFD simulation allows for the visualization of the melting and solidification of PCM, aiding in the optimization of the system for better thermal performance.
- Heat transfer rate: CFD analysis provides information on the heat transfer rate between the heat transfer fluid (HTF) and the PCM, as well as within the PCM itself. This helps to optimize the system's design and operational parameters.
- Flow pattern and velocity distribution: CFD results show the flow pattern and velocity distribution of the HTF within the storage tank, which is essential for understanding the mixing and heat transfer processes.
- Energy storage capacity: The simulation can be used to calculate the total energy storage capacity of the system, which is essential for sizing and design considerations.
- System efficiency: The results from the CFD analysis can be used to evaluate the overall efficiency of the thermal storage system, helping to identify areas for improvement and optimization.
- Transient behavior: CFD simulation can provide insights into the transient behavior of the storage tank with PCM, which is crucial for understanding the dynamic response of the system during operation.
- Thermal stratification: The analysis can reveal the extent of thermal stratification within the storage tank, which is a crucial factor affecting the performance of thermal energy storage systems.

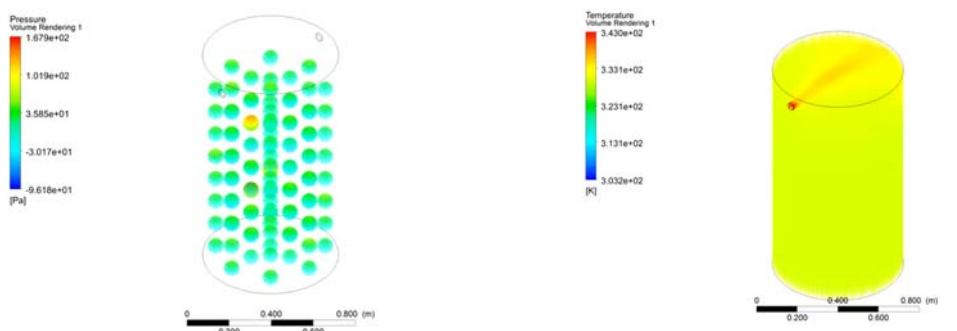

a) b)

Fig. 2. a) Contours of Pressure Magnitude; b) Temperature Magnitude

4. Discussion

A discussion over the CFD analysis of a storage tank with PCM may involve several aspects, such as the benefits and limitations of CFD analysis, factors affecting the accuracy of simulations, and the importance of validation and verification. Here are some points that can be considered for such a discussion:

- Benefits of CFD analysis: Using CFD for analyzing storage tanks with PCM allows engineers to gain insights into the complex fluid dynamics and heat transfer

processes that are otherwise difficult to observe experimentally. CFD analysis enables the visualization of temperature distribution, phase change, and flow patterns, which helps in optimizing the design and operational parameters of the thermal storage system.

- Limitations of CFD analysis: Although CFD simulations provide valuable insights, they are based on mathematical models and assumptions that may not always perfectly represent the real-world scenarios. Factors such as mesh quality, turbulence modeling, and numerical schemes can affect the accuracy of the results. Additionally, CFD analysis can be computationally expensive and time-consuming, especially for large-scale or highly detailed simulations.
- Factors affecting CFD accuracy: The accuracy of CFD simulations depends on various factors, including the selection of appropriate boundary conditions, numerical models (e.g., turbulence models), discretization schemes, and the quality of the mesh. Proper selection of these factors is crucial for obtaining reliable and accurate results.
- Importance of validation and verification: To ensure the reliability of CFD analysis, it is essential to validate and verify the simulation results. Validation involves comparing the simulation results with experimental data or other established benchmarks, while verification ensures that the numerical solution converges and the discretization error is minimized. This process helps to build confidence in the simulation results and identifies areas where improvements can be made.
- Sensitivity analysis: A sensitivity analysis can be performed to evaluate the impact of various input parameters and assumptions on the CFD results. This helps to identify critical factors affecting the simulation outcomes and provides a better understanding of the uncertainties involved in the modeling process.
- Optimization of storage tank design: CFD analysis can be used to optimize the design of a storage tank with PCM, such as the shape and size of the tank, the configuration of PCM containers, and the placement of heat exchangers. This allows engineers to enhance the performance, efficiency, and reliability of the thermal storage system.
- Applications in different industries: The CFD analysis of storage tanks with PCM is applicable to various industries, including renewable energy (e.g., solar thermal power plants), building energy systems (e.g., heating and cooling), and process industries (e.g., waste heat recovery and storage). The insights gained from CFD simulations can help in the development of innovative and efficient thermal storage solutions.

5. Conclusion

In the first instance, the temperature of the environment increases with the addition of hot water, which raises the average temperature of the PCMs and demonstrates the melting process in 343 seconds, as shown by the graph of the average temperatures of the environment and PCMs.

Gives. The average temperature diagram shows the impacts of the flow of cold water entering the domain after 1500 seconds, which results in a fall in the domain's average temperature. All of the PCMs have entirely melted by this point. As a result, the average temperature of PCMs drops more slowly when the heat is gradually released.

The PCMs begin to solidify 500 seconds after being submerged in the cold water, and they finish solidifying 4500 seconds later.
You can get the geometry and mesh file you need as well as a thorough training movie that explains how to fix the issue and get the desired outcomes.

References

[1] Sharma, A., Tyagi, V. V., Chen, C. R., & Buddhi, D. (2009). Review on thermal energy storage with phase change materials and applications. Renewable and Sustainable Energy Reviews, 13(2), 318-345.
[2] Zalba, B., Marín, J. M., Cabeza, L. F., & Mehling, H. (2003). Review on thermal energy storage with phase change: materials, heat transfer analysis and applications. Applied Thermal Engineering, 23(3), 251-283.
[3] Farid, M. M., Khudhair, A. M., Razack, S. A. K., & Al-Hallaj, S. (2004). A review on phase change energy storage: materials and applications. Energy Conversion and Management, 45(9-10), 1597-1615.
[4] Kuznik, F., David, D., Johannes, K., & Roux, J. J. (2011). A review on phase change materials integrated in building walls. Renewable and Sustainable Energy Reviews, 15(1), 379-391.
[5] Cabeza, L. F., Castell, A., Barreneche, C., de Gracia, A., & Fernández, A. I. (2011). Materials used as PCM in thermal energy storage in buildings: A review. Renewable and Sustainable Energy Reviews, 15(3), 1675-1695.
[6] Rathod, M. K., & Banerjee, J. (2017). Phase change materials for low temperature solar thermal applications: A review. Solar Energy, 147, 77-94.
[7] Sarı, A. (2016). Thermal energy storage materials with phase change for solar heating applications: A brief review. Renewable and Sustainable Energy Reviews, 61, 317-328.
[8 Kosny, J., & Kossecka, E. (1996). Infiltration of phase-change materials (PCM) into porous building materials. International Journal of Heat and Mass Transfer, 39(12), 2513-2523.
[9] Mondal, S. (2018). Phase change materials for smart textiles – An overview. Applied Thermal Engineering, 131, 284-298.

Indoor climate influence related human performance. Case Study

Influenta climatului interior asupra performantei umane. Studiu de caz

Cristian Pacurar [1], Adriana Tokar [1], Marius Adam[1]

[1] Politehnica University of Timisoara, Romania
Traian Lalescu 2, Timisoara 300223, Romania
E-mail: cristian.pacurar@upt.ro, adriana.tokar@upt.ro , marius.adam@upt.ro

DOI: 10.37789/rjce.2023.14.4.6

Abstract. *The indoor air quality is one of the main factors that influence the thermal confort and, consenquently, the human performance inside buildings. Throughout the years, a lot of studies described the relation between the climate confort and the performance .This study follows the thermal sensations of students in a seminar room during the summer and winter periods and presents the results between them.*

Key words: thermal comfort, productivity, performance, PMV, PPD, environmental comfort, indoor environment1. Introduction

1. Introduction

Currently people spend up to 87% of their time in indoor environments, be it in residential, academic or commercial buildings, and another 6% in their vehicles, and thus are continually being exposed to the indoor environment [1]. According to Wong et al. (2007) [2], the acceptance of an environment by its occupants depends on environmental parameters, namely thermal comfort, indoor air quality (IAQ), sound and visual comfort, which are identified to determine indoor environmental quality.

This study focuses mainly on education because children spend 30% of their time in schools and educational activity has major repercussions on the future development of young people [3]. Indoor Environmental Quality (IEQ) includes factors such as indoor air quality, thermal comfort, acoustic comfort and visual comfort. It is very important to study these factors, because people spend very long time inside buildings [4]. Besides this to provide comfort to its occupants, buildings should have low energy consumption and concern with sustainability [5].

In many studies it has been proven that poor IEQ may cause diseases, negatively affecting the worker's well-being and reduce its productivity [6]. The thermal environment is one of the main factors that influence thermal comfort and the productivity of occupants inside buildings. It was noted that there was a large number

of publications in the last years related of the importance of the IAQ in people's quality of life. Air temperature is a commonly used indicator in thermal environment in IEQ and in performance research [6]. Many studies held in the last decades have reported the connection between air temperature and the performance of its occupants [7]. The physical effects obtained in the thermal environment may vary and may affect the performance of workers, affecting their productivity.

In the case of an academic environment the performance and the productivity can be measured using different methods. There are many factors who can affect the productivity and it can be mentioned environmental, organizational, social and personal factors. It is a limit to the studies which determine mathematical models and relations between productivity and physical factors of the indoor environment, such as thermal comfort, visual comfort, acoustic comfort and air quality. Very many years the aspects of IEQ were analyzed separately and there are other factors that should be considered, such as multisensory interactions [5]. Occupant's productivity could be measured: physiologically, objectively or subjectively. Physiological measurements mean to monitor the indicators of the nervous system, the cardiovascular system, the respiratory system and biochemistry. In subjective assessment, occupants' feedback on changes in the physical environment can be gathered by means of field research (interviews and questionnaire) and objective assessments (calculations and metrics) [8].

2. Content of the paper

The study highlights the possible links between the learning activity of students in their classes and specific parameters of indoor climate. More exactly, based on tests of attention, the study is trying to determine approximate values for efficiency of a person at a certain period of time. Knowing the indoor climatic parameters (measurements were performed earlier), and based on the correlation relationship, the dependency that exists between a person's efficiency and the climatic conditions will be highlighted. Measurements were made in cold period at indoor temperature values ranged between (22 ÷ 28) ±0.8°C and in hot period at temperature values between (16 ÷ 22) ±0.8°C. The average humidity was 50±10 % and the air speed of approx. 0.22 m/s. The seminar room was without mechanical ventilation, with central heating and SPLIT air conditioning cooling. The study described in this article was realized based on several series of measurements for the following climatic parameters: indoor temperature, air velocity and relative humidity [9]

The measurements were made with a device (type meter Testo 350) connected to a sensor which has the following characteristics: temperature (range: +20…70 °C, accuracy: ±0,4°C), air velocity (range: 0…10 m/s, accuracy: ±0,03m/s), humidity (range: 0…+100 %, accuracy: ±2%RH), CO_2 probe measures (range 0 …10000 ppm CO_2, accuracy: ±50 ppm CO_2). At the beginning and end of each measurement session, participants were asked to fill out a questionnaire for determining the IAQ sensation. To determine the PMV and PPD comfort indices according to the Fanger

model, the activity of the occupants was estimated to be 1.2 met (69.84 W/m^2), and the thermal resistance of the clothing was 0.5 clo in summer and 1 clo in winter.

In the study is presented a comparation between representatives' relations for relative performance in order to analyze the best option to be used in the futures studies. For the study are used the below relations related to relative performance (RP) with indoor temperature (T_i) and relative humidity (RH_i) .

Koehn, E. and Brown, G. presents relative performance (RP) with indoor temperature (T_i) (^{0}F) and relative humidity (RH_i) differentiated used in cold climate (equation (1.1)) and in hot climate (equation (1.2)).

$$RP = 0{,}0144 \cdot T_i - 0{,}00313 \cdot RH_i - 0{,}000107 \cdot T_i^2 - 0{,}000029 \cdot RH_i^2 - 0{,}0000357 \cdot (T_i \cdot RH_i) + 0647 \quad (1.1)$$

$$RP = 0{,}0517 \cdot T_i + 0{,}0173 \cdot RH_i - 0{,}00032 \cdot T_i^2 - 0{,}000985 \cdot RH_i^2 - 0{,}0000911 \cdot RH_i - 1459 \quad (1.2)$$

Relative performance (RP) could be represented with another formula for the both type of climate performance is related in equation (2) and is in dependence only with indoor temperature (Ti) (^{0}C)

$$RP = 0{,}1647524 \cdot T_i - 0{,}0058274 \cdot T_i^2 + 0{,}0000623 \cdot T_i^3 - 0{,}4685328 \quad (2)$$

Thomas, H.R. and Yakoumis, I. presents relative performance (RP) in dependence with indoor temperature (T_i) (^{0}F) and relative humidity (RH_i) in equation (3).

$$RP = \frac{1}{9{,}448 + 0{,}0518 \cdot T_i - 0{,}2{,}819 \cdot ln(T_i) + 3{,}89 \cdot 10^{-37} \cdot e^{RH_i}} \quad (3)$$

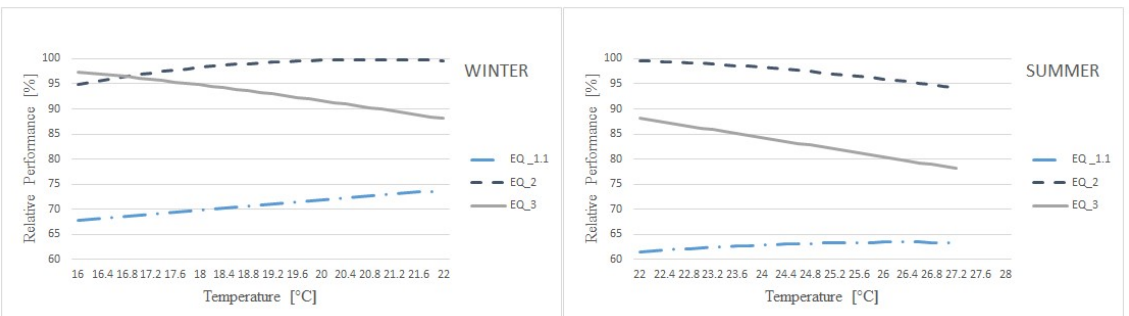

Fig. 1. Relative performance depending on the indoor temperature and relative humidity

Based on these equations, the final model resulting from the superimposition of the relative performance results depending on the season, indoor temperature and relative humidity are shown in the graph above. Most of the research studies in this area agree on the premise that indoor temperature and relative humidity have a very influential effect on people' productivity.

Conclusions

This study provides new insights into the indoor environment that maximizes the productivity of those who occupies a certain space and thermal satisfaction. Thermal comfort evaluation becomes even more relevant when the aim is to maximize performance/productivity, which occurs in a lot of domains. It is necessary to ascertain how environmental variables (air temperature, average radiant temperature, air velocity and relative air humidity) and people (metabolism and clothing) influence thermal comfort and productivity.

References

[1] N.E. Klepeis, W.C. Nelson, W.R. Ott, J. Robinson, A.M. Tsang, P. Switzer, J.V. Behar, S.Hern, W. Engelmann, The National Human Activity Pattern Survey (NHAPS): A Resource for Assessing Exposure to Environmental Pollutants. J. Expos. Anal. Environ. Epidem. 2021, 11, 231–252.
[2] Wong, L.T., Mui, K.W., Hui, P.S., A multivariate-logistic model for acceptance of indoor environmental quality (IEQ) in offices. Build. Environ. 2008, 43, 1–6.
[3] F. R. Alfano d'Ambrosio et all.: Environment and Energy Efficiency in Schools (Part 1), REHVA Guidebook, vol. 13, Brussels, Belgium, ISBN 978-2-930521-03-9, 2010
[4] Gani, A.Z., Zamberi, M.M., Teni, M.H.M. A Review of Ergonomics towards Productivity. Int. J. Sup. Chain. Mgt. 2018, 7, 306.
[5] Bellia, L., d'Ambrosio Alfano, F.R., Fragliasso, F., Palella, B.I.; Riccio, G., On the interaction between lighting and thermal comfort: An integrated approach to IEQ, Energy Build, 2021, 231.
[6] Cui, W., Cao, G., Ouyang, Q., Zhu, Y. Influence of dynamic environment with different airflows on human performance. Build. Environ 2013, 62, 124–132.
[7] Roelofsen, P., The impact of office environments on employee performance: The design of the workplace as a strategy for productivity enhancement. J. Facil. Manag. 2002, 1, 247–264.
[8] Zhao, J., Zhu, N., Lu, S., Productivity model in hot and humid environment based on heat tolerance time analysis. Build. Environ. 2009, 44, 2202–2207.
[9] A. Retezan, A. Tokar, C. Pacurar, M. Adam, A model for efficiency estimation of student activity depending on relative humidity, ICCA, 2015

Power supply insurance solutions for fire protection

Sisteme de menținere a alimentării cu energie electrică pentru protecție la incendiu

Cătălin Dragotă [1], Adriana Tokar [2], Alexandra Rusen [2]

[1] Border Police Territorial Inspectorate
Sever Bocu Street, No. 49, 300278 Timisoara, Timis county, Romania
E-mail: catalindragota1996@gmail.co

[2] Politehnica University Timisoara
Piaţa Victoriei Nr. 2, 300006 Timişoara, jud. Timiş, Romnia
E-mail: alexandra.rusen@student.upt.ro

DOI: 10.37789/rjce.2023.14.4.7

Abstract. *The study analyzes the benefits of implementing automatic transfer systems of the main electricity supply with one or more backup supplies in the event of a breakdown caused by a fire or other unforeseen events. Transfer switch using relays as phase failure protection is a gear switch control system with the main purpose of transferring load between a primary source (Public Utility) and a secondary power supply sources (Generator1 and Generator2) which are stand by power sources and eliminating frequent manual switching of change over device when there is power outage.*

Key words: backup supplies, fire, control system, maintenance

1. Introduction

The power supply insurance of the electrical installations serving buildings is very important, especially in buildings where a large number of people work (hospitals, hotels, commercial premises, public buildings, subways) [1].

Usually, the backup power sources (alternative) used are:

- accumulators;
- fixed or portable generators capable of operating independently;
- separate power supply that is independent from the main power supply with reduced risk of failure at the same time.

On the other hand, consideration may also be given to installing a duplicate power supply from a three-phase source, where possible [1].

A link between the main and back-up power sources is an important aspect in ensuring the continuity of the electrical energy supply. This connection can be

achieved through low voltage automatic transfer switch assemblies (ATS) that provide a reliable means of transferring the connection between the two sources.

Basically, an automatic transfer switch (ATS) is an intelligent, self-acting power switching device governed by dedicated control logic. The main purpose of an ATS is to ensure the continuous supply of electrical energy from one of two power sources to a connected load circuit (electrical equipment - lights, motors, computers, etc.). The automatic controller is usually microprocessor-based and constantly monitors the electrical parameters (voltage, frequency) of the primary and alternative power sources. Upon failure of the connected power source, the ATS will automatically transfer (switch) the load circuit to the other power source (if available). As a general rule, most automatic transfer switches seek connection to the primary power source (utility) by default and will connect to the alternate power source (motor-generator, backup utility) only when required (primary source failure) or when prompted to do so (operator command) (Fig.1) [2], [3], [4].

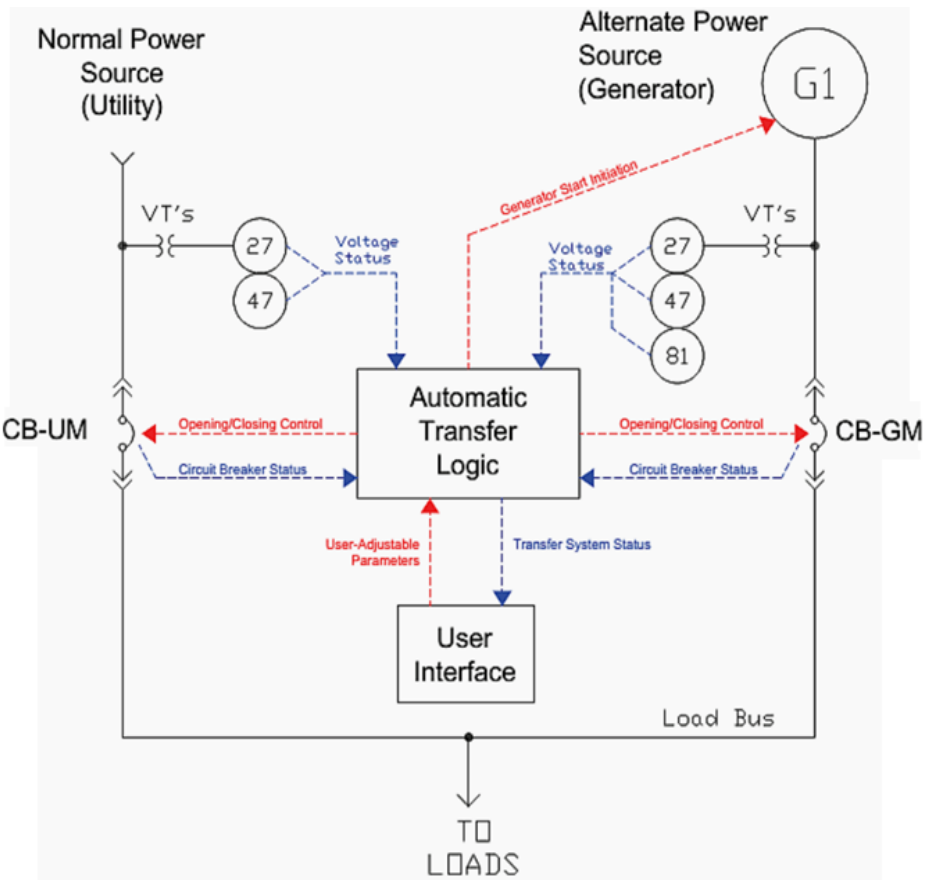

Fig.1. Automatic Transfer Scheme Detail [4]
CB-UM/GM – Circuit Breaker Utility/Generator Module, VT's – Voltage Transformers, 27 – Undervoltage indicator, 47 – Negative sequence voltage, 81 – Frequency indicator

When the primary source (utility) fails and the load is transferred to the generator or any other secondary power source, the ATS system also monitors the

main supply, and when power is restored, or the supply power characteristics return to normal, it transfers the load back to the main supply and sends signals to stopping the generator or simply interrupting any other secondary source of electricity supply [3].

A variety of arrangements using two or three power supplies are available [1]:

- *with two power sources:*

- main power source (mains) and backup generator;

- main source-main source (ensures redundancy in the distribution system and allows rapid restoration of service to the load if a failure of upstream equipment occurs). This configuration is suitable for dual power supply or redundant power supply.

- generator-generator: for the use of energy (remote installations) between two sets of generators, transfer switches are applied

- *with three power sources:*

- main source-generator-generator: this configuration additionally has a second connection to a generator considered as an emergency redundant backup that can be used during periods of bad weather or when the first generator is scheduled for maintenance. In this configuration, as a rule, the first generator is fixed, and the second is mobile and is installed only when necessary.

- main source-main source-generator: this configuration extends the redundancy provided by a dual main source configuration and includes an emergency standby generator source.

From the point of view of transfer types ATS switches ensures the transit of loads between the main and backup power sources with the options [1]:

- open: the switch interrupts the connection to one power source before making the connection to the other;

- closed: the switch makes the connection to the second power source before breaking the connection to the first source.

2. Use of ATS systems in case of damage caused by fires

The utility of these systems in case of breakdowns in the electrical power supply installation of the building's vital systems in emergency situations, such as the emergency lighting system, HVAC systems, security, and access control systems, etc., is very important and brings important benefits in the operation of these installations.

The concept of the utility of automatic transfer systems in case of emergencies caused by the occurrence of a fire consists in ensuring the continuous supply of the safety installations of the building if the main supply suffers a breakdown. You can also use the double feeding method and it is very efficient.

This method is based on a main supply which at a certain point, usually in the basement of the building, is divided into two supply routes, as far as possible from each other, so that if there is a fire in one part of the building, the main supply is damaged, the automatic transfer system switches the supply of all emergency

installations with the secondary supply from the other individual route, thus gaining reaction time and evacuation of the building in maximum safety conditions (Fig.2) [4].

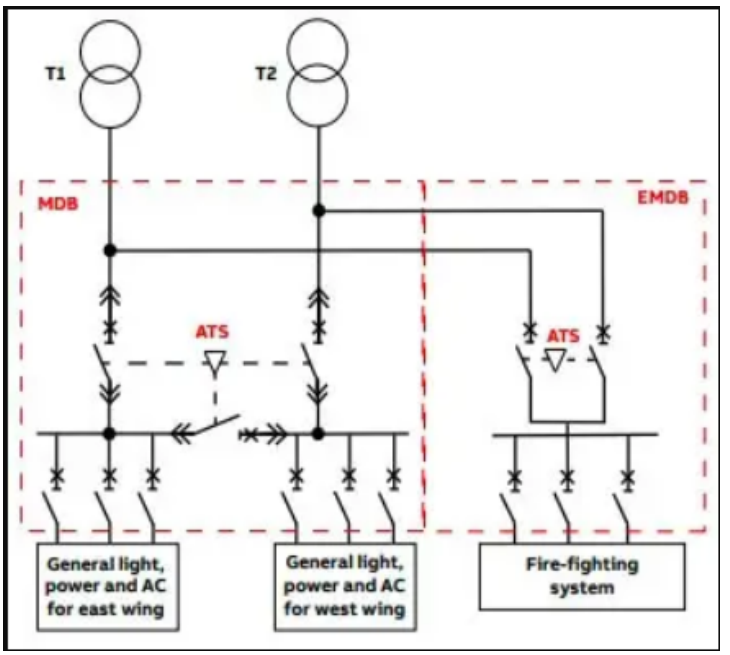

Fig. 2. ATS backing up supply for loads [4]
T1, T2 – Divided supply routes, MDB – Main Distribution Board,
EMDB – Emergency Main Distribution Board

Transfer switch needs can vary considerably from type to type,depending upon your structure's capacity and the purpose of the building.

The dimensioning of the transfer system must be done correctly in order to optimize its operation in the building installation and avoid malfunctions.

3. ATS types and maintenance

There are three general ATS types [4], [5]:

- Open transition (break-before-make): This breaks the load during the transfer between primary and secondary power. This is the most common type of ATS, however, it has the disadvantage of interrupting the supply even for a short period of time.
- Closed transition (make-before-break): When the load is affected, this type of ATS allows a transfer between two power sources without interruption during the transfer. This type of ATS is typically found in applications that require uninterruptible power supply to equipment.
- Delayed transition: This type of ATS operates similarly to the open transition type but affords a delay in load transition and is typically used in situations where residual voltages on inductive loads can dissipate before transition.

If an ATS works with a generator, they are independent. An ATS can be mounted in an electrical panel in a premises but is usually mounted on the generator housing. Fig. 3 highlights a typical ATS [4].

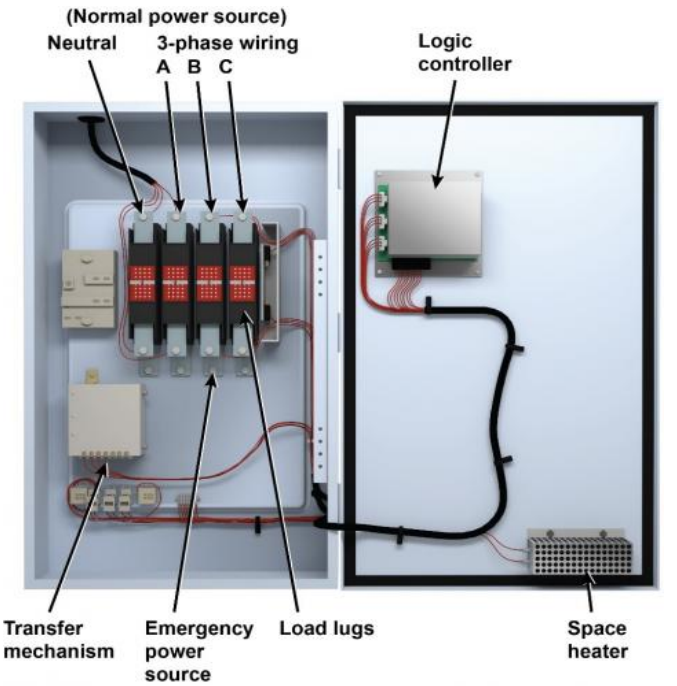

Fig. 3. Typical ATS configuration [4]

The example checklist in Table 1 [4] below provides recommended actions for ATS maintenance.

Maintenance must be performed periodically to ensure proper operation and to issue periodic installation inspection certificates.

Table 1

ATS Maintenance checklist

Component	Action	Maintenance Frequency		
		Monthly	Semi-Annually	Annually
ATS	Inspect all wiring, insulation, and connectors, look for crack's deformation, or discoloration due to excessive heat.	x		
	Check and replace any batteries if equipped.		x	
	Lubricate all mechanical parts as needed.			
	Conduct infrared (IR) thermography scan of connections and contacts; note areas of high heat conduction.			x

Component	Action	Maintenance Frequency		
		Monthly	Semi-Annually	Annually
	Check ATS operation to verify proper transfer from Emergency to Normal and back again. Initiate standby generator operation and run system for 1 hour under full building load.			x
	Performing inspection measurements of the installation to which the ATS is connected, checking electrical impedances and resistances.			x

4. Conclusions

In conclusion, automatic transfer systems are very beneficial in the operation of a building's installations, especially residential and office buildings, where the crowding of people speaks for itself in case of emergencies caused by fires.

These systems can ensure safe evacuation of buildings and at the same time ensure the quality of the energy supplied in the building to avoid possible failures caused by variations in the main power supply characteristics.

References

[1] Eaton, „Fundamentals of automatic transfer switches (ATS)", Powering Bussines Worldwide, 2023.
[2] CFPA Europe, „Fire safety measures with emergency power supplies", Guideline No 34-F, 2015.
[3] D. Idoniboyeobu, „Design and Implementation of a Three Phase Automatic Transfer Switch Using Relays as Phase Failure Protection", in International Journal of Engineering Technologies IJET, Rivers State University Port Harcourt, 2022.
[4] Pacific Northwest National Laboratory, „Best Practices for Automatic Transfer Switches Operation and Maintenance", O&M Best Practices, https://www.pnnl.gov/projects, 2021.
[5] Institute of Electrical and Electronics Engineers (IEEE), „Guide for Performing Arc Flash Hazard Calculations", Institute of Electrical and Electronics Engineers, New York, https://standards.ieee.org, 2018.

Energy parameters of construction elements in the passive house concept

Parametrii energetici ai elementelor de construcție în conceptul de casă pasivă

Alexandra Rusen [1], Dănuț Tokar [1], Cătălin Dragotă [2]

[1] Politehnica University Timisoara
Square Victoriei No. 2, 300006 Timișoara, Timiș county, Romania
E-mail: alexandra.rusen@student.upt.ro

[2] Border Police Territorial Inspectorate
Sever Bocu Street, No. 49, 300278 Timisoara, Timis county, Romania
E-mail: catalindragota1996@gmail.com

DOI: 10.37789/rjce.2023.14.4.8

Abstract. *Newly built houses are subject to requirements with high levels of energy performance including the creation of houses with zero energy consumption (passive houses) and respectively without carbon emissions. Building regulations, processes and control will need to be rethought in light of these ambitions and a development of performance guarantees in the construction sector.Many mandatory standards and rating systems for the energy efficiency of buildings have been developed globally, but those for passive houses are still voluntary, and for this reason there is little data on the performance of houses built to these standards. They have emerged as a promising approach to mitigating and solving many energy problems, and constructive visions and solutions and testing or demonstrating their feasibility are undoubtedly major steps in the process of solving the energy problem.*

Key words: *passive house, energy parameters, performance of materials, operational costs*

1. Introduction

This article studies the influence of energy parameters in building materials for the certification of passive houses. Through a case study, the influence of building insulation on consumption and building operating costs is presented according to the performance of insulating materials, emphasizing comparisons between consumption and operating costs according to the type of insulation.

2. The influence of building insulation on the consumption and operating costs of construction materials

The most important aspect of an insulation material is its performance to consistently ensure resistance to heat transfer throughout the life of the building. Although performance expectations given by the manufacturer are essential, other factors associated with the "real" installation of the material must be considered as part of the design process, namely [1]:

- ease of installation - final performance will be determined by how efficiently a builder can install a material using conventional skills. For example, insulation boards must be installed so that there are no gaps either between adjacent boards or between the boards and other building components that are part of the overall insulation envelope, such as rafters or joists. Any remaining gaps will allow air to pass through and result in reduced performance.

- shrinkage, compaction, settlement - some materials may experience some degree of dimensional instability during installation. In many cases this is anticipated and can be overcome by careful design and installation methods. In all other cases, the builder should seek guidance from the insulation manufacturer regarding the associated risks, particularly where the materials have not performed stably at installation.

– humidity protection - some insulating materials suffer performance degradation when they are wet. The designer must, through technical details, ensure that the vulnerable insulation is protected from humidity. If humidity is at high risk (penetration or above 95% RH), then a resistant material should be chosen.

3. Consumption and operating costs of buildings depending on the type of insulation. Comparative study

The calculation was made using the Hydrolution program provided by Mitsubishi Heavy Industries [2]. For the analyzed building, a hot water consumption of 45 l/day/person was considered. The conventional external calculation temperature for the chosen town of Lugoj is -12 ^{o}C and as equipment we chose an air-water heat pump in parallel with an electric boiler. In the following, the simulations performed for each of the insulation materials analyzed (mineral glass wool, polyurethane foam and straw) are analyzed:

-Mineral glass wool [2]

Made from fused glass, typically with 20% to 30% recycled industrial waste and post-consumer content. The material consists of glass fibers arranged using a binder in a wool-like texture. The process traps many small air pockets between the glass, and these small air pockets result in high thermal insulation properties. The density of the material can be varied by pressure and binder content (Fig. 1).

- Thermal conductivity / λ , W / m^2 K = 0,035;
- Thermal resistance at 100mm K m^2/ W = 2,85;

- Specific heat capacity J / (kg. K) = 1030;
- Density kg / m^3 = circa 20;
- Thermal diffusivity m^2/ s = 0,0000016;
- Built-in energy MJ / kg = 26;
- Vapor permeable: Yes.

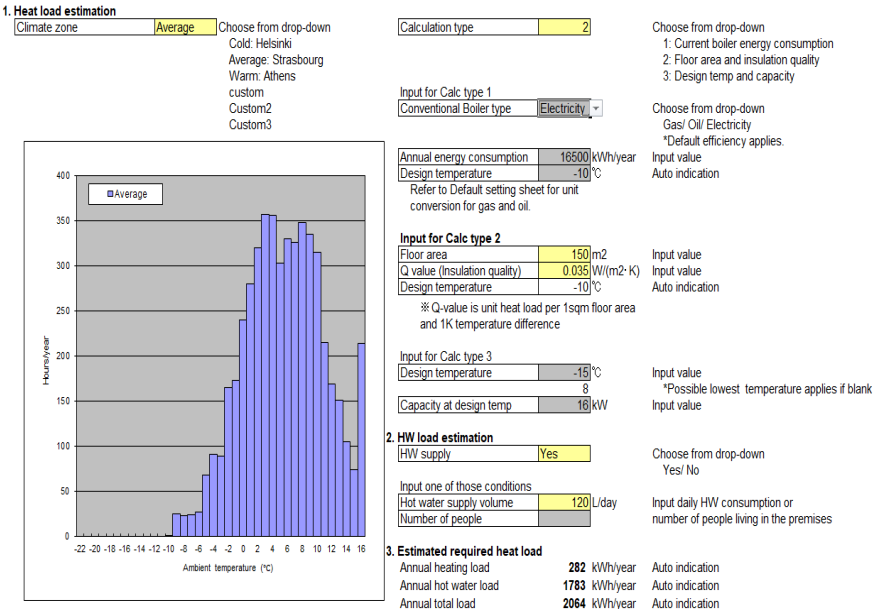

Fig.1. Vitrified mineral wool input data

For a thermal conductivity value of 0.035 W/m^2 K, an annual requirement of 2064 kWh/year results.

Annual energy consumption of the heat pump compared to the electric boiler (Fig. 2).

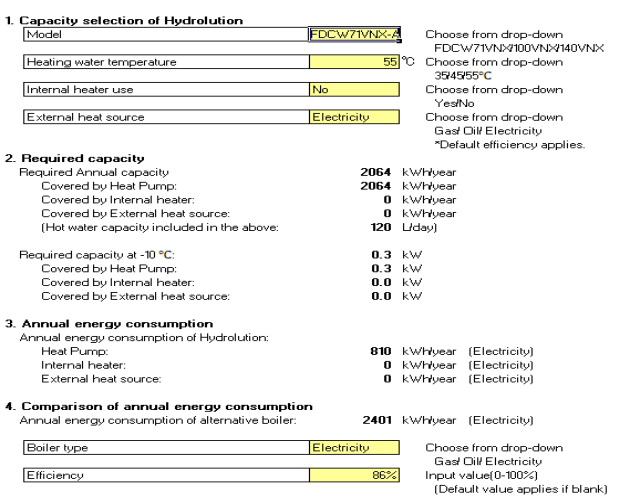

Fig. 2. Energy consumption (glass wool)

Depending on these annual consumptions, the comparison of costs and the time in which the air-to-water heat pump amortizes its investment results (Fig. 3).

Life time cost comparison

Hydrolution	FDCW71VNX-A		Alternative Boiler		
1. Initial Cost					
Equipment	6500	EUR	Equipment	1500	EUR
Installation	2000	EUR	Installation	2000	EUR
2. Running Cost					
Maintenance cost	500	EUR/year		1200	EUR/year
Night time operation ratio	75%	Input value (0-100%)			
Annual energy cost					
Electricity	60.7	EUR/year	Gas	0.0	EUR/year
Gas		EUR/year	Oil		EUR/year
Oil		EUR/year	Electricity	360.1	EUR/year
Total	60.7	EUR/year	Total	360.1	EUR/year
Payback Time	**5.0**	**years**			

Fig. 3. Costs (mineral wool)

- Polyurethane foam [2]

Polyurethane (PUR and PU) is a polymer composed of organic units joined by carbamate (urethane) bonds. Polyurethane can be manufactured in a variety of densities and hardnesses by varying the isocyanate, polyol or additives (Fig. 4).

- Thermal conductivity / λ (lambda) W / m. K = 0,023-0,026;
- Thermal resistance at 100mm K m^2/ W = 4,50;
- Specific heat capacity J / (kg. K) = n / a;
- Density kg / m^3 = 30 – 40;
- Thermal diffusivity m/ s = n / a;
- Built-in energy MJ / kg = 101;
- Vapor permeable: No.

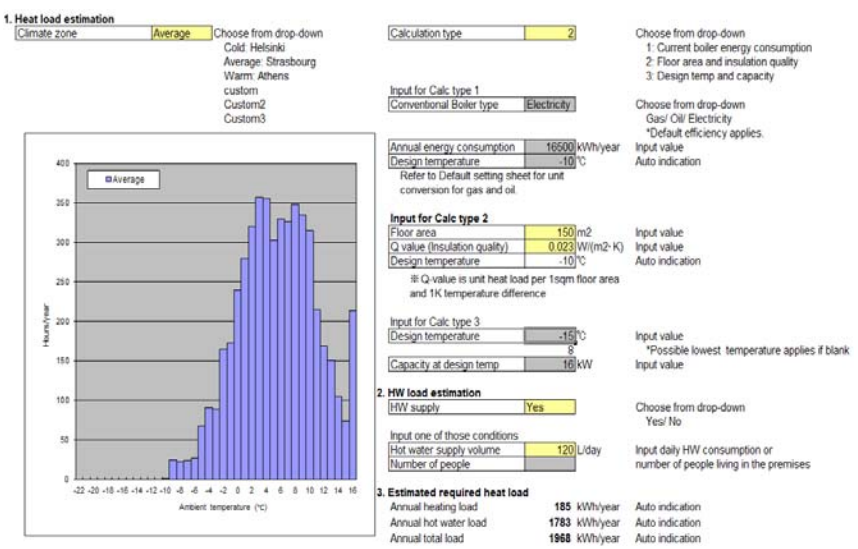

Fig. 4. Polyurethane foam (input data)

For a thermal conductivity value of 0.023 W/m^2 K, an annual requirement of 1968 kWh/year results.

The annual energy consumption of the heat pump compared to the electric power plant (Fig. 5).

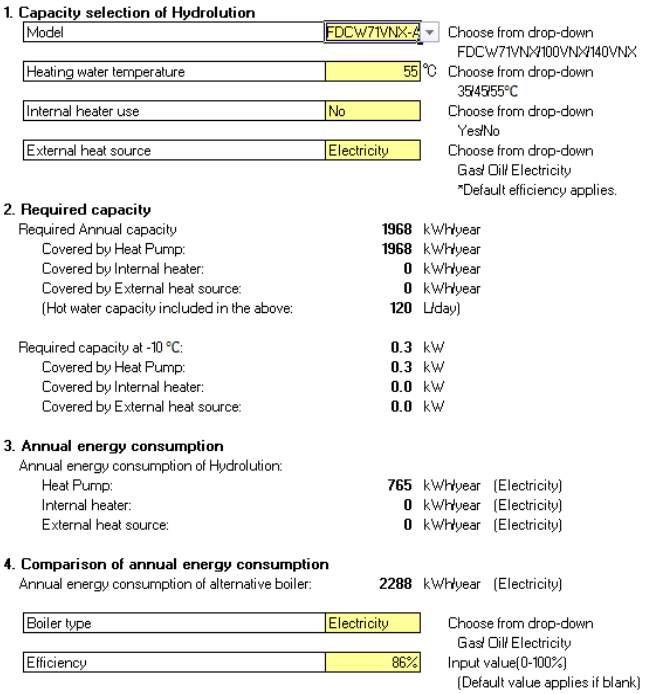

Fig. 5. Annual consumption (polyurethane foam)

Cost comparison and the time in which the air-to-water heat pump amortizes its investment (Fig. 6).

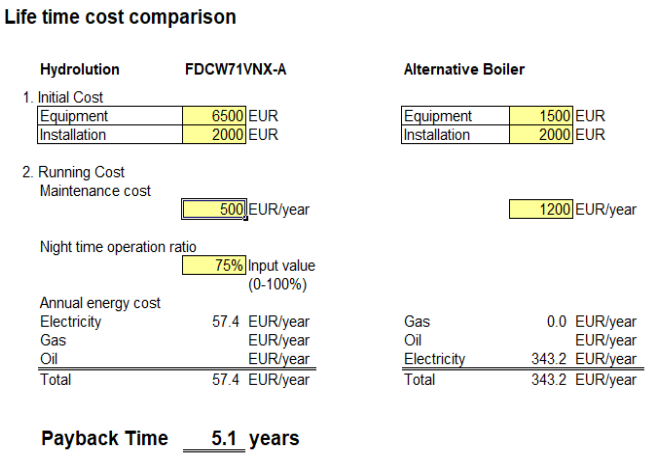

Fig. 6. Costs (polyurethane foam)

- Straw [2]

Straw is an agricultural by-product, the dried stalks of cereal plants after the grain and chaff have been removed.

Straw accounts for about half of the yield of cereal crops such as barley, oats, rice, rye and wheat (Fig. 7).

- Thermal conductivity / λ (lambda) W / m. K = 0,08 (for load-bearing structures);
- Thermal resistance at 350mm K m^2/ W = 4,37 la 350mm;
- Specific heat capacity J / (kg. K) = unavailable;
- Density kg / m^3= 110 – 130;
- Thermal diffusivity m^2/ s = unavailable;
- Built-in energy MJ / kg = 0,91 (source ICE database 2011);
- Vapor permeable: Yes.

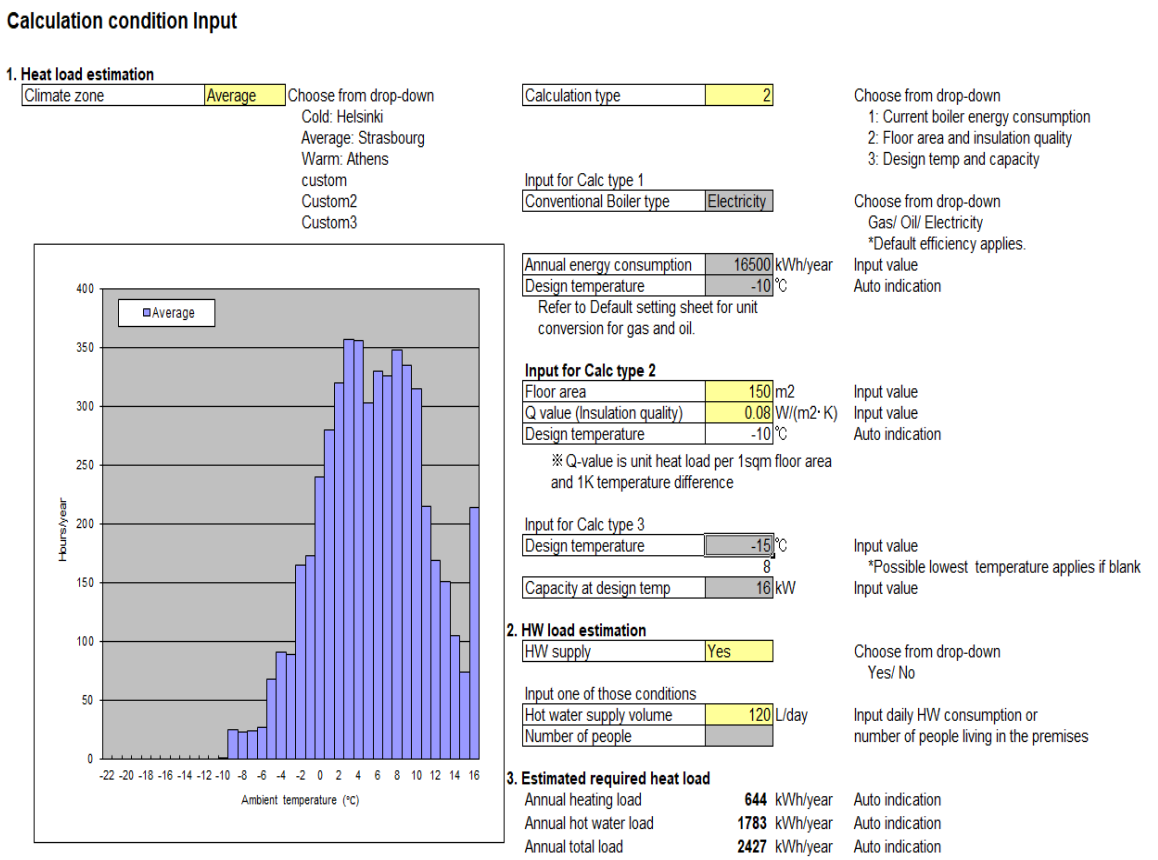

Fig. 7. Straw input data

For a thermal conductivity value of 0.08 W/m^2 K, an annual requirement of 2427 kWh/year results.

The annual energy consumption of the heat pump compared to the electric power plant (Fig. 8).

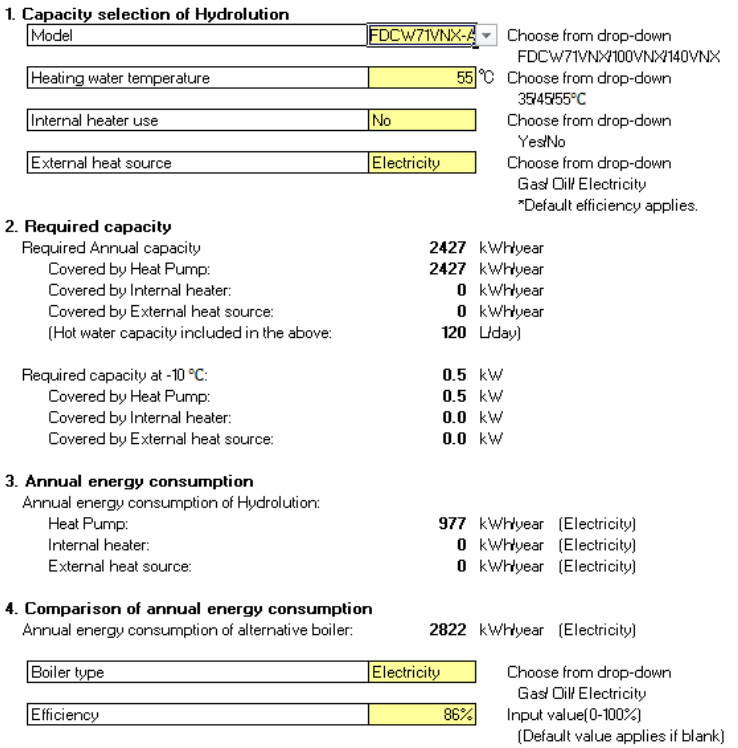

Fig. 8. Consumables (straw)

Cost comparison and the time in which the air-to-water heat pump amortizes its investment (Fig. 9).

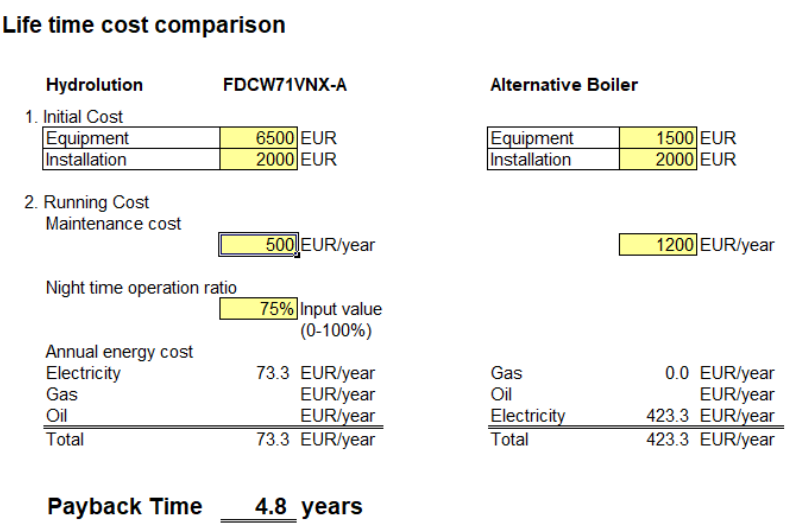

Fig. 9. Costs (straw)

4. Concluzii

Following these comparisons, we observe how and how much consumption varies depending on the type of insulation chosen, this is just one factor, quite important in fact, in the process of designing and building an energy passive building. The tightness of the buildings was evaluated in terms of hourly air changes. The hourly exchange rate at 50 Pa is n50 = 0.2 air exchanges/h. The reference building is not equipped with window shades. Solar4S + Low-e6 + Clear triple pane windows were chosen for the windows, with "U" coefficient values of 0.6 W/m^{2}K, resulting in a thermal resistance R of 1.66 m^{2}K/W.

References

[1] Agoria, „EPB policy framework: an introduction into the measure and the ongoing discussions”, in Buildings-Climateneutral, comfortable and secure (re)construction, 07 February, 2020.
[2] Mitsubishi Heavy Industries, „Hydrolution program provided”, 2022.

Thermography – new trends in heating installation inspection

Termografia – noi tendinţe în inspecţia instalaţiilor de încălzire

Viorica David[1], Alina-Corina Bălă[1], Floarea - Maria Brebu[1], Maria - Roberta Jianu[1]

[1] University Politehnica Timişoara
Square Victoriei No. 2, 300006 Timisoara, Timis county, Romania
E-mail: viorica.david@upt.ro , alina.bala@upt.ro , floarea.brebu@upt.ro , roberta.gridan@upt.ro

DOI: 10.37789/rjce.2023.14.4.9

Abstract. *Technology is always evolving at a quick rate and specialists try to integrate it in their works, either if we are discussing engineering, or any other domain. Furthermore, the most important accomplishments, in a research domain, are achieved when using the latest technology and research interdisciplinary.*
So, starting from all the above, in this paper we are trying to create a connection between monitoring methods and technologies, used in Thermography, and the installation inspection which is a part of Building Services. Data was acquired from thermal images and processed to establish the integrity of a heating installation.

Key words: *thermography, thermal images, heating installations, thermal inspection, clogged pipes*

1. Introduction

A picture says a thousand words; infrared thermography is the only diagnostic technology that lets you instantly visualize and verify thermal performance. Infrared cameras show you thermal problems, quantify them with precise non-contact temperature measurement, and document them [1].

Recent innovations in the development of thermal cameras have made them available to specialists in many industries, making them a common presence in industries such as building inspection, electrical, plumbing, fire, law enforcement and more [2].

Infrared thermography (IRT), thermal video and/or thermal imaging, is a process by which a thermal camera captures and creates an image of an object using the infrared radiation emitted by that object in a process, which are examples of the science of infrared imaging [3].

Thermographic cameras typically detect radiation in the long infrared range of the electromagnetic spectrum (approximate 9,000-14,000 nanometres' or 9-14 μm) and produce images of this radiation, called thermograms [4, 5]. Because infrared radiation is emitted by all objects with a temperature above absolute zero, according to the law of blackbody radiation, thermography makes it possible to observe the environment with or without visible illumination [6]. The amount of radiation emitted by an object increases with temperature, so thermography makes it possible to observe temperature variations [7,8].

Today, infrared thermography is one of the most effective technology available to locate problems quickly, accurately, and safely prior to failure [1].

2. Materials and methods

Everything in life gives off electromagnetic radiation, most of which goes unnoticed and is completely invisible to our eyes. The human eye perceives a very small window known as the visible light spectrum that makes up the colours that we can see [9].

Like the principle of ordinary camera, thermal radiation is equivalent to visible light, first through the lens to the detector, in the processing of images, and finally output stream, forming a video image for human observation [10].

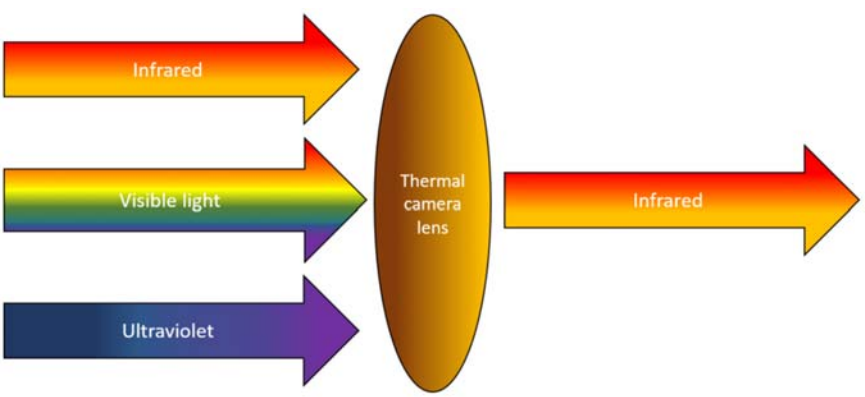

Fig. 1. Thermal radiation output for human observation [starting from [10]

An object emits more IR radiation the hotter its temperature rises. Infrared thermography cameras allow us to use our eyes to measure the temperature of an object instead of having to risk contact with something potentially dangerous. With the use of thermal imaging, we can "see" and "measure" thermal energy that was previously invisible to us. This type of heat radiation is known as infrared radiation [10].

A FLIR Vue Pro R 640 thermal camera (with radiometric recordings and a resolution of 640 x 512 pixels) was used for acquiring the thermal images and FLIR Tools software was the image analysing software.

The first steps before the image acquiring phase were to set up the technical parameters for the thermal camera. For that we used FLIR UAS software where we set the following:

- the measurement type (indoor);
- the capture mode (single);
- thermal IR zoom (100%);
- the photo format (radiometric JPEG)
- the thermal colour palette (Lava)
- the emissivity of the material (0,95);
- the atmospheric temperature (23℃) and humidity (30%);
- the weather type (sunny);
- the distance between the camera and the studied object (2,5m).

Our data interpretation and processing are based on the fundamentals of the physical principles of thermal energy exchange between two different environments (in our case: hot water inside the heating pipe and air inside the office), thus resulting in an energy exchange.

The data processing software that we used in our case study was FLIR TOOLS. Using this software, we analysed each thermal image and after that we selected the most clear and suggestive ones. After that, on those images we established the "critical areas" (surfaces on the interest areas where significative emissions of thermal energy appeared) and on those areas specifical measurements were made using tools available from the software.

3. Discussions

For the experimental part we chose to acquire thermal images of a heating installation from inside an office from the Faculty of Civil Engineering of Politehnica University Timişoara.

From this heating installation we studied the radiator (Fig. 2) and the pipes, especially the connection point between two pipes (Fig. 4) and the pipe entering point from the celling of the office (Fig. 3).

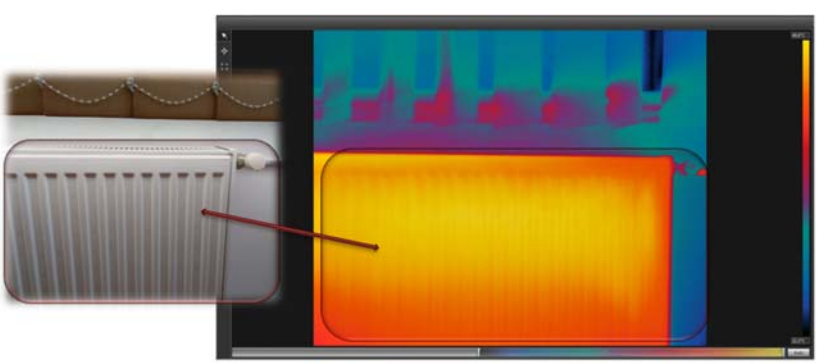

Fig. 2. The interest area from the radiator (left side - real image; right side: thermal image)

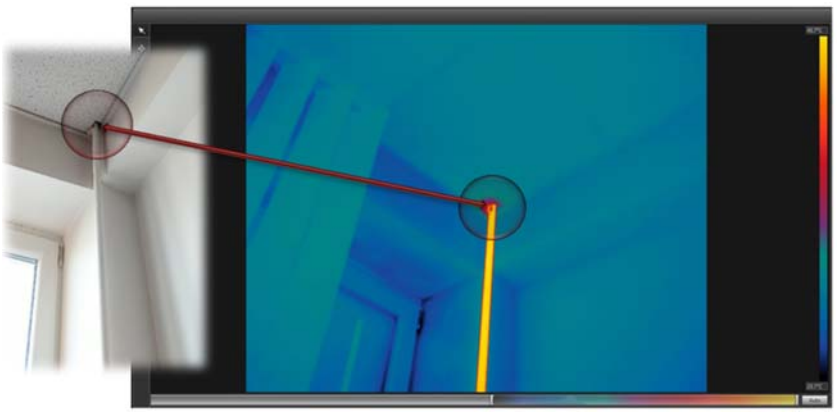

Fig. 3. The pipe entering point from the office' celling (left side - real image; right side: thermal image)

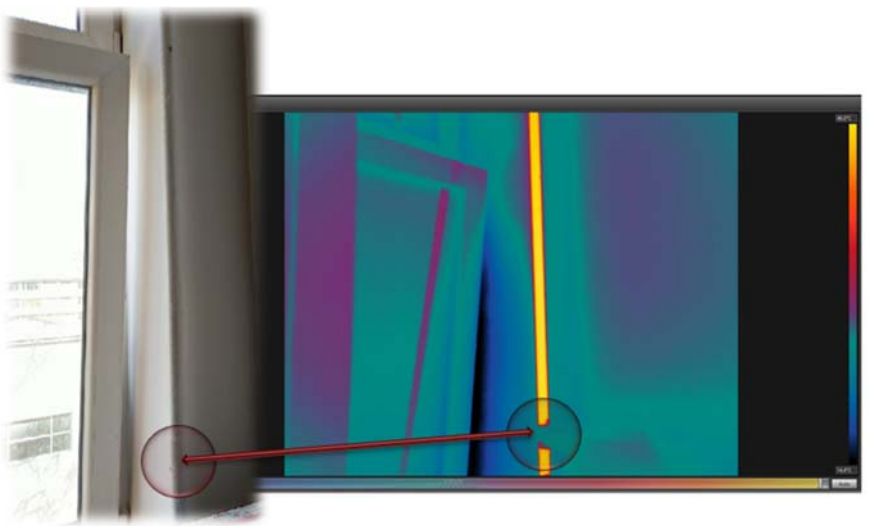

Fig. 4. The connection point between two pipes (left side - real image; right side: thermal image)

Because we desired an accurate interpretation of the thermal images, the first step that we took in this direction was to select the best images from the batch that was made during the photo session. The selection was made visually, in the processing software, by comparing multiple images of the same area and selecting the one with the higher clarity and an increased detail density.

After selecting the images for each of the three cases we selected the interest areas:

- on the radiator, the interest area contained both its upper and lower part, and the area around the radiator valve;
- on the heating pipe we chose two interest areas: first - around the pipe connector, and second – on the pipe entering point from the office' celling.

Further, for better measurements and image interpretation the images were adjusted using predefined filters from the processing software.

4. Results

On the radiator image, firstly we made a visual analysis in which we concluded the lack of uniformity of the temperature both on its lower and upper parts, even if the radiator surface is made from the same material, which reflects the heating uniformly on its surface.

Furthermore, we analysed the image by making punctual temperature measurements, in order to determine the temperature difference between different areas on the radiator. For this, we used the thermos-spots Sp2, Sp3 and Sp4 on the radiator area and, for comparison we used thermo-spots Sp1 and Sp5 around the radiator valve.

Analysing the thermos-spots around the radiator valve (Fig. 5) we observed a temperature difference about 2,4℃ (Sp1 has 42,4℃ – the temperature before the valve; and Sp5 has 40,0℃ –the temperature after the valve).

Meanwhile, the thermos-spots on the radiator surface (Fig. 5) have larger temperature differences, depending on where they were measured:

- on the bottom of the radiator surface Sp2 has 42,6℃ – like Sp1;
- on the upper part of the radiator surface Sp3 has 45,8℃ – a higher temperature than the previous spots;
- on the middle of the radiator surface Sp4 has the highest temperature 49,3℃.

It can be concluded, that in its inside are air gaps and residual deposits, which must be eliminated in order that the radiator to be warmed up the same on all its surface and to emit the optimum heat quantity.

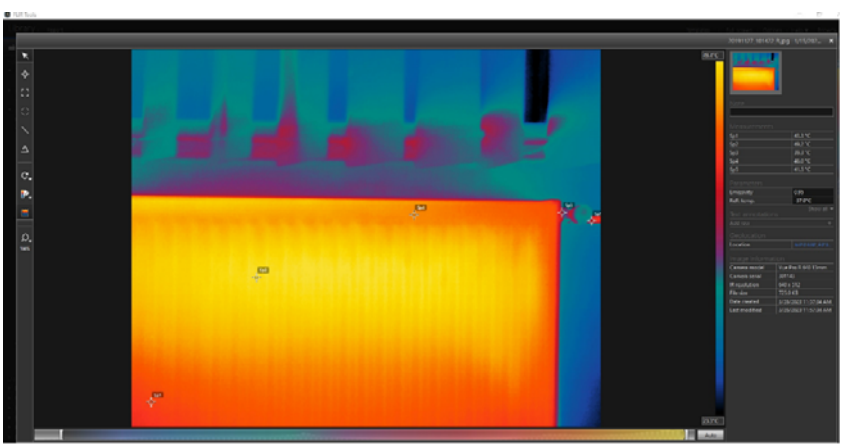

Fig. 5. The interest area from the radiator

In the second part of our study case, when visually analysing the image with the connection point between two heating pipes (Fig. 6), we conclude that: the uniformity of the thermal reflection that appears on the pipe connector indicates that the connection is not fully isolated.

Also, when analysing the image using thermo-spots, we observe a temperature difference between Sp4 (taken on the pipe connector) and Sp5 (taken on the lower part of the pipe connector, where a temperature inconsistency appears) of 4,2℃. This can be

caused either by a very thin crack (not visible with the human eye) in the material from which the connector is made.

Furthermore, when comparing the thermo-spots Sp1 with Sp7, thermal spots taken on the two pipes (above and under the connector – Fig. 6), we observe that the emitted radiation is almost the same (Sp1 – 46,0℃ and Sp7 – 45,3℃ resulting only a 0,7℃ difference which can appear due to the interaction between two different environments - the air inside the office, which has a lower temperature, and the heating pipe, which has a higher temperature because of the hot water circulating through it).

Moreover, when analysing the area around the pipe connector (Sp2 - 36,6℃, Sp3 - 37,8℃ and Sp6 - 34,7℃) we observe that the radiation values are all around 36,37℃, a lower value comparing to the emitted radiation from the pipes (Sp1 and Sp7 – a medium value of 45,65℃), that can be caused to the residual deposits on the area where the two pipes are connected.

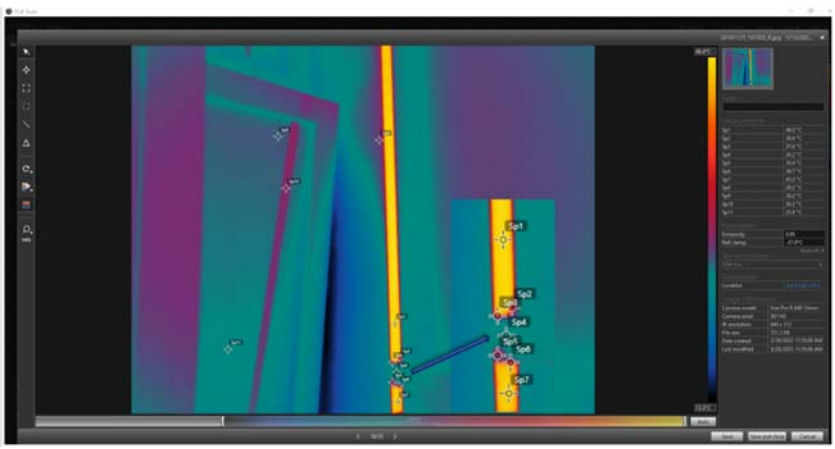

Fig. 6. The connection point between two pipes

In the third part of our study case, on the pipe entering point from the office' celling, when visually analysing the image, inconsistencies of the emitted radiation can be observed (around the entering point on the celling and also on the pipe – Fig. 7).

These inconsistencies are also confirmed when analysing the image using the thermos-spots function from the processing software:

- thermo-spot Sp1 was taken on the pipe, where the first inconsistency appears. It can be observed that is an isolated area which reflects a lower quantity of radiation, so we can conclude that in that area, a residual deposit is inside the pipe;
- comparing the radiation vales of thermo-spots Sp2 and Sp4 (points selected on the celling, on both sides of the pipe) it can be observed that Sp4 has a lower radiation value than Sp2, indicating that on the celling may be a leakage around the entering point.

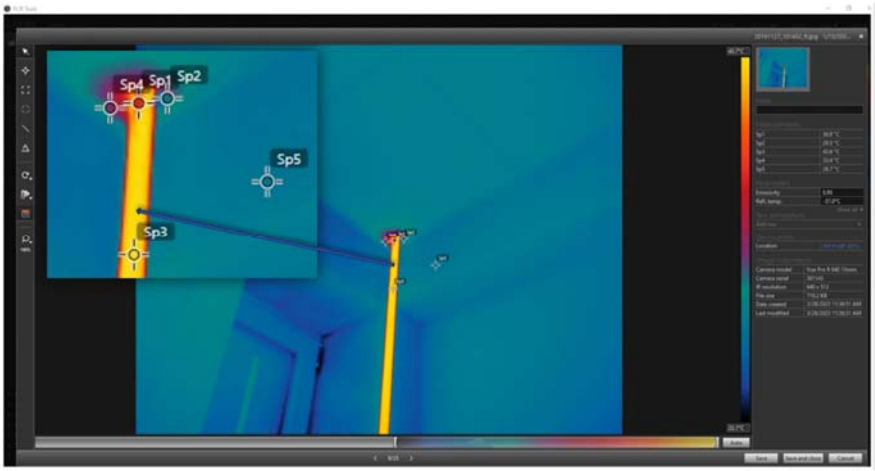

Fig. 7. The pipe entering point from the office' celling

4. Conclusions

So, we can conclude that Thermography is a useful method for heating installation monitoring because:

- it is contactless – the thermal scanning is made from a distance, where both the operator and the target are safe;
- it is bi-dimensional – the thermal footprint can be visualized/analysed, the obtained information regarding the analysed object are complete and different areas of the studied object can be compared;
- it is obtained in real time – it permits both moving and standing object thermal scanning.

Furthermore, when analysing the data both a qualitative and quantitative analyse can be done (Fig. 8).

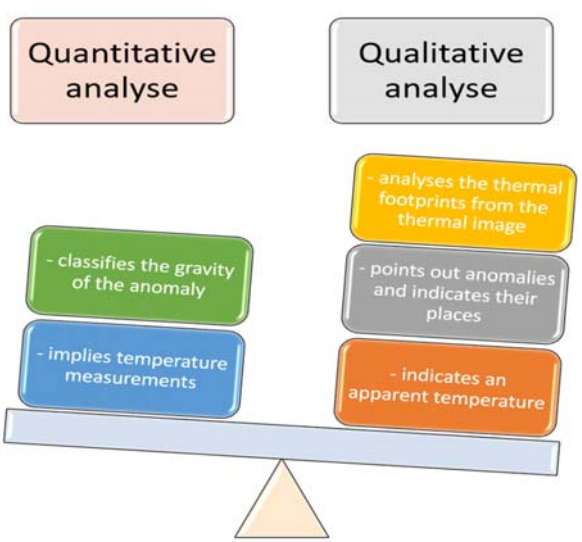

Fig. 8. The quantitative and qualitative analyse of a thermal scanning

But always must be taken into account that the material type, the surface structure and geometry are key factors that can influence the emissivity and of course the quality of data interpretation and processing.

References

[1] https://www.flir.com/discover/why-use-infrared/
[2] Tartarini, F., Schiavon, S., Cheung, T., Hoyt, T., 2020. CBE Thermal Comfort Tool: online tool for thermal comfort calculations and visualizations. SoftwareX 12, 100563. https://doi.org/10.1016/j.softx.2020.100563
[3] Parkinson, Thomas; de Dear, Richard (2014-12-15). "Thermal pleasure in built environments: physiology of alliesthesia". Building Research & Information. 43 (3): 288-301. ISSN 0961-3218. S2CID 109419103. doi:10.1080/09613218.2015.989662.
[4] Carlos Lerma, Eva Barreira, Ricardo M.S.F. Almeida A discussion concerning active infrared thermography in the evaluation of buildings air infiltration, Energy and Buildings, Volume 168, 2018, pp. 56-66, https://doi.org/10.1016/j.enbuild.2018.02.050
[5] Zhi Qu, Peng Jiang and Weixu Zhang, Development and Application of Infrared Thermography Non-Destructive Testing Techniques, Sensors 2020, 20, 3851; doi:10.3390/s20143851
[6] Tartarini, F., Schiavon, S., Cheung, T., Hoyt, T., 2020. CBE Thermal Comfort Tool: online tool for thermal comfort calculations and visualizations. SoftwareX 12, 100563. https://doi.org/10.1016/j.softx.2020.100563
[7] Ameersing Luximon, Huang Chao2, Ravindra S. Goonetilleke and Yan Luximon Theory and applications of InfraRed and thermal image analysis in ergonomics research, Computer Vision Volume 4 –2022 | https://doi.org/10.3389/fcomp.2022.990290
[8] Thermography Theory—Physical Basics|InfraTec GmbH. Available online: https://www.infratec.eu/thermography/service-support/glossary/theory/ (accessed on 9 april 2023).
[9] https://www.flir.com/discover/what-is-infrared/
[10] https://hti-instrument.com/blogs/news/thermal-imaging-principle

Theoretical and Experimental Aspects of Sustainable Rainwater Management in a Residential Area

Aspecte teoretice și experimentale privind gestionarea sustenabilă a apelor meteorice într-un ansamblu rezidențial

Andrei Bolboacă[1], Dan Mureșan[1], Anagabriela Deac[1], Cristina Iacob[1], Teodor Chira[1]

[1]Technical University of Cluj-Napoca, Faculty of Plant Engineering
B-dul. 21 Decembrie 1989, nr. 128-130, Mun. Cluj-Napoca
E-mail: andrei.bolboaca@insta.utcluj.ro, muresan.dan@insta.utcluj.ro, cristina.iacob@insta.utcluj.ro, anagabriela.deac@insta.utcluj.ro, teodor.chira@insta.utcluj.ro

DOI: 10.37789/rjce.2023.14.4.10

Abstract. *In the paper, the authors address the issue of rainwater management, which represents a renewable, clean, and cost-free resource. However, currently, the way to reintroduce it into the environment is not sustainable because it is done with high energy consumption and at significant expenses. The case study presents a solution whereby, with a small investment, rainwater is returned to the natural water cycle in nature.*

Keywords: rainwater, rainwater management, circular economy

1. Introduction

Rainfall collection has been used historically to conserve water, especially in areas with little or difficult access to alternative water sources.

Rising water demand, greater interest in conservation of water and energy, and increased regulatory emphasis on reducing stormwater runoff volumes and related pollutant loads have all led to a renewed interest in water use techniques among researchers and policymakers in recent years [1].

Understanding the importance of rain and making the most use of both the rain and the place where it falls are important aspects of rainwater harvesting and conservation [2].

Urban stormwater management practices in place today are meant to quickly collect, transport, and evacuate excessive runoff outside the urban areas. This can lead to flash floods, downstream flooding in significant stream channels, costly property damage, and washout of structures. The problem is made even more complicated by the unpredictability of the climate in the future. For localities with existing infrastructure, the change in precipitation in the future may have very serious ramifications for managing and controlling flooding.

With the application of best practices management within the watershed, stormwater quantity can be decreased, and stormwater quality can be increased. Detention/retention basins, infiltration basins or trenches, dry wells, sediment traps, vegetated swells, bioretention, and artificial wetlands are a few examples of structural best management techniques. By containing peak flows, eliminating pollutants via physical and biological processes, and allowing stormwater to seep in to recharge aquifers, the placement of these structures within a watershed has the potential to lessen flooding [3].

Due to climate change, there is a general increase in rainfall and especially an increase in extreme events such as 'cloudbursts', which, due to the high intensity of rainfall in a short period of time, cause flooding with negative effects on the quality of life. In this context, the sustainable management of stormwater is a highly topical issue, especially as it is found in very large quantities in short periods of time. The technical solution of using stormwater retention tanks and subsequent controlled discharge into sewerage networks is not a sustainable solution in terms of recycling, infiltration, and reuse.

One solution is the use of storage tanks and the gradual infiltration of water into the ground, thus returning the water to its natural circuit and at the same time relieving the sewage network of these quantities of stormwater and, perhaps more importantly, relieving municipal wastewater treatment plants of the need to process these flows of water. In this respect, the concept of circular water economy is becoming increasingly important [4].

In other locations around the world, considering the climatic zone, it may be important to collect rainwater for later use, especially if we do not have an even distribution of rainfall throughout the year [5], [6]. The collected rainwater can be used for gardening, watering green areas, washing driveways and so on. However, care should be taken to avoid collecting rainwater from heavily polluted areas in the immediate vicinity of industrial areas that release pollutants into the environment if reuse is intended.

With this paper, the authors aim to present a case study of stormwater storage in a residential development using retention and infiltration tanks.

2. Case study

The solution chosen to be implemented in this particular case is to store stormwater collected from the built-up areas of a residential area in a retention and infiltration tank that can be placed either in the green area, under the alleys or in the

traffic zone with a maximum speed of 60 km/h. The material used for this kind of tanks is tested for high load resistance. Another point to note is that new technologies on the manufacturing lines can produce these tanks from recyclable materials, the one used in this case being made from PP-B polypropylene.

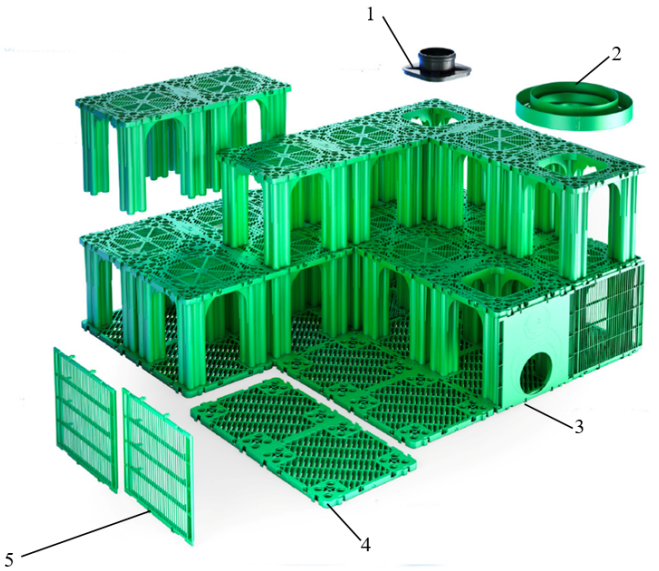

Fig. 1. Retention and infiltration tank [4]
1 and 2 - adapters, 3 - connection plate, 4 - bottom plate, 5 - side wall.

The design of an infiltration tank can be adapted to the available space because it has a modular design. A parallelepiped module measures 1200×600×600 mm and occupies a volume of 432 l, which can store 412.6 l of water. For situations where the holding capacity is too low, several interconnected reservoirs could be provided, thus forming a larger capacity reservoir. Three horizontal tunnels 295 mm wide and 500 mm high are provided inside the infiltration tank according to the components to facilitate cleaning and video inspection when needed.

A geotextile or geomembrane membrane shall be provided on the entire outer surface of the tank to prevent soil particles from infiltrating into the tank, depending on the role of the tank. The arrangement of the perforations in the tank elements are designed to ensure protection of the geotextile/geomembrane during the pressure cleaning process. The bottom plate is designed to facilitate the cleaning direction.

a b c

Fig. 2. Examples of tank intervention [5].
a - video inspection camera, b and c - pressure water cleaning.

A compacted gravel layer is required when installing the system. Its grain size depends on the use to which the water accumulating in the tank will be put and on the nature of the soil in which it is placed.

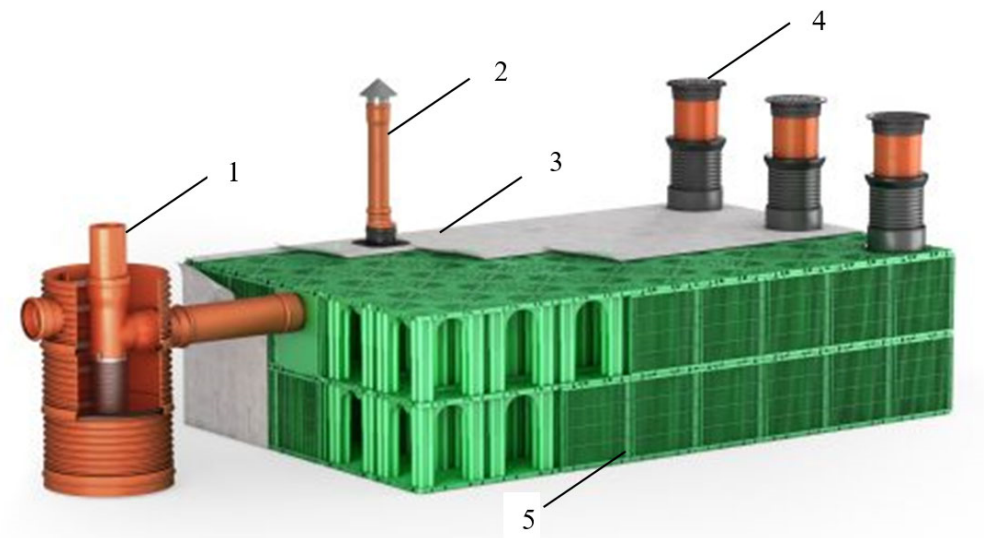

Fig. 3. Tank component elements in final form [5].
1 - sand trap, 2 - vent pipe, 3 - geotextile or geomembrane, 4 - manhole, 5 - tank itself

Thus, in the following we present an application of the system described above, in the case of a residential complex in the Cluj - Napoca area.

The residential complex consists of four buildings A, B, C and D with a height of D+P+7E+R. The total roof terrace area of the four buildings completed so far is 3600 sq m. The residential complex was developed in successive stages: the A building with a terrace area of 732 sqm was completed in 2018, the B building with a terrace area of 1290 sqm was completed in 2019, the D building with a terrace area of 853 sqm was completed in 2020 and the C building with a terrace area of 725 sqm was completed in 2022. Construction work is currently underway on buildings E and F, whose terraces total 1450 square metres. The total area of the terraces will be 5050 sqm.

For the above situation, a retention and infiltration tank with a volume of 48 m^3 was used. The installation was carried out in parallel with the construction of the first two buildings in the complex. After the land was cleared and the site for the tank was excavated, the geomembrane was spread to cover all six outer sides of the parallelepiped tank (see fig. 5). In the next step, the bottom plate was assembled (see fig.5). After the base of the tank was made, it was mounted vertically and the four corners were provided with double-walled polypropylene manholes of DN 400 (see Figs. 6 and 7) to ensure ventilation of the tank.

Fig. 5. Geomembrane preparation and tank bottom plate installation stage

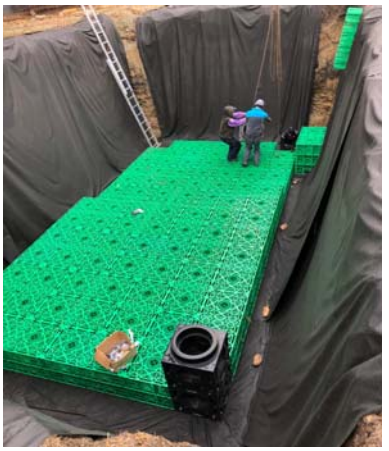

Fig. 6. Details from the tank assembly stage

Once the assembly of the tank components was completed, the tank was covered with geomembrane (see fig. 8). All around the tank, an 80 cm compacted gravel fill was made and covered with soil. (see fig. 9).

Fig. 7. Preparation for geomembrane coating

Fig. 8. Covering the tank with geomembrane

Fig. 9. Preparing the soil for final landscaping

For the built-up areas shown above, we will determine the stormwater flows collected from the buildings. According to current regulations and standards, the design flow rate for stormwater collected from the surfaces of terraces is determined with the relation below [9]:

$$V_{ci} = 0.0001 \cdot i \cdot \Sigma\phi \cdot S_c \qquad [l/s] \quad (1)$$

where i is the design rainfall intensity in [l/s-ha];

ϕ - the coefficient of stormwater water runoff from the design surface;

S_c - design area, in [m^2], corresponding to the drainage coefficient ϕ.

A design rainfall intensity of 320 l/s-ha for a design rainfall duration of 5 minutes with a rainfall frequency of ½ was used to determine these flows collecting from the walkable terraces of the buildings and a design surface runoff coefficient of stormwater, $\phi = 0.85$, was applied.

Table 1

Stormwater flow per building

Building	S_c	t	f	i	ϕ	V_{ci}
	[m^2]	[min]	[-]	[l/s-ha]	[-]	[l/s]
A	732,00	5	1/2	320	0.85	19.91
B	1290.00	5	1/2	320	0.85	35.09
C	725.00	5	1/2	320	0.85	19.72
D	853.00	5	1/2	320	0.85	23.20
E	600.00	5	1/2	320	0.85	16.32
F	850.00	5	1/2	320	0.85	23.12
TOTAL	5050.00	5	1/2	320	0.85	137.36

According to the phased implementation of the building complex, in 2018 a flow of 19.91 l/s was collected from the built-up areas, in 2019 a flow of 55.00 l/s was collected, in 2020 and 2021 78.20 l/s and in 2022 97.92 l/s.

Reviewing the statistical data on the average amount of precipitation that fell in the years 2018-2022, in the following we will examine how much water accumulated in the reservoir.

Table 2

Monthly precipitation amount in Cluj - Napoca [10]

Month	2018	2019	2020	2021	2022
January	9.90	59.00	8.80	30.30	16.70
February	27.10	19.40	39.30	23.60	11.40
March	40.90	18.00	48.60	41.60	9.90
April	23.00	73.20	30.70	41.70	49.30
May	36.40	136.20	56.90	74.30	97.40
June	173.40	36.40	109.30	33.60	19.90
July	68.60	37.80	60.20	130.60	25.20
August	22.00	57.20	88.30	70.60	87.80
September	48.80	18.40	42.60	31.10	91.70
October	61.60	18.10	50.70	12.10	29.20
November	32.00	18.90	21.00	23.00	20.10
December	74.80	16.40	37.20	73.70	24.20

Table 3

Annual rainfall amounts collected in the case study

Year	Collecting surface	Amount of precipitation accumulated in the tank annually	
	m^2	l	m^3
2018	732	452742	452.7
2019	2022	1029198	1029.2
2020	2875	1706600	1706.6
2021	2875	1685325	1685.3
2022	3600	1143360	1143.4

These volumes of water infiltrated back into the ground during the non-rainfall period and were returned to the natural water cycle without the need for additional costs associated with disposal. Since the collecting surface is represented by the walkable terraces of the buildings, the water quality is considered conventionally clean and can therefore be returned to the soil.

3. Conclusions

According to the data presented above, there is a continuous increase in the volume of water discharged into the reservoir, reaching a significant volume of 1143.40 m^3 of stormwater in 2022, exceeding the reservoir capacity by 23.81 times. From periodic visual checks of the tank, it was found that the water level in the tank never reached the level of the overflow pipe, so the amount of water reaching the tank was fully infiltrated into the soil, indicating the functionality of the proposed technical solution.

In this context, the use of storage and infiltration tanks is a sustainable solution as a first step in "Turning stormwater into a valuable asset".

References

[1] *Environmental Protection Agency (EPA)* Rainwater Harvesting Conservation, Credit, Codes, and Cost Literature Review and Case Studies, 2013

[2] *Celeste Allen Novak, Eddie Van Giesen, Kathy M. DeBusk* - Designing Rainwater Harvesting Systems: Integrating Rainwater into Building Systems

[3] R. Ghazal, A. Ardeshir, I.Zahedi Rad Climate Change and Stormwater Management Strategies in Tehran 16th Conference on Water Distribution System Analysis, Procedia Engineering Volume 89, 2014, Pages 347-354

[4] *Mbavarira, T.M.; Grimm, C.* A Systemic View on Circular Economy in the Water Industry: Learnings from a Belgian and Dutch Case. Sustainability 2021, 13, 3313. pg. 1 – 62. https://doi.org/10.3390/su13063313

[5] *Liaw, Chao-Hsien and Yao-Lung Tsai*, 2004. Optimum Storage Volume of Rooftop RainWater Harvesting Systems for Domestic Use. Journal of the American Water Resources Association (JAWRA) 40(4): pg.901-912.

[6] *Shuster, William D., Dennis Lye, Armah De La Cruz, Lee K. Rhea, Katharine O'Connell, and Amanda Kelty*, 2013. Assessment of Residential Rain Barrel Water Quality and Use in Cincinnati, Ohio.Journal of the American Water Resources Association (JAWRA) 49(4): pg. 753-765. DOI: 10.1111/jawr.12036,

[7] https://www.pipelife.com/buildings/rainwater-and-drainage.html, accessed at 04.04.2023.

[8]https://www.pipelife.ro/content/dam/pipelife/romania/marketing/general/cataloage/Stormbox_VF_BT_2021.pdf, accessed at 04.04.2023.

[9] Standard for the design, execution and operation of plumbing installations in buildings, indicative I9-2022.

[10] https://www.casomes.ro/wp-content/uploads/2014/12/Arhiva-precipitatii.pdf, accessed at 04.04.2023.

[***]1-s2.0-S1877705814026228-main.pdf

Causes and consequences of work events in electrical and technical-sanitary installation enterprises from Timis County

Cauze si consecinte ale evenimentelor de muncă în întreprinderile de instalații electrice și tehnico-sanitare din județul Timis

Rudolf Mirescu[1], Dumitru Tucu[1]

[1]Politehnica University Timișoara,
Piata Victoriei Nr.2, 300006 Timisoara, Romania
E-mail: rudolfmirescu@yahoo.com, dumitru.tucu@upt.ro

DOI: 10.37789/rjce.2023.14.4.11

Abstract. *The paper identifies and hierarchize all factors and causes of work events in the field of enterprises specialized in building facilities and environmental comfort, from Timiș County, considered as integrated part in the process of optimization of specific occupational health and safety risk management systems (OHSRMS). Based on activities (CAEN code 4321 and 4322), the work events from the last 10 years were extracted from official statistics, correlated with number of employees, factors and causes (also, special conditions). 1397 enterprises were selected. The relevance was verified by Fisher test and ANOVA, and possible relations based on work events were identified.*

Key words: work accident/event, optimization, occupational health and safety risk management system

1. Introduction

The technical-sanitary installation industry is usually intensive, and even accident rates in this industry have been steadily decreasing [1], work accidents rate are still higher related to other industries [2]. According to an Eurostat report on total work accidents, 3 355 fatal accidents at work were in the EU during 2020 (for Romania during 2019 a 3,0 incidence rate per 100 000 persons employed), a decrease of 53 deaths compared with the year before [3].

Several studies of root causes were carried out to eliminate fatal incidents in the construction/installation industry [4, 5]. Many studies indicate that such work is not an ergonomics-friendly job, often involving heavy physical labour, unconventional postures, constant bending and reaching movements, unfavourable climatic conditions [6].

Because the most fatal incidents occur during the construction phase, the best way to prevent such incidents was considered to identify their potential occurrence in advance.

The fatal incidents in the construction industry can be identified in advance considering the characteristics of the project.

The main characteristics of construction accidents are the following (7, 8, 9, 10):

- there are various tasks depending on the project type (usually `all' is a major fatal incident during building/installation construction projects; also 'Traffic accident', and however, `Overturning the banks of ditches`);
- the work is different ('Fall', 'Slip' are major causes of accident; 'Electric shock' is the hazard that should be considered most importantly during electrical work [11];
- the accident type should be subdivided clearly (example: the categories of 'Fall', 'Be hit', and 'Traffic accident');
- in the field of construction/installation, the perception of risk factors at work, almost consequences of accidents, still remaining at low level, [12, 13, 14, 15].

Starting at authors experience in the frame of health & safety work requirements, the paper has the main objective to account and hierarchize the significant work events in electrical and technical-sanitary installation enterprises, in Timiș County, the factors, causes and consequences, considering all actions as integrated parts in the process of assessment and general optimization of specific occupational health and safety risk management systems (OHSRMS).

2. Methods

Starting at specific activity of enterprises (CAEN code 4321 (Electrical works), and 4322 (Plumbing, heating, and air conditioning works)), 1397 enterprises were selected for study.

All the work events from 10 years (2012-2021 year), were extracted from official statistics, in the same time correlated with number of employees, factors and causes (if necessary, special conditions). 12 groups were selected. Based on statistical methods and reports of work events/employee, the groups were evaluated according to the work and healthy risks.

Only enterprises with accidents were considered for statistical analysis. The relevance of results was verified using Fisher test. Possible relations between activities and work events were identified using ANOVA.

Statistical analysis used Microsoft Excel and STATEGRAPHICS Centurion XVI. Conclusions and results of present work were prepared to be generally used in practical optimization of the OHSRMS for improve the conformity with EU and national strategy.

3. Results and discussion

Table 1 presents information collected (enterprises with minimum one accident/year).

Table 1

Recorded accident in electrical and technical-sanitary installation enterprises, Timiș County between 2012-2021

Year	CAEN	Enterprise	Dead			Invalidity			T I W					
			E	Ad	AR	E	Ad	AR	E	Ad	AR	D	N	EN
2012	4322	CASITHERM SERVICE SRL	0	0	0	0	0	0	1	0	0	46	1	16
		CONFORT SRL	0	0	0	0	0	0	1	0	0	55	1	579
		BEMAD YCE SRL	0	0	0	1	0	0	0	0	0	272	1	15
TOTAL c						**1**			**2**	**0**	**0**	**373**	**3**	**610**
2013	4321	GRUP SIN ELECTRIC SRL	0	0	0	0	0	0	1	0	0	31	1	3
		DEMARK CONSTRUCT SRL	0	0	0	0	0	0	0	0	1	268	1	42
		DEMARK CONSTRUCT SRL	0	0	0	0	0	0	0	0	1	87	1	42
		DEMARK CONSTRUCT SRL	0	0	1	0	0	0	0	0	0		1	42
		COMANDOR SRL	0	0	0	0	0	0	0	0	1	22	1	59
		COMANDOR SRL	0	0	0	0	0	0	0	0	1	45	1	59
TOTAL c					**1**				**1**		**4**	**453**	**6**	**247**
	4322	CONFORT SA	1	0	0	0	0	0	0	0	0	0	1	151
		MI TAM AIR CON-DITIONERS SRL	0	0	0	0	0	0	0	0	1	65	1	12
TOTAL c			**1**								**1**	**65**	**2**	**163**
TOTAL y			**1**		**1**				**1**		**5**	**518**	**8**	**410**
2014	4321	SC ELECTRIC SG INSTAL SRL	0	0	0	0	0	0	0	1	0	15	1	8
		SC MELBO INSTAL SRL	0	0	0	0	0	0	1	0	0	38	1	34
		SC COMANDOR SRL	0	0	0	0	0	0	1	0	0	51	1	58
TOTAL c									**2**	**1**		**104**	**3**	**100**
2015	4321	LOGIMAETICS ELECTRIC SRL	0	0	0	0	0	0	1	0	0	86	1	31
	4322	FLEXIK AUTOMATION SRL	0	0	0	0	0	0	1	0	0	60	1	207
		TERMODINAMICA SRL	0	0	0	0	0	0	1	0	0	3	1	16
TOTAL c									**2**			**63**	**2**	**223**
TOTAL y									**3**			**149**	**3**	**254**
2016	4322	HIDROPLUS SRL	0	1	0	0	0	0	0	0	0		1	14
		DINU INSTAL SRL	0	1	0	0	0	0	0	0	0		1	46
		AGASI SRL	0	0	0	0	0	0	1	0	0	24	1	157
		RADEL & HAHN SRL	0	0	0	0	0	0	1	0	0	14	1	30
		MI TAM AIR CON-DITIONERS SRL	0	0	0	0	0	0	1	0	0	90	1	15
		AGASI SRL	0	0	0	0	0	0	0	1	0	24	1	157

		AGASI SRL	0	0	0	0	0	0	1	0	0	148	1	157
TOTAL c				**2**					**4**	**1**		**300**	**7**	**576**
2017	4321	ELECTRO BENCONS SRL	0	0	0	0	0	0	0	1	0	180	1	21
		GLOBAL SOLUTIONS SRL	0	0	0	0	0	0	0	0	1	31	1	14
		GLOBAL SOLUTIONS SRL	0	0	0	0	0	0	0	0	1	82	1	14
TOTAL c										**1**	**2**	**293**	**3**	**49**
	4322	PIPETECH SRL	0	0	0	0	0	0	1	0	0	152	1	13
TOTAL c									**1**	**1**	**2**	**445**	**4**	**62**
2018	4322	ROLIFT SERV SRL	0	0	0	0	0	0	1	0	0	24	1	5
TOTAL c									**1**			**24**	**1**	**5**
2019	4322	RADEL & HAHN SRL	0	0	0	0	0	0	1	0	0	59	1	27
		DISTRI-REVIZII-VERIFI-CARI DPM S.R.L.	1	0	0	0	0	0	0	0	0	0	1	2
		DINU INSTAL SRL	0	0	0	0	0	0	1	0	0	47	1	34
		AGASI SRL	0	0	0	0	0	0	1	0	0	32	1	147
TOTAL c			**1**						**3**			**138**	**4**	**210**
2020	4321	ELECS MONTAJ S.R.L.	0	0	0	0	0	0	1	0	0	17	1	13
		CONS ELECTRIFICAREA INSTAL SRL	0	0	0	0	0	0	0	0	1	51	1	115
		DANNYS-M.D. SRL	0	0	0	0	0	0	1	0	0	5	1	12
TOTAL c									**2**		**1**	**73**	**3**	**140**
2021	4321	GLOBAL SOLUTIONS SRL	0	0	0	0	0	0	1	0	0	72	1	13
	4322	INSTGAT SRL	0	0	0	0	0	0	1	0	0	12	1	51
TOTAL y									**2**			**84**	**2**	**64**
TOTAL P			**2**	**2**	**1**	**2**			**21**	**3**	**8**	**2208**	**38**	**2431**

In table 1, the significance are: E – accidents caused by the employee; Ad - accidents caused by administration or responsible work safety; AR – accident on road from/to workplace; D – days of temporary inability; N – number of accidents cumulated on enterprise/year; EN – employee's number/year; TOTAL c– total on activity's code; TOTAL y – total on year (more cods); TOTAL P – total for all considered activities and years (panel).

Analyzing processed data Microsoft Excel, next conclusions could be formulated:

- In the analyzed period both groups of activity generated work accidents, with small differences between groups (17 versus 21);

- The results used in statistic were calculated at 1000 employees according to actual used solutions [16].

The first analysis studied the character of relationship between number of accidents on year, N, and number of employees NE, starting at simple regression considering relevant S-curve model ($Y = \exp(a + b/X)$). (Such model was considered adequate after linear or/and nonlinear models were tested). Here Y is total yearly number of accidents (column N at rows TOTAL y in table 1), and X is the total

number of employees (NE, in same conditions). The results of STATGRAPHICS indicated the optimum equation of the fitted model:

$$N = exp(1.37568 - 7.10394/NE) \quad (1)$$

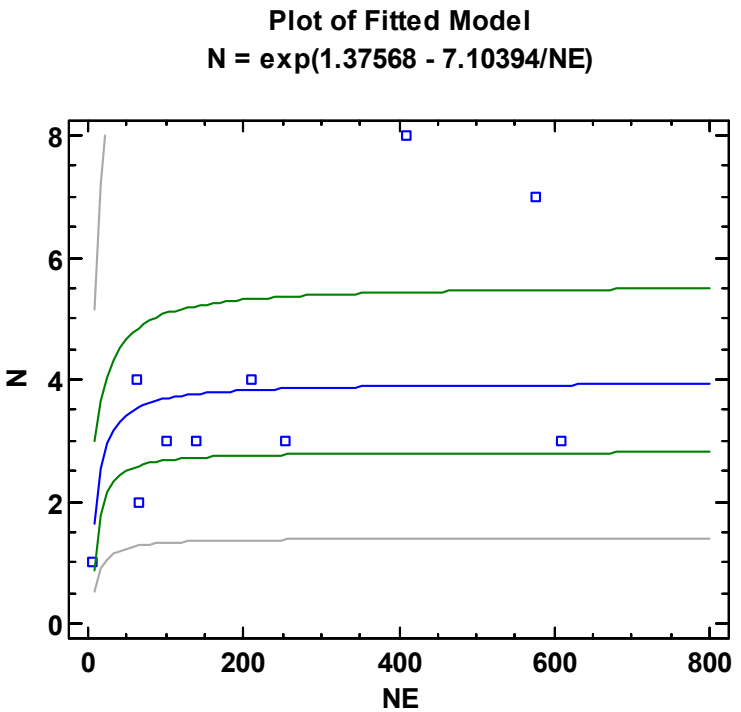

Fig. 1 The plot of fitted model for function N=f(NE)

Table 2

Results for coefficients and analysis of variance for function N=f(NE)

Coefficients

	Least Squares	Standard	T	
Parameter	Estimate	Error	Statistic	P-Value
Intercept	1.37568	0.146888	9.36553	0.0000
Slope	-7.10394	2.30229	-3.0856	0.0150

Analysis of Variance

Source	Sum of Squares	Df	Mean Square	F-Ratio	P-Value
Model	1.70407	1	1.70407	9.52	0.0150
Residual	1.43185	8	0.178982		
Total (Corr.)	3.13592	9			

In Figure 1 can be seen the position in graphic and in Table 2 the results for coefficients and analysis of variance. The R-Squared statistic indicates that the model

as fitted explains 54.3402% of the variability in N. The correlation coefficient equals -0.737158, indicating a moderately strong relationship between the variables. The standard error of the estimate shows the standard deviation of the residuals to be 0.423062. The mean absolute error (MAE) is 0.30368. Since the P-value is greater than 0.05, there is no indication of serial autocorrelation in the residuals at the 95.0% confidence level.

Regarding the possible relationship between number of days of temporary inability, D, and number of employees NE, in Fig. 2 can be seen the plot of fitted model in graphic and in table 3 the results for coefficients and analysis of variance in the same conditions of regression.

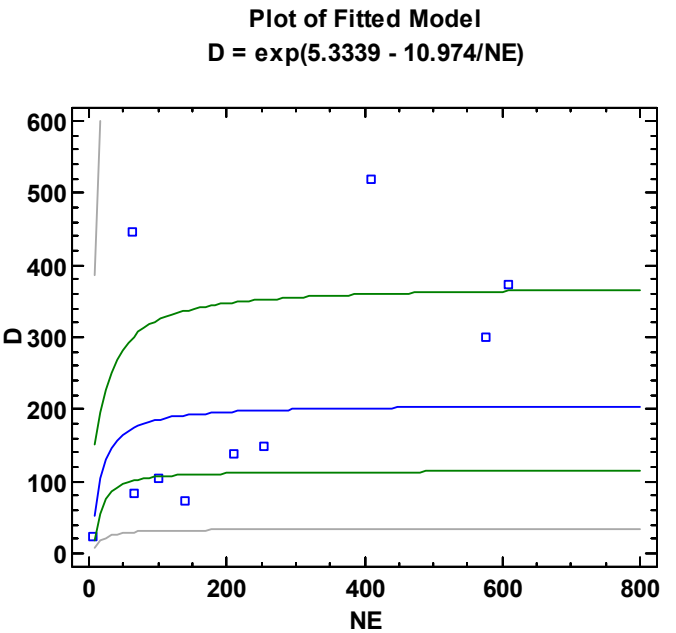

Fig. 2 The plot of fitted model for function D=f(NE)

Table 3

Results for coefficients and analysis of variance for function N=f(NE)

Coefficients

	Least Squares	*Standard*	*T*	
Parameter	*Estimate*	*Error*	*Statistic*	*P-Value*
Intercept	5.3339	0.254694	20.9424	0.0000
Slope	-10.974	3.99203	-2.74898	0.0251

Analysis of Variance

Source	*Sum of Squares*	*Df*	*Mean Square*	*F-Ratio*	*P-Value*
Model	4.06647	1	4.06647	7.56	0.0251
Residual	4.30492	8	0.538115		
Total (Corr.)	8.37139	9			

The results shows the results of fitting a S-curve model to describe the relationship between D and NE. The equation of the fitted model is

$$D = exp(5.3339 - 10.974/NE) \quad (2)$$

Since the P-value in the ANOVA table is less than 0.05, results a statistically significant relationship between D and NE at the 95.0% confidence level. The R-Squared statistic indicates that the model as fitted explains 48.5758% of the variability in D. The correlation coefficient equals -0.696964, indicating a moderately strong relationship between the variables. The standard error of the estimate shows the standard deviation of the residuals is 0.733563. The mean absolute error (MAE) is0.583515. Because P-value is greater than 0.05, there is no indication of serial autocorrelation in the residuals at the 95.0% confidence level.

4. Conclusions

The obtained results justify once again the necessity to extend health and safety measures in the technical-sanitary installation industry and continuous improvement of occupational health and safety risk management systems, because, opposite to present measures, the work is still usually intensive, and even accident rates in this industry have been steadily decreasing, work accidents rate are still higher related to other industries (The present statistics demonstrated an average about one day of temporary incapacity of work/employee/year!). A special mention was justified for enterprise less than 50 employees (micro and small enterprises), when the number of work accidents is dependent of number of employees. If the number of employees is greater than 100, the number of work accidents keep the same. All hypothesis from introduction were demonstrated.

References

[1] B.H. Guo, T.W. Yiu, V.A. Gonzalez, Predicting safety behavior in the construction industry: development and test of an integrative model, Saf. Sci. 84, 1–11, 2016, https://doi.org/10.1016/j.ssci.2015.11.020, accessed March 2023

[2] S.S., Man, A.H.S., Chan, S. Alabdulkarim, and T., Zhang, "The effect of personal and organizational factors on the risk-taking behavior of Hong Kong construction workers", Safety Science, Vol. 136, 105155, 2021

[3] ***, EUROSTAT, Statistic Explained, 2020, https://ec.europa.eu/eurostat/statistics-explained/index.php?title=Accidents_at_work_statistics, accessed March 2023

[4] W.M. Alruqi, M.R. Hallowell, U. Techera, Safety climate dimensions and their relationship to construction safety performance: a meta-analytic review, Saf. Sci. 109 165–173, 2018 https://doi.org/10.1016/j.ssci.2018.05.019, accessed March 2023

[5] R.S. Fediuk, V.S. Lesovik, Y.L. Liseitsev, R.A. Timokhin, A.V. Bituyev, M. Y. Zaiakhanov, A.V. Mochalov, Composite binders for concretes with improved shock resistance, Mag. Civ. Eng. 85 (1), 2019 145, https://doi.org/10.18720/MCE.85.3, accessed March 2023

[6] BY., Jeong, Occupational deaths and injuries in the construction industry, Appl. Ergon, 29(5), 355–360, doi:10.1016/S0003-6870(97)00077-X, 1998

[7] H.B. Zhou, H. Zhang, Risk assessment methodology for a deep foundation pit construction project in Shanghai, China, J. Construct. Eng. Manag. 137 (12) 1185–1194, 2011, https://doi.org/10.1061/(ASCE)CO.1943-7862.0000391, accessed March 2023
[8] M.W. Moon, K.Y. Yang, A study on the major construction accidents analysis using work classification system, in: Proceedings of the Architectural Institute of Korea Structure & Construction Conference, pp. 711–713, 16(2), 1996
[9] J.B. Lee, M.R. Ro, S.S. Go, The property of building construction accident according to the analysis of building accident cases, J. Kor. Soc. Saf. 19 (3) 101–107, 2004
[10] T. Niskanen, O. Saarsalmi, Accident analysis in the construction of buildings, J. Occup. Accid. 5 (2), 89–98, 1983, https://doi.org/10.1016/0376-6349(83) 90014-7, accessed March 2023
[11] M. Suarez-Cebador, J.C. Rubio-Romero, A. Lopez-Arquillos, Severity of electrical accidents in the construction industry in Spain, J. Saf. Res. 48 63–70, 2014, https://doi.org/10.1016/j.jsr.2013.12.002, accessed March 2023
[12] D.,Bodescu, A.-D., Robu, A.F., Jiťareanu, I., Puiu, A.M., Gafencu, F.D., Lipşa, Work Satisfaction in the Food Industry—A Premise for Economic Performance. In: Agriculture. 12, 1015. 2022, https://doi.org/10.3390/agriculture12071015, accessed March 2023
[13] G.C., Crisan, D., Tucu, R., Boboescu, Improvement of safe & healthy work systems in agricultural SME's. In: ACTUAL TASKS ON AGRICULTURAL ENGINEERING, Book Series: Actual Tasks on Agricultural Engineering-Zagreb, vol.45, 657-663, 2017
[14] D., Tucu, G.C., Crisan, A., Tucu, The use of self-assessment in occupational risk management system in SMEs from agriculture. In: Book Series: Actual Tasks on Agricultural Engineering-Zagreb, vol.47, 479-485, 2019.
[15] A., Tucu, G.C., Crisan, D., Tucu, A., Vasilica, Motivational factors in systems of occupational risk management in agriculture. In: Actual Tasks on Agricultural Engineering, Zagreb, Vol. 48, 521-526, 2021.
[16] R., Mitchell, R., Lystad, Occupational injury and disease in the Australian aquaculture industry. Marine Policy 99, 216–222, 2019.

Agro-waste addition in the mixture for building geopolymer concrete manufacture

Adăugarea unui deșeu agricol în amestecul pentru fabricarea betonului geopolimeric pentru construcții

Bogdan Valentin Păunescu[1], Lucian Păunescu[2], Enikő Volceanov[3,4]

[1] Consitrans SA
56 Polona street, sector 1, Bucharest 010504, Romania
E-mail: pnscbogdan@yahoo.com

[2] Cosfel Actual SRL
95-97 Calea Grivitei street, M4 room, sector 1, Bucharest 010705, Romania
E-mail: lucianpaunescu16@gmail.com

[3] University „Politehnica" of Bucharest
313 Independence Splai, sector 6, Bucharest 060042, Romania
E-mail: evolceanov@yahoo.com

[4] Metallurgical Research Institute SA
39 Mehadia street, sector 6, Bucharest 060543, Romania
E-mail: evolceanov@yahoo.com

DOI: 10.37789/rjce.2023.14.4.12

Abstract. *Geopolymer concrete based on fly ash including an agro-waste (corn cob ash) was chosen as the optimal version as a result of the experiment in which granulated blast furnace slag was also used in the other versions. The alkaline activator solution for developing the geopolymerization reaction was kept. Also, usual curing technique was used to increase the mechanical strength. The geopolymer concrete specimen with corn cob ash addition made in the optimal version had the following features: density-2369 $kg \cdot m^{-3}$, porosity-34.8 %, heat conductivity-0.509 $W \cdot m^{-1} \cdot K^{-1}$, compressive strength-25.9 MPa (after 7 days) and 39.8 MPa (after 28 days).*

Key words: *geopolymer concrete, agro-waste, corn cob ash, alumino-silicate waste, alkaline activator.*

Rezumat. *Betonul geopolimeric pe bază de cenușă zburătoare incluzând un deșeu agricol (cenușa de știulete de porumb) a fost ales ca variantă optimă ca urmare a experimentului în care zgura granulată de furnal a fost de asemenea utilizată în celelalte variante. Soluția de activator alcalin pentru dezvoltarea reacției de geopolimerizare a fost menținută. De asemenea, tehnica uzuală de întărire a fost aplicată pentru creșterea rezistenței mecanice. Proba de beton geopolimeric cu adaosul cenușii de știulete de*

porumb produs in varianta optimă a avut următoarele caracteristici: densitatea-2369 kg·m^{-3}, porozitatea-34,8 %, conductivitatea termică-0,509 W·m^{-1}·K^{-1}, rezistența la compresiune-25,9 MPa (după 7 zile) și 39,8 MPa (după 28 zile).

Cuvinte cheie: beton geopolimeric, deșeu agricol, cenușă de știulete de porumb, deșeu aluminosilicatic, activator alcalin.

1. Introduction

Ever since the beginning (in the middle of the 19th century), the modern manufacturing process of conventional construction materials has represented a high carbon footprint. According to [1, 2], the manufacture of cement, that requires high consumption of fossil fuel to reach the process temperature of 1450 ºC, releases about 0.85 tons of CO_2 for each ton of cement, being one of the excessive sources of greenhouse gases emitted into the atmosphere worldwide. The need to develop ecological and sustainable construction materials and at the same time, cheap and accessible without affecting their quality, represents the main challenge of scientific research in this field.

Agricultural waste such as sugarcane bagasse, wheat straw, rice husk, etc. are not yet valorized properly. The usual strategies include throwing them in landfills and incinerating, which aggravates the problems of environmental protection. However, recent experimental results regarding the use of agro-waste for the manufacture of viable construction materials are known. Except recycled demolition waste of building and industrial waste, the incorporation of agro-waste has been tested for the production of concrete blocks [3]. Rice husk, sawdust, peanut shell, rice straw, and coconut shell have been tried. The results showed that the blocks with agricultural waste had acceptable mechanical strength, but the durability was satisfactory only in the case of using coconut shell and peanut shell.

According to Rahman et al. [4], the fly ash bricks were significantly improved by the addition of 10 % palm oil ash and the highest value of compressive strength was achieved by combining fly ash with palm oil ash in a 1:1 weight ratio.

According to [5], several agro-waste biomass types were analyzed for their possible use in the construction sector. The main type of cereal crop that generates straw is composed of wheat (65 %), rice (50 %) and to a lesser extent barley, sorghum, rye and oats. Coconut husk is one of the main types of agro-waste biomass as well as corn cob, oil palm, and maize husk. Most of the component parts of crops (leaves, stems, fruits, seeds, etc.) are suitable for the manufacture of new bio-based products. In the manufacture of building materials in concrete industry as well as in bricks production, the use of rice husk and sugarcane bagasse as biomaterials in the form of ash and to a lesser extent as fibers is known.

Several works note that silica (SiO_2) is the main component of the ash of agricultural waste. According to [6], the silica content in rice husk ash and sugarcane bagasse is much higher, reaching values within the limits of 60-95 %. Also, the pozzolanic properties of these ashes determine their effectiveness for increasing the

level of physical, mechanical, and thermal characteristics (durability, strength, heat conductivity, porosity, workability, etc.) of bio-based products.

Fibers from cereal straws are used in the manufacture of bricks and as filler in polymer molds for structural reinforcement and thermal/ acoustic insulation [7, 8]. These fibers used in making bio-composites replace partially or totally the wood. Due to the high content of natural fibers, coconut husk is also used in this field. According to [9], coconut husk and rice husk are suitable for the manufacture of biopolymers used in construction.

Currently, one of solutions for the thermal insulation of buildings is the use of flax and hemp fibers, but the level of their application is quite limited. A growing interest in ecological and renewable materials has been noted lately. The use of natural fibers as a component of the insulation is directed especially towards the construction sector. Cellulosic insulations having a higher moisture regain compared to inorganic materials are recommended for old wooden buildings. Recently, several types of mattresses and loose-fill insulations have been developed. Despite their previous use, flax and hemp insulations are considered as new materials in the field of insulations [10].

According to [11], agriculture can become a major source of raw material for different sectors of the economy including the construction sector as a priority. The energy saving due to the efficient thermal insulation of the building is a basic factor of the rational use of energy, directly influencing the level of environmental pollution and greenhouse gas emissions in the atmosphere [12]. The paper [11] analyzes the role of agricultural waste in the concrete industry as aggregate substitutes (sawdust, rice husk, coconut kernel, and cork granules), and Portland cement substitutes (rice husk ash) as well as straw bales used in construction [13] and considers that the use of agricultural waste creates interesting perspectives in the field of ecological construction.

The research team of the authors of the current work has already made a concrete composite with coal fly ash and granulated blast furnace slag as main raw materials reinforced with hemp fibers as agricultural waste [14]. The made product was a concrete geopolymer using alumino-silicate materials representing industrial by-product activated with aqueous alkaline solution composed of sodium silicate (Na_2SiO_3) and sodium hydroxide (NaOH). The experimental results showed the following geopolymer features: density of 327 $kg \cdot m^{-3}$, heat conductivity of 0.094 $W \cdot m^{-1} \cdot K^{-1}$, compressive strength of 8.1 MPa (after 28 curing days), and water absorption of 2.6 vol. %.

The present work aimed at the use of an agricultural waste (corn cob ash) together with industrial alumino-silicate by-products (such as fly ash and granulated blast furnace slag) which by their pozzolanic properties allow the complete replacement of Portland cement for manufacturing a strength geopolymer concrete. Considering that all these raw materials are recycled agricultural or industrial waste, the deeply ecological particularity of the manufacturing process is obvious contributing to the valorization of these residual materials and the significant reduction of greenhouse gas emissions in the atmosphere. The originality of this paper is the addition in variable weight proportions of agro-waste to the already known

combination of alumino-silicate waste, the effects on the geopolymer concrete features being analyzed.

2. Materials and methods

Corn cob is the hard part in the middle of the corn and base of the kernel. Generally, it is used as firewood in the household, but also for the production of numerous food and industrial products including corn oil, starch, sweeteners, beverage, industrial alcohols, etc. [15] and the resulting ash is thrown into landfills creating environmental problems. Corn cob ash can be considered an agricultural by-product, can be recycled and re-used in various ways. One of the possible utilization is as a pozzolanic material in cement and concrete. The ash is silica-rich [16]. According to [17], the chemical composition of corn cob ash contains: 79.3 % SiO_2, 1.0 % Al_2O_3, 0.6 % Fe_2O_3, 9.0 % CaO, 1.5 % MgO, 3.8 % K_2O, 10.8 % LOI.

In this experiment, corn cobs were dried outdoor in the sun heat for 1-2 days to remove the moisture, after which the calcination process took place in a ceramic crucible inserted in a muffle oven at 700 ºC for at least 5 hours, transforming the crystalline state of ash in an amorphous state. The grain size of corn cob ash was under 40 μm. Several calcination methods of corn cobs (relatively similar) were described in the literature [18-20].

Alumino-silicate industrial by-products used in experiment were coal fly ash recycled from energy industry and granulated blast furnace slag recycled from metallurgy industry. Fly ash was provided by Paroseni-Thermal Power Plant (Romania) about six years ago. The oxide composition of fly ash was the following: 54.8 % SiO_2, 24.2 % Al_2O_3, 8.6 % Fe_2O_3, 4.8 % CaO, 3.4 % MgO, 4.2 % (Na_2O + K_2O). The grain size of this material was under 200 μm and required an additional grinding to grain size under 80 μm. Granulated blast furnace slag was provided by ArcelorMittal Galati (Romania) 7-8 years ago and had the following chemical composition: 37.4 % SiO_2, 6.4 % Al_2O_3, 6.9 % Fe_2O_3, 39.9 % CaO, 3.5 % MgO, 2.3 % MnO, 0.1 % Na_2O, 0.2 % K_2O. The slag granulation was within the limits of 2-6 mm and its mechanical processing reduced the grain size under 100 μm.

Quartz sand with a content of about 98.8 % SiO_2 and a grain size below 2 mm was used in the starting mixture as fine aggregate, while gravel with a chemical composition of 87.5 % SiO_2, 6.1 % Al_2O_3, 2.1 % Na_2O, and 1.6 % Fe_2O_3 and grain size below 6 mm was chosen as coarse aggregate.

According to the invention of the French scientist Davidovits, J. [21] and the principle of alkaline activation of alumino-silicate materials [22], the mixture of sodium hydroxide (NaOH) soluble in water and aqueous solution with a concentration of 38 % of sodium silicate (Na_2SiO_3) was used. NaOH was commercially purchased in the form of flakes. Also, the Na_2SiO_3 solution was available on the market and could be diluted with distilled water to correct the solution viscosity.

The remarkable invention of the transformation of alumino-silicate waste into a superior geopolymeric material in terms of quality by activation in a highly alkaline medium, which facilitates the development of geopolymerization reaction, was the

basis of the method adopted in this experiment. The effect of transforming alumino-silicate waste into a geopolymer is the possibility of significantly reducing or completely eliminating ordinary Portland cement from the composition of traditional concrete and obtaining a product with higher physico-mechanical properties under the conditions of its manufacture without greenhouse gas emissions (CO_2). The addition to the mixture of alumino-silicate materials of an agricultural waste with a very high availability (corn cob ash), silica-rich and having pozzolanic properties that give it the ability to be used in the manufacture of cement and construction concrete constitutes the completion of the mentioned adopted method.

The geopolymerization reaction is perceived by researchers as a complex reaction. The contact between the alkaline solution (NaOH) and the alumino-silicate materials generates the dissolution and hydrolysis of silicon and aluminum, which take place according to the reactions shown below [23-25].

$$Al_2O_3 + 3H_2O + 2OH^- = 2[Al(OH)_4]^- \quad (1)$$

$$SiO_2 + 2OH^- = [SiO_2(OH)_2]^{2-} \quad (2)$$

As a result of these reactions (at room temperature), a gel is formed, that modifies its structural features and several gel phases appear. At the end, the system is polymerized, forming a solidified mass due to its hardening. A three-dimensional polymeric chain and ring structure based on Si-O-Al-O bonds is generated [26].

A pozzolanic material is, in terms of chemistry, a material rich in silica and alumina without cementing properties. Water added to such material gives it cementing properties by forming calcium silicate hydrate (C-S-H) gel. C-S-H gel is the main product of hydration of Portland cement and has the ability of increasing the strength of cement-based materials [27, 28]. Corn cob ash is a silica-rich precursor and it was experimentally found that it can partially substitute the Portland cement in a cement concrete due to its pozzolanic properties. In the experiment described below, the cement was completely eliminated from the mixture composition, the alumino-silicate waste playing the role of cementitious materials.

The method of preparing geopolymer concrete included the following steps. The dry alumino-silicate materials (fly ash and granulated blast furnace slag) together with corn cob ash, quartz sand, and coarse aggregate (gravel) in the dosages adopted for each experimental version were mixed in a metal container with an electrically operated stirrer for 5 min. The preparation of the alkaline activator took place separately in a glass vessel, being mixed NaOH flakes dissolved in distilled water, Na_2SiO_3 solution, and water addition by stirring for 5 min. After mixing, the alkaline activator was slowly poured over the solid mixture, after which the stirring process continued for another 5 min, generally until the gel was formed. The gel representing the fresh geopolymer was poured into a metal mold protected on the inside with thin plastic film and placed in a thermally insulated room for the curing treatment carried out by blowing steam at 80 ºC for 24 hours. The hot curing process was followed by room temperature curing for 48 hours. Keeping the specimen removed from the mold

for free curing also at room temperature was carried out in an isolated room until the tests for characterizing the specimen were carried out after 7 and 28 days, respectively.

Composition of the four experimental versions is shown in Table 1.

Table 1

Composition of experimental versions

Composition	Experimental version ($kg \cdot m^{-3}$)			
	1	2	3	4
Fly ash	370	370	370	388
Granulated blast furnace slag	46	32	19	-
Corn cob ash	46	61	74	74
Quartz sand	670	670	670	670
Coarse aggregate (gravel)	850	850	850	850
NaOH 8M	120	120	120	120
Na_2SiO_3 solution	250	250	250	250
Water addition	60	60	60	60

According to [29], the calcium content could influence geopolymer gel products through the appearance of hydrated calcium alumino-silicate (C-A-S-H) along with hydrated calcium silicate (C-S-H) in alkali-activated geopolymer. The effect of Ca^{2+} on the geopolymerization process is still unclear. An improvement in compressive strength after 7 days for an addition of 3 % CaO in the material mixture was observed. Considering that the blast furnace slag provided by Arcelor Mittal Galati had a relatively high content of CaO (39.9 %) as well as the controversies in the literature regarding the effect of calcium, in this paper it was chosen to significantly reduce the weight proportion of blast furnace slag in the mixture, even up to zero, simultaneously with the increase in corn cob ash content.

Weight proportion of fly ash, blast furnace slag, and corn cob ash was varied according to the data in Table 1 as follows. In the first three versions, the proportion of fly ash was relatively constant around 80 %, while in version 4, the proportion of fly ash increased to 84 %. Blast furnace slag continuously decreased from 9.9 to 4.1 % between versions 1 and 3 and reached zero in version 4. The corn cob value increased from 9.9 % (version 1) to 16.0 % (version 3) and remained almost constant in version 4. The other components of the mixture had constant values in all four versions. The sand was 27.8 %, and coarse aggregate had the value of 35.2 %. Na_2SiO_3 and NaOH represented 10.4 and 5.0 %, respectively, their weight ratio being 2.08. The weight ratio between the total alumino-silicate materials (fly ash and slag) and the total alkaline activator decreased from 1.12 (in version 1) to 1.05 (in version 3), reaching 0.78 (version 4) in the case of complete elimination of the blast furnace slag. Water addition was kept constant at 2.5 %.

Characterizing methods of geopolymer specimens were the following. Density was determined by weighing the specimen mass relating to its volume [30]. Porosity was calculated identifying the proportion of porous material (apparent density) compared to the same material without pores obtained by melting and cooling (true density) [31]. The method utilized for measuring the heat conductivity was the heat-

flow method according to SR EN 1946-3:2004 standard. Compressive strength was measured with TA.XTplus Texture Analyzer and flexural strength was determined using SR EN ISO 1412:2000 [32]. The method of immersing under water the geopolymer specimen was applied for determining the water absorbed by this (ASTM D570). Investigation of the microstructural configuration was carried out with Biological Microscope TM5000 model with captured image, 1000 x magnification.

3. Results and discussion

The application of characterizing methods of geopolymer concrete specimens after 7 and 28 curing days led to the results shown in Table 2.

Table 2

Features of geopolymer concrete specimens

Feature	Experimental version			
	1	2	3	4
Density ($kg \cdot m^{-3}$)	2412	2400	2383	2369
Porosity (%)	29.8	31.7	33.7	34.8
Heat conductivity ($W \cdot m^{-1} \cdot K^{-1}$)	0.518	0.514	0.510	0.509
Compressive strength (MPa)				
- after 7 days	22.5	20.8	20.4	25.9
- after 28 days	31.4	31.1	30.8	39.8
Flexural strength (MPa)				
- after 7 days	2.9	3.0	2.9	3.7
- after 28 days	3.6	3.7	3.7	4.1
Water uptake (vol. %)	2.1	2.3	2.2	2.4

The analysis of the data in Table 2 showed a slight decrease of the geopolymer density with the reduction of blast furnace slag proportion in the starting mixture, the density value starting from 2412 $kg \cdot m^{-3}$ (version 1) and going down to 2369 $kg \cdot m^{-3}$ (version 4). The porosity fell within low limits (29.8-34.8 %) following a slightly increasing slope from the value corresponding to the specimen of version 1 to that of the specimen made in version 4. Due to the high density and low porosity of the samples, heat conductivity had relatively high values (0.509-0.518 $W \cdot m^{-1} \cdot K^{-1}$). The compressive strength was influenced by changing the weight proportion of alumino-silicate waste (fly ash and slag) and agricultural waste. It is possible that the high content of CaO in the slag composition, at least in version 1 in which the blast furnace slag represented 1/8 of the total fly ash-slag amount, favorably influences the compressive strength value after 7 days of curing (22.5 MPa) according to the hypothesis presented in [29]. In versions 2 and 3 characterized by reducing the proportion of slag and increasing the proportion of agricultural waste, the compressive strength slightly decreased, both after 7 and after 28 days, to increase significantly in both curing variants in version 4. The value of compressive strength after 28 days reached the maximum level of 39.8 MPa. An almost similar situation was also registered in the case of specimen flexural strength. After remaining relatively constant

in versions 1-3, the flexural strength reached its maximum value in the case of version 4 after 7 days (3.7 MPa) and also after 28 days (4.1 MPa), demonstrating that the best solution in terms of quality was the use of corn cob ash as an agricultural waste widely available in Romania mixed with coal fly ash, a by-product of energy industry, activated with the alkaline solution composed of NaOH and Na_2SiO_3. The maximum weight proportion of corn cob ash in the mixture with fly ash was 16 %.

The microstructural aspect of the four specimens corresponding to the tested experimental versions is presented in Fig. 1.

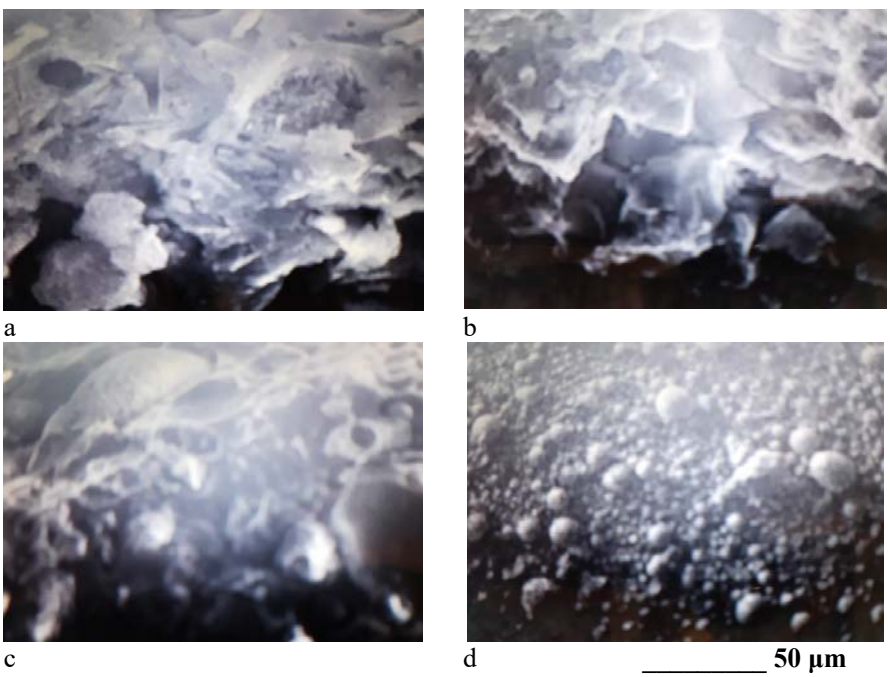

Fig. 1. Microstructural aspect of geopolymer concrete specimens
a – version 1; b – version 2; c –version 3; d – version 4.

Fig. 1 practically shows the transition from typical structures in which fly ash and granulated blast furnace slag are predominant (a) and (b), to structures in which the peculiarities of the fly ash structure become predominant, especially (d).

The results showed that the manufacture of geopolymer as designed by the French inventor Davidovits is an excellent modern technique of great importance for environmental protection based on residual alumino-silicate materials. The addition of other silicate wastes in the starting mixture, such as corn cob ash, is a very current trend that also contributes to the manufacture of products with suitable qualities for the construction sector. In this experiment, preparing the corn cob ash was made starting from corn cobs provided by an agricultural producer. Their transformation into ash by calcination was carried out in laboratory with electricity consumption. It should be noted that in reality, corn cob ash is practically an industrial by-product, which is thrown into the landfill. So, the energy consumption that generates ash as a secondary product is a useful consumption in several industrial activities, according to the

previous specification in this work (chapter 2). Practically, version 4 of this paper after removing the granulated blast furnace slag used in versions 1-3 and keeping fly ash as an alumino-silicate industrial by-product as well as the alkaline solution for its activation became a typical fly ash-based geopolymer concrete also including the agricultural waste (16 %).

4. Conclusions

The work aimed at manufacturing geopolymer concrete based on fly ash and granulated blast furnace slag as alumino-silicate waste activated with liquid solution of NaOH and Na_2SiO_3 combined with the addition of a silica-rich agricultural waste (corn cob ash) to the starting mixture. Considering the controversial influence in the literature of the calcium content in the material mixture on the geopolymer features as well as the high proportion of CaO (39.9 %) in the composition of blast furnace slag provided by ArcelorMittal Galati, the solution of using a low slag content and its reducing in versions 1-3 up to the zero level in version 4, at the same time as the agricultural waste content increases up to a maximum of 16 wt. % in the same experimental version was adopted. The solid and liquid components of the mixture were processed separately and then together until a gel was formed, which was poured into a mold and subjected to the curing process. The geopolymer concrete specimen with corn cob ash addition made in the optimal version (version 4 without slag content) had the following features: density of 2369 $kg \cdot m^{-3}$, porosity of 34.8 %, heat conductivity of 0.509 $W \cdot m^{-1} \cdot K^{-1}$, compressive strength of 25.9 MPa (after 7 days) and 39.8 MPa (after 28 days), flexural strength of 3.7 MPa (after 7 days) and 4.1 MPa (after 28 days). Compared to other geopolymer concrete characteristics reported in the literature, the product had excellent compressive and flexural strength being suitable for using in the construction sector. The viability of adding the agro-waste in the form of corn cob ash for making the geopolymer was confirmed.

References

[1] K. Wi, H. Lee, S. Lim, H. Song, M. Hussin, M. Ismail, „Use of an Agricultural By-Product, Nano Sized Palm Oil Fuel Ash as a Supplementary Cementitious Material", Construction of Building Materials, vol. 183, 2018, pp. 139-149. https://doi.org/10.1016/j.conbuildmat.2018.06.156

[2] C. Maraveas, „Production of Sustainable Construction Materials Using Agro-Wastes", Materials (Basel), vol. 13, no. 2, 2020. https://doi.org/10.3390/ma13020262

[3] N. Sathiparan, H.T.S.M. de Zoysa, „The Effect of Using Agricultural Waste as Partial Substitute for Sand in Cement Blocks", Journal of Building Engineering, vol. 19, Elsevier, 2018, pp. 216-227. https://doi.org/10.1016/j.jobe.2018.04.023

[4] M.E. Rahman, P.J. Ong, O. Nabinejad, S. Islam, N.A.N. Khandoker, V. Pakrashi, K.M. Shorowordi, „Utilization of Blended Waste Materials in Bricks", Technologies, vol. 6, no. 1, 2018. https://doi.org/10.3390/technologies6010020

[5] M. Duque-Acevedo, I. Lancellotti, F. Andreola, L. Barbieri, L.J. Belmonte-Ureña, F. Camacho-Ferre, „Management of Agricultural Waste Biomass as Raw Material for the Construction Sector: An Analysis of Sustainable and Circular Alternatives", Environmental Sciences Europe, vol. 34, no. 70, 2022.

[6] V. Balagopal, A. Rahim, T.S. Viswanathan, „Sustainable Supplementary Cementitious Materials Derived from Agro-Wastes-A Review", International Journal of Civil Engineering and Technology, vol. 8, 2017, pp. 572-582.
[7] T. Ashour, „Composites Using Agricultural Wastes", in: Handbook of Composites from Renewable Materials, K.T. Vijai, K.T. Manju, R.K. Michael (eds.), Wiley & Sons, Hoboken, USA, 2017.
[8] I. Kellersztein, U. Shani, I. Zilber, A. Dotan, „Sustainable Composites from Agricultural Waste: The Use of Steam Explosion and Surface Modification to Potentialize the Use of Wheat Straw Fibers for Wood Plastic Composite Industry", Polymer Composites, vol. 40, 2019, Wiley Online Library, pp. E53-E61. https://doi.org/10.1002/pc.24472
[9] C. Maraveas, „Production of Sustainable and Biodegradable Polymers from Agricultural Waste", Polymers (Basel), vol. 12, 2020. https://doi.org/10.3390/polym12051127
[10] H.R. Kymäläinen, A.M. Sjöberg, „Flax and Hemp Fibres as Raw Materials for Thermal Insulations", Building and Environment, vol. 43, no. 7, Elsevier, 2008, pp. 1261-1269. https://doi.org/10.1016/j.buildenv.2007.03.006
[11] C. Aciu, N. Cobirzan, „Use of Agricultural Products and Waste in the Building Materials Industry", ProEnvironment, vol. 6, 2013, pp. 472-478. http://journals.usamvcluj.ro/index.php/promediu
[12] J. Vėjelienė, A. Gailius, S. Vėjelis, S. Vaitkus, G. Balčiūnas, „Evaluation of Structure Influence on Thermal Conductivity of Thermal Insulating Materials from Renewable Resources", Materials Science, vol. 17, no. 2, 2011, pp. 208-212.
[13] G. Bou-Ali, „Straw Bales and Straw-Bale Wall Systems", University of Arizona, Tucson, USA, 1993. https://repository.arizona.edu/handle/10150/276292
[14] L. Paunescu, E. Volceanov, B.V. Paunescu, „Reinforced Concrete Composite with Vegetable Fibre", Academic Journal of Manufacturing Engineering, vol. 21, no. 1, 2023, pp. 120-125.
[15] D. Wojcieszak, J. Przbyl, L. Czajkowski, J. Majka, A. Pawlowski, „Effects of Harvest Maturity on the Chemical and Energetic Properties of Corn Stover Biomass Combustion", Materials (Basel), S. Bennici (ed.), vol. 15, no. 8, 2022. https://doi.org/10.3390/ma15082831
[16] P. Murthi, K. Poongody, R. Gobinath, „Effects of Corn Cob Ash as Mineral Admixture on Mechanical and Durability Properties of Concrete-A Review", IOP Conference Series: Materials Science and Engineering, vol. 1006, IOP Publishing, 2020. https://doi.org/10.1088/1757-899X/1006/1/012027
[17] F.F. Udoeyo, S.A. Abubakar, „Maize-Cob Ash as Filler in Concrete", Journal of Materials in Civil Engineering, vol. 15, 2003, pp. 205-208.
[18] O.S. Olafusi, A.P. Adewuyi, O.M. Sadiq, A.F. Adisa, O.S. Abiola, „Rheological and Mechanical Characteristics of Selfcompacting Concrete Containing Corncob Ash", Journal of Engineering Research, vol. 22, no. 1, 2017, pp. 72-85.
[19] J. Kamau, A. Ahmed, P. Hirst, J. Kangwa, „Suitability of Corncob Ash as a Supplementary Cementitious Material", International Journal of Materials Science and Engineering, vol. 4, no. 4, 2016, pp. 215-228. https://doi.org/10.17706/ijmse.2016.4.4.215-228
[20] S.A. Memon, M.K. Khan, „Ash Blended Cement Composites: Eco-Friendly and Sustainable Option for Utilization of Corn Cob Ash", Journal of Cleaner Production, vol. 175, 2017, pp. 442-455. https://doi.org/10.1016/j.jclepro.2017.12.050
[21] J. Davidovits, M. Davidovits, N. Davidovits, „Process for Obtaining a Geopolymeric Alumino-Silicate and Products thus Obtained", US Patent no. 5,342,595, August 30, 1994.
[22] D. Dimas, I. Giannopoulos, D. Panias, „Polymerization in Sodium Silicate Solutions: A Fundamental Process in Geopolymerization Technology", Journal of Materials Science, vol. 44, no. 14, 2009, pp. 3719-3730.
[23] L. Paunescu, A. Ioana, E. Volceanov, B.V. Paunescu, „Nonconventional Ecological and Low-Energy Consumption Technique to Produce High-Strength Geopolymer Composite Based on Residual Materials as a New Type of Construction Material", Nonconventional Technologies Review, vol. 27, no. 1, 2023, pp. 32-38.

[24]M.H. Nawaz, M. Sivakumar, „Geopolymers in Construction-Recent Developments", Construction and Building Materials, vol. 260, Elsevier, 2020, ISSN 0950-0618.
[25] J. Davidovits, „Geopolymers and Geopolymeric Materials", Journal of Thermal Analysis Calorimetry, vol. 35, no. 2, 1989, pp. 429-441.
[26] N.B. Singh, „Fly Ash-Based Geopolymer Binder: A Future Construction Material", Minerals, vol. 8, no. 7, 2018. https://doi.org/10.3390/min8070299
[27] I.G. Richardson, „The Calcium Silicate Hydrates", Cement and Concrete Research, vol. 38, no. 2, 2008, pp. 137-158. https://doi.org/10.1016/j.cemconres.2007.11.005
[28] K. Takemoto, H. Uchikawa, „Hydration of Pozzolanic Cements", Proceedings of the 7th International Congress on the Chemistry of Cement, vol. IV-2, 1980, pp. 1-29.
[29] X. Zhao, C. Liu, L. Zuo, L. Wang, Q. Zuo, M. Wang, „Investigation into the Effect of Calcium on the Existence Form of Geopolymerization Gel Product of Fly Ash Based Geopolymer", Cement and Concrete Composites, vol. 103, Elsevier, 2019, pp. 279-292.
[30] *** „Metrology in Laboratory-Measurement of Mass and Derived Values", in: Radwag Balances and Scales, 2nd edition, Randon, Poland, 2015, pp. 72-73.
[31] L.M. Anovitz, D.R. Cole, „Characterization and Analysis of Porosity and Pore Structures", Reviews in Mineralogy and Geochemistry, vol. 80, no. 1, 2005, pp. 61-164.
[32] I. Curtu, A.E. Stanciu, „Determinarea Caracteristicilor Mecanice ale Epruvetelor din Material Compozit de Tip Mat&Roving", Buletinul AGIR, no. 1, 2011, pp. 78-81.